Collot, J.-Y., Greene, H. G., Stokking, L. B., et al., 1992
Proceedings of the Ocean Drilling Program, Initial Reports, Vol. 134

11. SITE 831[1]

Shipboard Scientific Party[2]

HOLE 831A

Date occupied: 12 November 1990

Date departed: 13 November 1990

Time on hole: 23 hr

Position: 16°00.56′S, 166°40.34′E

Bottom felt (rig floor; m; drill-pipe measurement): 1077.6

Distance between rig floor and sea level (m): 11.20

Water depth (drill-pipe measurement from sea level, m): 1066.4

Total depth (rig floor; m): 1194.10

Penetration (m): 116.50

Number of cores (including cores with no recovery): 15

Total length of cored section (m): 115.50

Total core recovered (m): 25.85

Core recovery (%): 22.4

Oldest sediment cored:
Depth below seafloor (m): 115.50
Nature: coral grainstone and foraminiferal wackestone
Age: unknown
Measured velocity (km/s): 1.961

Comments: Beacon for Site 831 was dropped during approach to Site 830.

HOLE 831B

Date occupied: 13 November 1990

Date departed: 20 November 1990

Time on hole: 7 days, 12 hr, 30 min

Position: 16°00.56′S, 166°40.36′E

Bottom felt (rig floor; m; drill-pipe measurement): 1077.6

Distance between rig floor and sea level (m): 11.20

Water depth (drill-pipe measurement from sea level, m): 1066.4

Total depth (rig floor; m): 1929.60

Penetration (m): 852.00

Number of cores (including cores with no recovery): 84

Total length of cored section (m): 852.00

Total core recovered (m): 87.25

Core recovery (%): 11.6

Oldest sediment cored:
Depth below seafloor (m): 727.44
Nature: coral rudstone, bioclastic packstone, and foraminiferal grainstone
Age: unknown
Measured velocity (km/s): 3.062

Hard rock:
Depth below seafloor (m): 852.00
Nature: andesitic breccia
Measured velocity (km/s): 2.539

Comments: Washed to 102.4 mbsf.

Principal results: We arrived on Site 831 on 12 November 1990 at 0500 Universal Time Coordinated (UTC) and spent 8 days and 16.5 hr on site drilling two holes (Holes 831A and 831B). After obtaining all our objectives, we departed Site 831 at 1630 UTC on 20 November 1990.

Site 831 (proposed site DEZ-5) is located on the summit platform of the Bougainville Guyot (16°00.56′S, 166°40.35′E, water depth 1066.4 m), approximately 42 km southwest of the southern tip of Espiritu Santo Island, about 5 km west of the d'Entrecasteaux Zone (DEZ)–New Hebrides Island Arc subduction zone, and 15 km due west of Site 830. A short geophysical survey was undertaken to locate an area covered with sufficient sediment for spudding. A small rise located nearly in the center of the guyot was found that appeared promising, an area where approximately 700 m of reefal lagoon deposits were interpreted to overlie volcanic basement rocks.

The Bougainville Guyot impinges upon the forearc slope of the central New Hebrides Island Arc (Vanuatu) and is either being subducted beneath or accreted to the arc. Here the guyot clogs the New Hebrides Trench and indents the forearc slope by 10 km. The Bougainville Guyot represents the eastern terminus of the South d'Entrecasteaux Chain (SDC) of the DEZ, a two-ridge system that also includes the North d'Entrecasteaux Ridge (NDR). The SDC is a chain of conical volcanic seamounts and guyots located on the Australia-India plate that presently is converging with the New Hebrides Island Arc (Pacific plate) at about 10 cm/yr. Anomalous bathymetric features such as a subcircular topographic reentrant in the forearc-slope rocks east and south of the Bougainville Guyot suggest that other seamounts or guyots have been previously subducted. The number of seamounts subducted along the DEZ collision zone is indirectly related to the duration of convergence, which is important to understanding collision deformation. In addition, the style of deformation along the forearc slope of Vanuatu appears to differ considerably from where the NDR is colliding and from where the SDC, or Bougainville Guyot, is impinging upon the forearc slope. Therefore, the objective of drilling at Site 831 is to penetrate the carbonate cap of the guyot and recover basement rocks for dating, compositional analyses, and paleomagnetic measurements, which then can be compared with those samples recovered and analyzed from Site 828 on the NDR. This, along with dating and paleobathymetric studies of the carbonate rocks, is expected to indicate the age and origin of the SDC and to document the tectonic and paleoceanographic history of Bougainville Guyot.

We drilled to 115.5 mbsf in Hole 831A, retrieving only 25.85 m of core for a recovery of 22.4%. After washing to 102.4 mbsf in Hole 831B, we penetrated 852 mbsf, producing only 87.25 m of core for a recovery of 11.6%. Nevertheless, we were able to drill 120 m into the volcanic rocks at the base of the carbonate sequence, and our objectives were attained. Four lithostratigraphic units have been described from both holes, all but two (Subunits IIB and IIC) with conformable basal contacts. Unit I (0–16.9 mbsf, Hole 831A) is a Pleistocene, pelagic, bioclastic foraminiferal ooze. Unit II (Subunit IIA, 16.9–100 mbsf in Hole 831A; Subunit IIB, 102.4–256.0 mbsf in Hole 831B) consists of Pleistocene to Pliocene, neritic, coral rudstone and mollusc float-

---

[1] Collot, J.-Y., Greene, H. G., Stokking, L. B., et al., 1992. *Proc. ODP, Init. Repts.,* 134: College Station, TX (Ocean Drilling Program).

[2] Shipboard Scientific Party is as given in the list of participants preceding the contents.

stone with some marine-water carbonate cements. Subunit IIC (256.0–352.3 mbsf, Hole 831B) is also a neritic coral rudstone and floatstone, but of unknown age. It exhibits moldic and vuggy porosity (dissolution porosity) with mostly marine, but possibly with some meteoric (freshwater), carbonate cementation. Subunit IID (352.3–429.6 mbsf, Hole 831A) is a neritic, bioclastic floatstone of unknown age with little moldic and vuggy porosity and the first definite example of meteoric carbonate cementation. Subunit IIIA (429.6–592.6 mbsf, Hole 831B) consists of lower Miocene, neritic, bioclastic floatstone with moldic and vuggy porosity, highly altered and dissolved matrix, and abundant secondary, meteoric carbonate cementation. Subunit IIIB (592.6–621.6 mbsf, Hole 831A) is lower Miocene, neritic, skeletal floatstone and foraminiferal grainstone with considerable moldic and vuggy porosity, well cemented by meteoric processes; foraminiferal grainstone dominates the lithology. A possible unconformity separates Subunit IIIB from underlying Subunit IIIC. Subunit IIIC (621.6–669.2 mbsf) consists of upper Oligocene, neritic, bioclastic and foraminiferal grainstone with less moldic and vuggy porosity; it is less cemented than the overlying Subunit IIIB. Subunit IIID (669.2–727.5 mbsf) is an upper Oligocene, neritic, bioclastic packstone and foraminiferal grainstone, well cemented (almost a limestone) by meteoric processes. Within Subunit IIID a soil horizon (Terra Rosa) was identified at 688.1 mbsf that separates an upper sequence of algal packstone from a lower foraminiferal grainstone. A soil horizon at 707.6 mbsf separates an upper bioclastic packstone with chlorite veins from a lower bioclastic floatstone and mudstone and algal rudstone with chlorite veins. The base of Subunit IIID represents the base of the carbonate sequence and unconformably overlies Unit IV, the volcanic rock complex.

The volcanic base to the carbonate sequence is Unit IV (727.5–852.0 mbsf), the contact being a reddish-orange weathered zone (or bole) marking the top of the volcanic rocks and underlying the coral limestone. The volcanic rocks were penetrated 125 m and are a series of andesitic hyaloclastites. They consist of clasts of gray two-pyroxene andesite (plagioclase-clinopyroxene-orthopyroxene-phyric) in a brecciated glassy matrix. The clasts, or blebs, are generally subrounded but are sometimes flattened and elongate with wispy margins. The shapes suggest that they were still plastic at the time of incorporation into the matrix. Individual clasts are usually surrounded by a conspicuous corona or reaction rim. The breccia matrix is composed of crystal and lithic fragments set in altered glass, which is partly palagonite. The development of secondary clay minerals gives a greenish color to many of the rocks.

Unit IV is divided into five subunits: Subunit IVA (727–741.0 mbsf) is an andesitic breccia with weathered and altered (highly oxidized) fragments and reworked clasts. Subunit IVB (741.0–789.0 mbsf) consists of an andesitic breccia with green, palagonitic matrix. Subunit IVC (789.0–822 mbsf) consists of andesitic breccia with oxidized and reworked andesitic fragments. Subunit IVD (822–838.0 mbsf) is an andesitic breccia with green palagonitic matrix. Subunit IVE (838.0–852.0 mbsf) consists of andesitic breccia with oxidized and reworked andesite fragments; the base of this subunit contains a well-defined, cross-bedded, andesitic sandstone-like layer.

Initial interpretations of the cores obtained at Site 831 indicate that the Bougainville Guyot was an andesitic submarine (and at times an island) volcano that subsequently accumulated a 728-m carbonate cap. The guyot has gone through several episodes of emergence and submergence as indicated by the various soil horizons (Terra Rosa) and oxidized rocks identified in the cores. Carbonate lithologies indicate formation in lagoonal deposits that consist of two major sedimentary facies. Facies 1 (16.9–429.6 mbsf) is a sequence of coral-rich grainstone that contains fragments of mollusc, coral rubble, algae, echinoid spines, and giant clam (tridacnid). The upper part (16.9–246.4 mbsf) of this facies is Pleistocene or Pliocene (~0.5–5.1 Ma) in age. Facies 2 (429.6–727.5 mbsf) is a sequence of foraminiferal grainstone that contains coralline algae, algal fragments, and large benthic foraminifers. The lower part (563.6–727.5 mbsf) of the facies is early Miocene to late Oligocene (28.2-21.8 Ma) in age.

Unit IV is interpreted as a succession of submarine lava flows that largely disintegrated to hyaloclastite debris on contact with seawater; at several levels the hyaloclastite has been reworked as thin sedimentary horizons. Cycles of color variation in the hyaloclastite matrix are thought to reflect changes in water depth. The dark green color at some levels may represent deeper water and the appearance of reddish fragments at other levels may indicate shallow water and a subaerial input. The low-potassium tholeiite and calc-alkaline affinities of the andesitic clasts point unequivocally to an island-arc origin for the Bougainville Guyot.

Foraminifers and nannofossils were the best initial source of age information. Examination of core-catcher samples indicates three different ranges of ages: (1) Pleistocene (0–16.9 mbsf), (2) Pleistocene or Pliocene (16.9–246.4 mbsf), and (3) early Miocene to late Oligocene (573.3–727.5 mbsf). Ages could not be determined from 246.4 to 563.6 mbsf and from 727.5 to 852.0 mbsf, the total depth of the hole. Benthic foraminifers indicate that the Pleistocene strata cored from 0 to 6.4 mbsf were deposited in the middle bathyal zone, those cored from 6.4 to 16.9 mbsf were deposited in the outer sublittoral zone, and Pleistocene or Pliocene strata cored from 16.9 to 246.4 mbsf were deposited in the inner sublittoral zone. The predominant occurrence of corals and other shallow-water bioclasts throughout the carbonate sequence suggests an inner sublittoral environment for deposits cored below 246.4 mbsf. Initial paleomagnetic analyses indicates normal polarity–Brunhes Chron–in the upper 16 m of Holes 831A and 831B.

Physical properties measurements appear to correlate well with the lithologic units identified from the cores. For example, water content, porosity, bulk density, and velocity all show a direct relationship to lithology with distinct and profound increases in values occurring beneath 727.5 mbsf, the contact between the carbonate sequence and the underlying volcanic rocks.

A considerable amount of logging was undertaken at this site. Data were obtained using the standard Schlumberger geophysical and geochemical tool strings. In addition, the formation microscanner, digital borehole televiewer, and magnetometer/susceptibility tools were run twice. All tools produced good data and initial interpretation indicates good correlation between logging data and lithology.

BACKGROUND AND OBJECTIVES

Site 831 is the fifth of a series of sites (Sites 827–831) located within the collision area of the d'Entrecasteaux Zone (DEZ) and the central New Hebrides Island Arc (Vanuatu). The site is located on the summit platform of the Bougainville Guyot, approximately 42 km southwest of the southern tip of Espiritu Santo Island, about 5 km west of the trace of the subduction zone, and 15 km due west of Site 830 (Fig. 1). This guyot rises 3 km above the abyssal seafloor, and Seabeam bathymetric data (Daniel et al., 1986) indicate that the guyot is generally oriented northwest-southeast and has an approximate surface dimension of 16 km long by 10 km wide. The guyot is an irregularly shaped feature with a planar outline that resembles the profile of a buzzard. The primary purpose of drilling the guyot was to determine the origin and composition of the rocks that comprise the guyot so that comparisons of the forearc deformation along the DEZ collision zone can be made.

Bougainville Guyot represents the eastern terminus of the South d'Entrecasteaux Chain of the DEZ, a two-ridge system that also includes the North d'Entrecasteaux Ridge (NDR). Presently the guyot appears to have been partially subducted beneath the forearc slope of the New Hebrides Island Arc (Fisher et al., 1986; in press). Here the guyot clogs the trench and indents the forearc slope by 10 km to form an antiform structure whose surface has been elevated 800 m above the eastern platform of the guyot. Marking the separation of the guyot from the deformed forearc slope is a swale that trends northwest-southeast, parallel to the long axis of the guyot (Fig. 2), and extends into well-developed submarine canyons

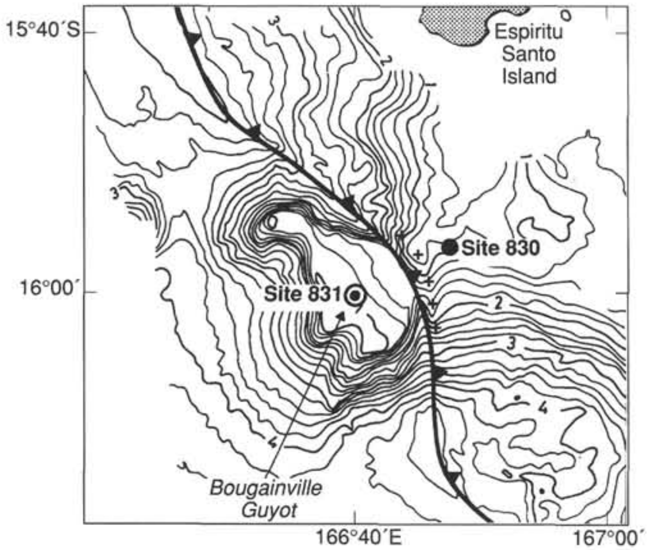

Figure 1. Bathymetric map showing location of Site 831. Isobaths are in kilometers. Bold line with teeth indicates approximate position of subduction zone; teeth are on upper plate.

to the north and south. This swale and the submarine canyons prevent all but the fine-grained materials eroded from the arc from reaching the surface of the guyot by directing sediment-laden currents north and south where the transported sediment are deposited in the New Hebrides Trench (Fisher et al., in press).

Bougainville Guyot is a volcanic edifice capped with a thick (~700 m), well-layered, flat carbonate sequence of lagoonal and coral reef deposits (Fisher et al., in press). Seismic reflection and Seabeam bathymetric data along with observations and sampling during *Nautile* dives (Daniel et al., 1986; Collot and Fisher, 1989; Fisher et al., 1986) show that several coral pinnacles are scattered about the flat, gently (~5°) eastward-dipping summit platform; local topographic highs along the periphery of the summit platform appear to be remnant fringing reefs. The edge of the summit platform is defined by steep scarps that are about 700 m high whose base is at the smooth upper flank of the guyot. Fisher et al. (in press) describe the flanks of the guyot as a debris apron composed of carbonate and volcanic rocks that have been shed from the guyot by mass wasting. Subcircular slump scars appear to indent and shape the guyot's western edge with one forming the "buzzard's neck" to the northwest and another shaping the southwestern edge.

Island-arc basalts, andesite, and middle Eocene to middle Oligocene sedimentary rocks, including carbonate rocks, have been recovered from the flanks of the Bougainville Guyot (Collot et al., unpubl. data).[3] This guyot, like many of the conical seamounts and guyots of the SDC, appears to be an andesitic seamount that is being carried along eastward upon the Australia-India plate, which is converging with the central New Hebrides Island Arc at a rate of 10 cm/yr (Minster and

[3] Collot, J.-Y., Lallemand, S., Pelletier, B., Eissen, J.-P., Glaçon, G., Fisher, M. A., Greene, H. G., Boulin, J., Daniel, J., and Monzier, M. Geology of the d'Entrecasteaux–New Hebrides island arc collision: results from a deep-sea submersible survey (submitted to *Tectonophysics*).

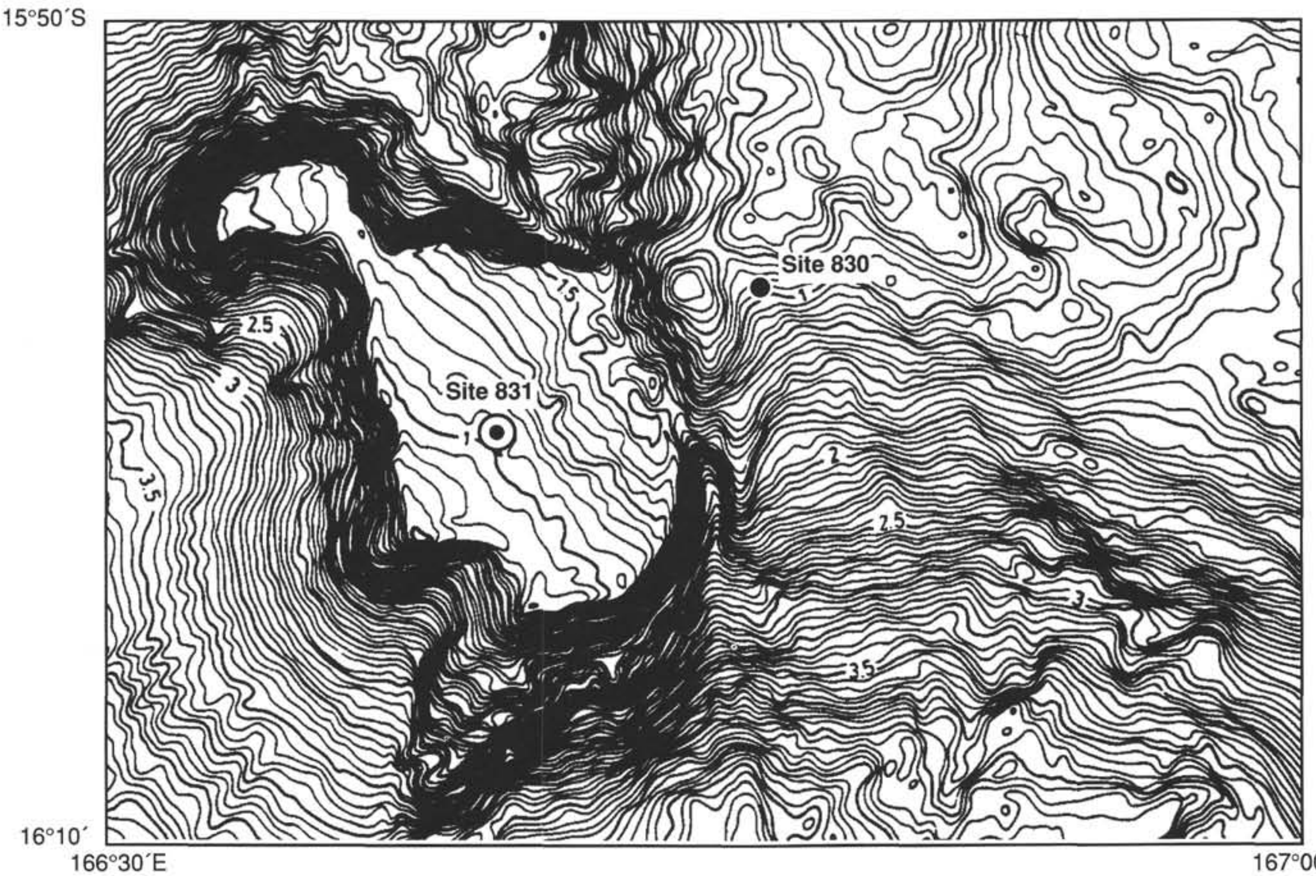

Figure 2. Seabeam map of Bougainville Guyot showing flat, eastward-dipping summit platform, swale and submarine canyons, and antiform dome immediately east of the guyot (modified after Daniel et al., 1986). Bathymetry in kilometers; contour interval is 50 m.

Jordan, 1978). While being carried along on the Australia-India plate, the Bougainville Guyot uplifted as it approached the New Hebrides Island Arc and possibly emerged on the outer rise before sliding down the subduction zone (Dubois et al., 1988). Collot et al. (unpubl. data) suggest that the guyot was last emergent between 2.2 and 0.5 Ma. The Bougainville Guyot is now in active collision with the arc and at least one-third of the guyot is interpreted to have been broken off the eastern edge and been buried beneath the forearc slope (Fisher et al., in press). The guyot is either being subducted beneath the arc or is being accreted to the forearc slope.

A short single-channel seismic reflection survey was made in the area of proposed site DEZ-5 (see "Seismic Stratigraphy" section, this chapter). From this survey we were able to locate an area upon a small rise that is covered with sediment, which would facilitate spudding of the drill; this site is nearly in the center of the guyot, in the area that is interpreted to be the guyot's lagoon. Onboard processing of the seismic reflection profile collected at this site indicated that acoustic basement, which may be the volcanic basement of the guyot, lies at about 700 mbsf.

Because the Bougainville Guyot is colliding with the New Hebrides Island Arc and is actively deforming the forearc slope, both by collisional processes and possible accretion and tectonic erosion, we hope to obtain information about the structure and composition of the guyot from drilling at this site. The principal objectives of drilling at Site 831 are as follows:

1. To penetrate the carbonate cap of the guyot and recover samples of the basement rocks for comparison with those recovered from the NDR.
2. To sample the basement rocks so that the lithology, age, and origin of the guyot and SDC can be understood.
3. To sample the carbonate rocks of the guyot and determine the age, subsidence history, and tectonic elevation of the guyot as it approached the outer bulge and started down the subduction zone.

Data obtained from the cores of Site 831 will be compared and contrasted with data from Sites 827–830 because the type of deformation that occurs along the forearc slope of the New Hebrides Island Arc is probably related to the structure and composition of the ridges that are impinging upon the slope. Information about the composition, physical properties, and fluids of the Bougainville Guyot is critical to understanding the style of deformation taking place at the collision zone and will be used to model the collision processes.

SEISMIC STRATIGRAPHY

Multichannel Seismic Data

Multichannel seismic lines that cross over the Bougainville Guyot show that the guyot summit is nearly planar and dips about 5° east. Parallel-bedded rocks, about 700 m thick, underlie the seafloor and form a carbonate cap composed of neritic reef debris. Migrated multichannel seismic line 100 (Figs. 3 and 4) crosses the guyot cap from east to west and reveals that Site 831, located near the center of the guyot, penetrated the cap at its thinnest; the cap thickens from the site in all directions toward the guyot rim. The small seafloor feature that has a square cross-sectional shape below shotpoint (SP) 720 is a reef. Reflections from within the cap vary little in amplitude, spacing, or frequency content, suggesting that cap rocks are mainly homogeneous and that layering is only faintly expressed. Poorly reflective rocks below the cap have been shown by drilling to be andesite breccia; seismic data are too scattered to reveal a consistent dip direction within the volcanic rocks.

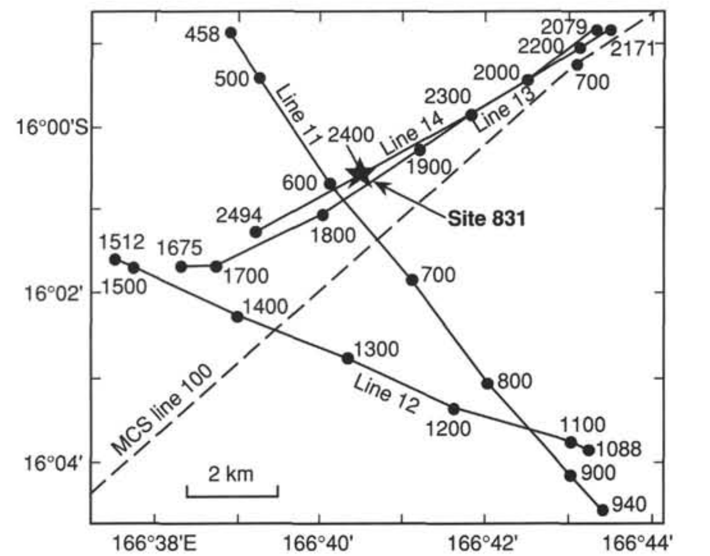

Figure 3. Trackline map showing the locations of Site 831, single-channel seismic lines 11 and 13, as well as multichannel seismic line 100 (USGS, L5-84-SP).

Single-Channel Seismic Data

Single-channel seismic reflection data were collected over Site 831, using two 80-in.^{3} water guns for the source and a streamer that has a 100-m-long active section. Aboard-ship processing included predictive deconvolution, bandpass filtering, and automatic gain control. Velocity data used to convert depth in the hole to traveltime come primarily from the sonic log, but the preliminary version of this log that was available aboard ship contained numerous zones of poor data marked by cycle skipping; the resulting depth-time conversion yields only a rough indication of the traveltime. Velocities from measurements of physical properties were used to calculate traveltimes to features in the shallowest part of the hole, where well-log data were not obtained.

Seismic lines 11 and 13 (Figs. 3, 5, and 6) cross just west of Site 831, which is located in the middle of a low-relief swell in the seafloor (Fig. 5). This swell is probably a horst bounded by normal faults at SP 1880 and 1815. Reflections in these single-channel data appear to be more discontinuous than are those in multichannel seismic data. Whether this results from the higher spatial resolution of the single-channel data or from a high noise content in these data is unknown. However, rock bodies deposited within lagoonal environments may be highly discontinuous. The strong reflection from near the top of the andesite breccia occurs at 2.01 seconds (s), and reflections from within the breccia appear to dip east.

Lithostratigraphic Unit I is Pleistocene foraminiferal ooze; Unit II includes neritic carbonates; Unit III, which also includes mainly neritic carbonates, shows a marked increase, relative to overlying rocks, in the degree of carbonate cementation; and Unit IV is andesite breccia (see "Lithostratigraphy" section, this chapter). The validity of the comparison between data of seismic line 13 and lithostratigraphic units (Fig. 7) depends critically on the accuracy of the sonic log, as described above. In this comparison, the contact between Units I and II appears to be lost within the reflection from the seafloor, and the contact between Units II and III does not coincide with any strong reflection. Contrary to our initial interpretation the strong reflection near 2.0 s does not correlate with the top of the andesite breccia (the contact between Units III and IV).

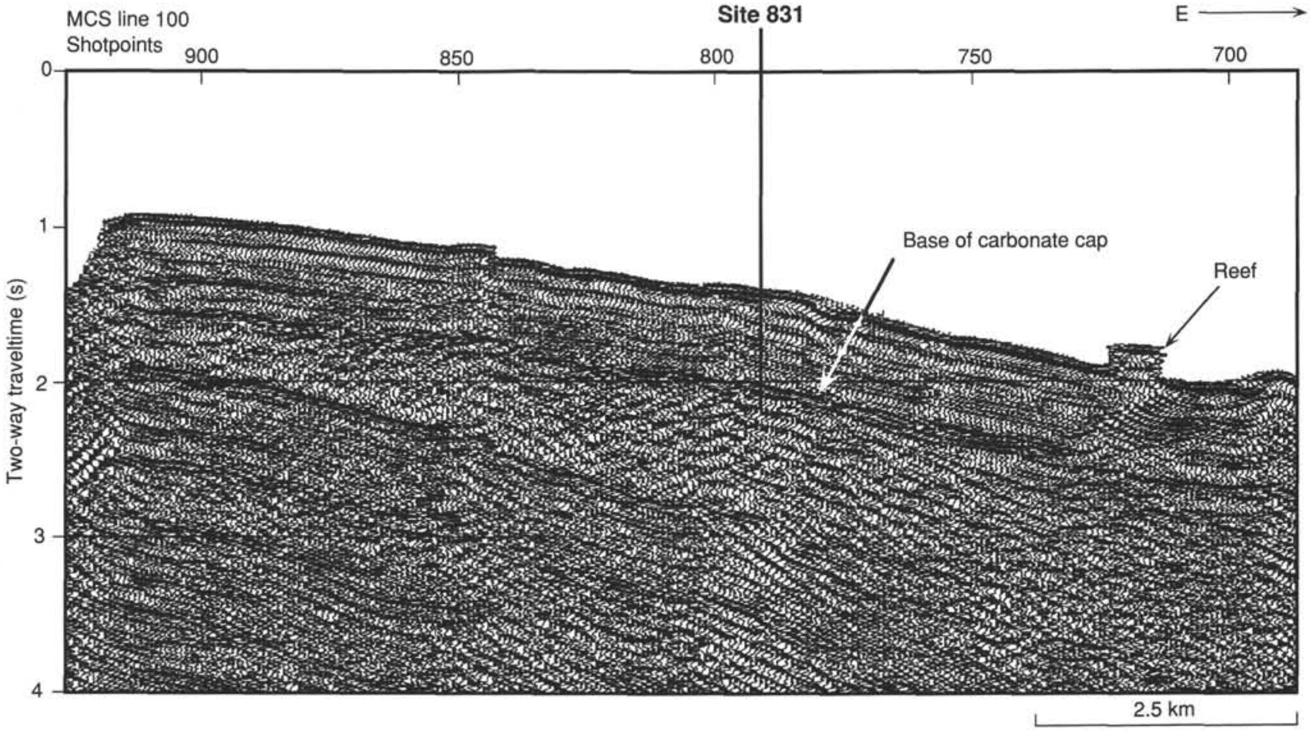

Figure 4. Part of migrated multichannel seismic line 100 that crosses the arc near Site 831.

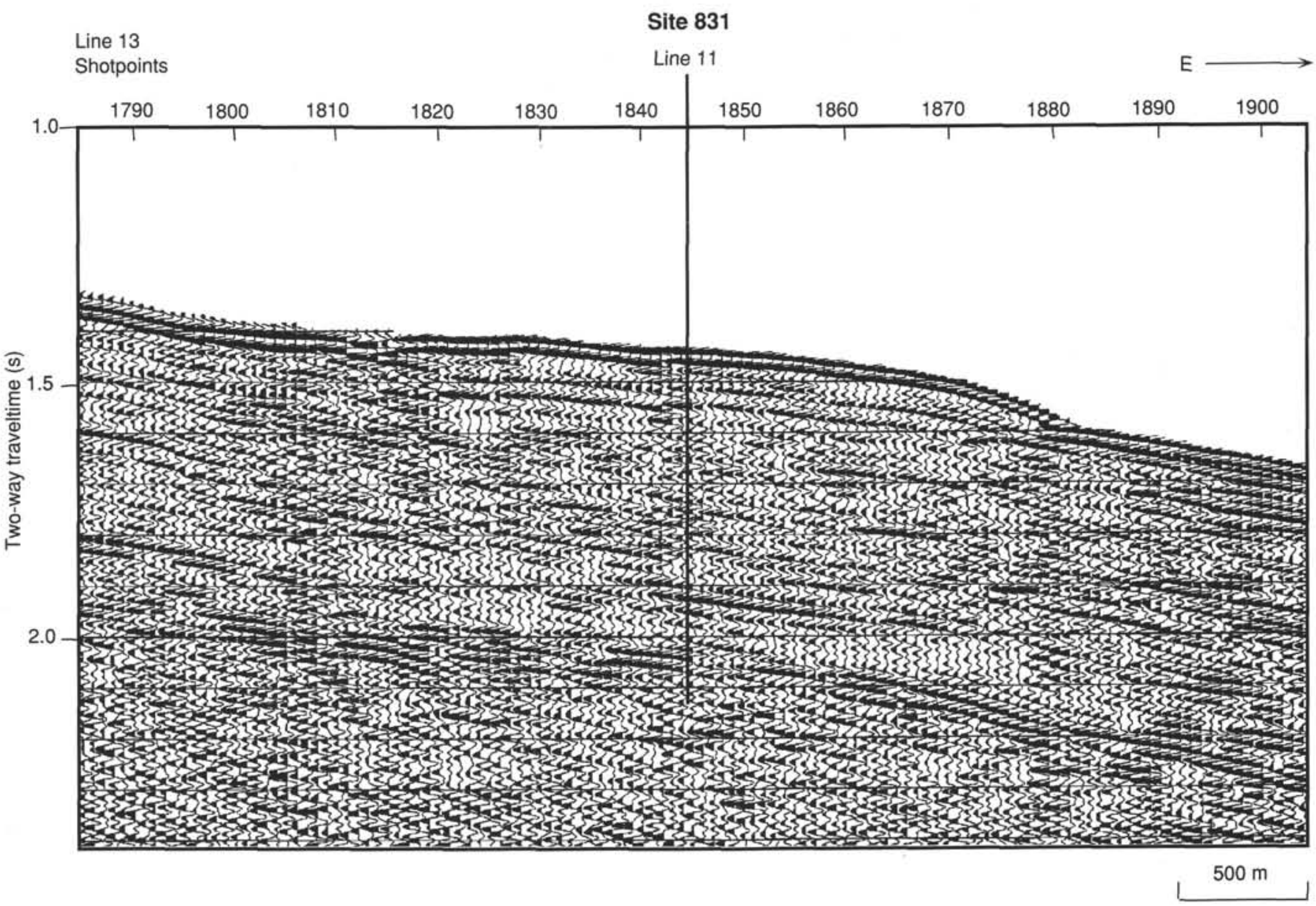

Figure 5. Part of single-channel seismic line 13 that crosses just west of Site 831.

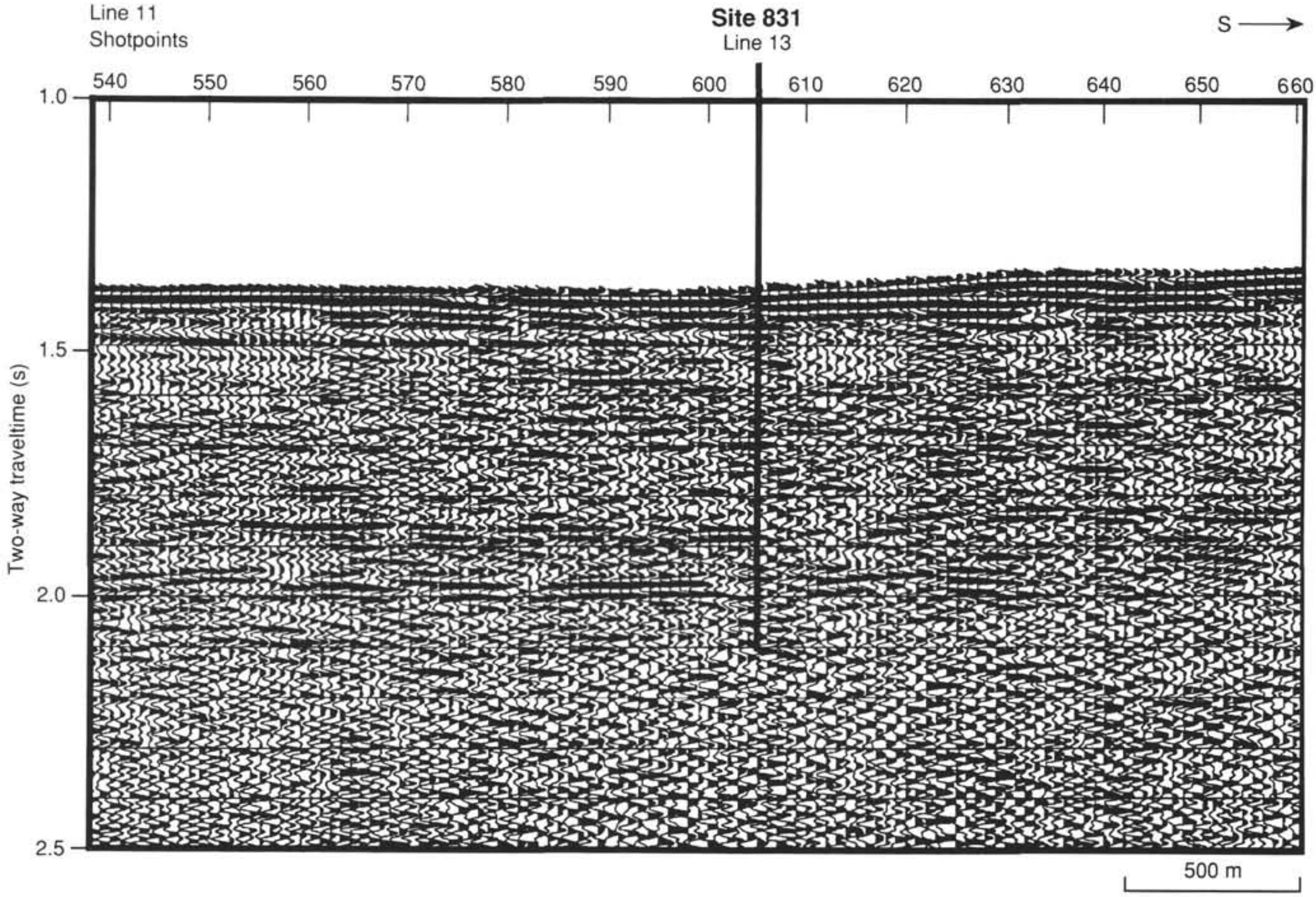

Figure 6. Part of single-channel seismic 11 that crosses Site 831.

The asterisk symbols (*) along the center vertical line in Figure 7 denote the traveltime to strong velocity gradients on the sonic log where velocities change by as much as 700 to 1000 m/s. Such gradients should produce strong reflections. The correlation between velocity gradients and seismic reflections is moderately strong: gradients 1 and 3 lie near horizontally continuous reflection peaks, and the reflection from near the top of the andesite breccia actually appears to be from two, close-spaced gradients (4 and 5) that lie within the carbonate section. Gradient 2, however, does not correlate with any continuous reflection. Surprisingly, the top of the andesite itself is seemingly not a strong reflector; this result may be due to the strongly weathered condition of the upper 10 to 20 m of andesite. The andesite breccia generates lower frequency reflections than do the overlying carbonate rocks.

Depths shown along the central bar in Figure 7 indicate the depths below the seafloor to horizons that produce particularly strong or continuous reflections evident on the seismic section. The reflector at 329 mbsf coincides with a borehole zone in which velocity data are poor and density values show little or no variation; therefore, the cause of this reflection cannot be determined. Similarly, the reflection at 496 mbsf coincides with parts of both the sonic and density logs that show only subdued variation, yielding no explanation for the cause of this reflection.

OPERATIONS

Site 831 (proposed site DEZ-5) is located on the summit of the Bougainville Guyot, 7.3 nautical miles (nmi) west-southwest of Site 830. Because the beacon had been dropped prior to drilling at Site 830, the vessel was moved in dynamic positioning mode while the drill string was tripped and the bottom-hole assembly was changed. No operating time was lost during the transit and the beacon signal was found easily.

Hole 831A

The advanced piston coring system (APC) penetrated the seafloor at 1066.4 meters below sea level (mbsl) and recovered 4.4 m of mud, sand, and coral rubble. The presence of coral fragments in the otherwise soft sediment (see "Lithostratigraphy" section, this chapter) prevented the use of the APC system below 17 mbsf. In addition, incomplete piston strokes and the flow of sandy sediment into the hole degraded the quality of the APC cores recovered.

The extended core barrel system (XCB) was then used. Although the rate of penetration was high, recovery remained poor. The motor-driven coring system (MDCB) was tried at 88 mbsf, but only 27 cm of coral fragments were recovered. Two downhole temperature measurements were attempted but were unsuccessful because the probe could not be completely inserted into the hard sediments. After two unsuccessful attempts to core using the MDCB, coring was stopped at 116.5 mbsf. A total of 25.85 m of core were obtained for a recovery of 22.4% (Table 1).

Hole 831B

After the round trip to change to the rotary core barrel (RCB) system, Hole 831B was spudded at 0815 UTC on 13 November. The hole was drilled to 102.4 mbsf, where continuous RCB coring began. Hole-filling problems started before the first core barrel was in place, and keeping the hole clean

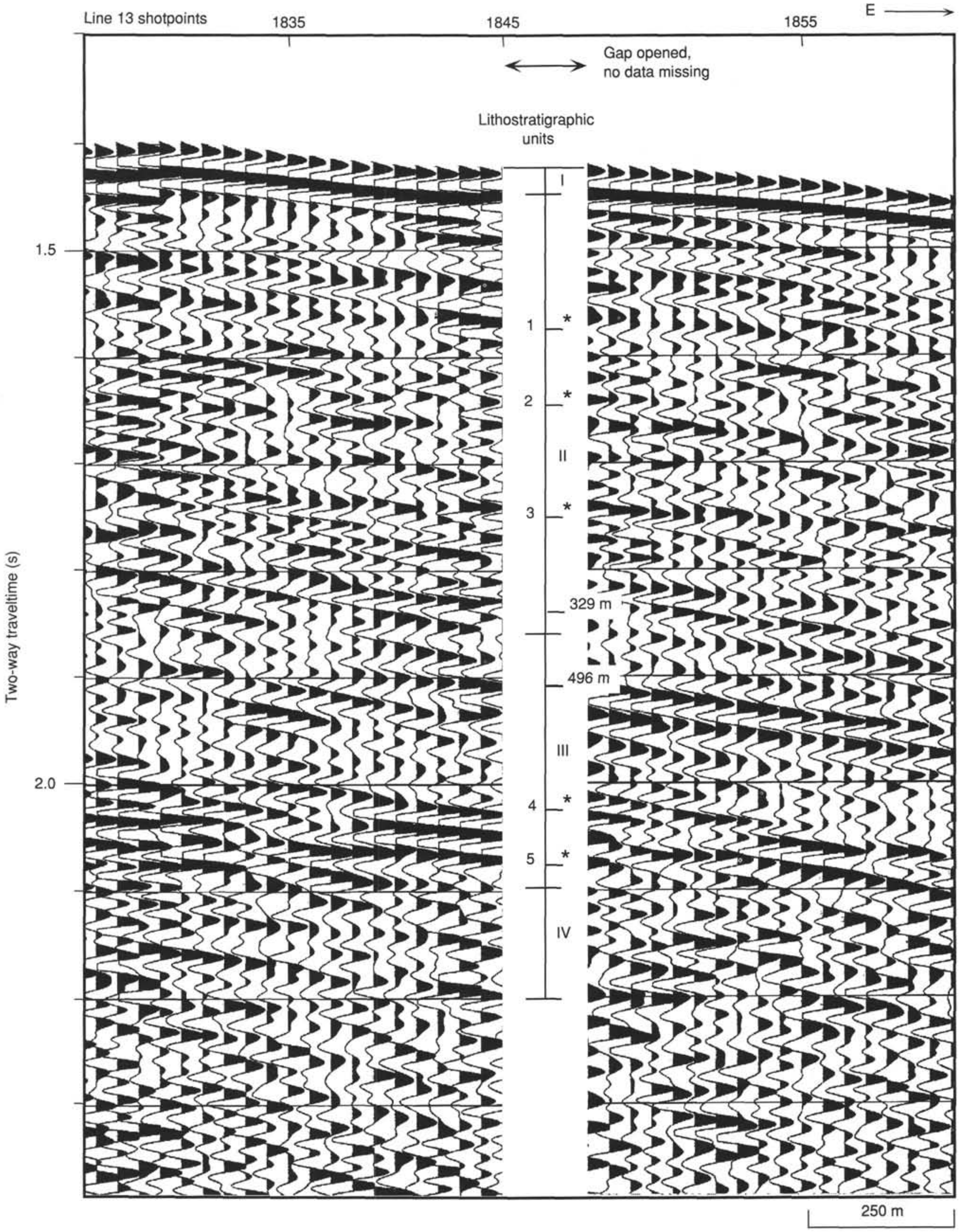

Figure 7. Detailed part of single-channel seismic line 13 that crosses Site 831. Lithostratigraphic units are explained in the "Lithostratigraphy" section (this chapter). Vertically along the line in the gap at the center of the section are asterisk symbols and numbers that are explained in the text.

Table 1. Coring summary, Holes 831A and 831B.

Core	Date (1990)	Time (UTC)	Depth (mbsf)	Length cored (m)	Length recovered (m)	Recovery (%)	Age
134-831A-							
1H	12 November	0950	0.0–4.4	4.4	4.36	99.1	Pleistocene
2H	12 November	1100	4.4–6.4	2.0	9.64	482.0	Pleistocene
3H	12 November	1200	6.4–15.9	9.5	9.70	102.0	Pleistocene
4H	12 November	1300	15.9–16.9	1.0	0.00	0.0	—
5X	12 November	1350	16.9–20.0	3.1	0.06	1.9	?Pleistocene
6X	12 November	1425	20.0–29.6	9.6	0.97	10.1	?Pleistocene
7X	12 November	1500	29.6–39.1	9.5	0.05	0.5	?
8X	12 November	1530	39.1–48.6	9.5	0.29	3.1	?Pleistocene
9X	12 November	1730	48.6–58.0	9.4	0.00	0.0	?
10X	12 November	1800	58.0–67.7	9.7	0.46	4.7	?
11X	12 November	1845	67.7–77.3	9.6	0.05	0.5	?
12X	12 November	1945	77.3–87.0	9.7	0.00	0.0	?
13N	12 November	2330	88.0–100.0	12.0	0.27	2.3	?
14X	13 November	0045	100.0–106.8	6.8	0.00	0.0	?
15X	13 November	0145	106.8–116.5	9.7	0.00	0.0	?
Coring totals				115.5	25.85	22.4	
134-831B-							
1W	13 November	1130	0.0–102.4	102.4	0.42	(wash core)	
2R	13 November	1230	102.4–111.9	9.5	0.16	1.7	?
3R	13 November	1320	111.9–121.3	9.4	0.17	1.8	?
4R	13 November	1400	121.3–130.9	9.6	0.30	3.1	?
5R	13 November	1600	130.9–133.9	3.0	5.92	197.0	?
6R	13 November	1830	133.9–140.5	6.6	0.18	2.7	?
7R	13 November	1920	140.5–150.1	9.6	0.19	2.0	?
8R	13 November	2000	150.1–159.8	9.7	0.08	0.8	?
9R	14 November	0000	159.8–161.4	1.6	0.00	0.0	?
10R	14 November	0200	161.4–169.4	8.0	0.06	0.8	?
11R	14 November	0250	169.4–179.1	9.7	0.05	0.5	?
12R	14 November	0500	179.1–188.8	9.7	0.07	0.7	?
13R	14 November	0700	188.8–198.5	9.7	0.06	0.6	?
14R	14 November	0835	198.5–208.2	9.7	0.09	0.9	?
15R	14 November	0930	208.2–217.8	9.6	0.07	0.7	?
16R	14 November	1035	217.8–227.5	9.7	0.19	2.0	?
17R	14 November	1130	227.5–237.2	9.7	0.09	0.9	?
18R	14 November	1225	237.2–246.4	9.2	1.86	20.2	?
19R	14 November	1345	246.4–256.0	9.6	0.09	0.9	?
20R	14 November	1510	256.0–265.5	9.5	0.31	3.3	?
21R	14 November	163	265.5–275.2	9.7	0.11	1.1	?
22R	14 November	1740	275.2–284.8	9.6	0.09	0.9	
23R	14 November	0000	284.8–294.4	9.6	0.12	1.3	
24R	14 November	1950	294.4–304.1	9.7	0.15	1.5	
25R	14 November	2050	304.1–313.7	9.6	0.16	1.7	
26R	14 November	2150	313.7–323.4	9.7	0.08	0.8	?
27R	14 November	2300	323.4–333.0	9.6	0.19	2.0	?
28R	15 November	0000	333.0–342.7	9.7	0.10	1.0	?
29R	15 November	0110	342.7–352.3	9.6	0.11	1.1	?
30R	15 November	0200	352.3–362.0	9.7	0.15	1.5	?
31R	15 November	0300	362.0–371.6	9.6	0.12	1.3	?
32R	15 November	0415	371.6–381.3	9.7	0.07	0.7	?
33R	15 November	0450	381.3–391.0	9.7	0.09	0.9	?
34R	15 November	0530	391.0–400.6	9.6	0.21	2.2	?
35R	15 November	0650	400.6–410.3	9.7	0.05	0.5	?

continued to be a problem until the drill reached 140 mbsf. Below this depth, conditions began to improve gradually, and progressively less time was required to clean the hole between cores, although frequent mud flushes and moderately high circulation rates were required. Core recovery was poor and typically consisted of a handful of coral and limestone fragments per core (see "Lithostratigraphy" section, this chapter). Rate of penetration, weight on bit, and other drilling parameters indicated that the recovered fragments corresponded to hard, partially lithified intervals. At 731 mbsf, an andesite breccia was penetrated and core recovery increased dramatically to the total depth of the hole at 852 mbsf, where the drilling objectives were considered fulfilled. A total of 87.25 m of core was obtained in Hole 831B for a recovery rate of 11.6%.

The wiper trip undertaken in preparation for logging went smoothly and indicated that the hole was stable and in very good condition. Two Schlumberger logging combinations were run (see "Downhole Measurements" section, this chapter). The first was the geophysical combination, consisting of the dual induction tool, the long-spaced sonic tool, the lithodensity tool, and the LDGO temperature tool. The second was the geochemical combination, including the natural gamma-ray spectrometry tool, the aluminum clay tool, the induced gamma-ray spectrometry tool, and the LDGO temperature tool. In addition, the magnetic susceptibility/magnetometer tool and the digital borehole televiewer were run successfully and the formation microscanner was employed successfully twice (see "Downhole Measurements" section, this chapter). The hole remained open, but fill increased from 30 m to 106 m during logging operations. Upon completion of logging, the drill string was recovered and the vessel departed for Site 832 at 1630 UTC on 20 November.

Table 1 (continued).

Core	Date (1990)	Time (UTC)	Depth (mbsf)	Length cored (m)	Length recovered (m)	Recovery (%)	Age
36R	15 November	0930	410.3–420.0	9.7	0.17	1.8	?
37R	15 November	1200	420.0–429.6	9.6	0.04	0.4	?
38R	15 November	1325	429.6–439.3	9.7	0.17	1.8	?
39R	15 November	1430	439.3–448.9	9.6	0.16	1.7	?
40R	15 November	1540	448.9–458.6	9.7	0.42	4.3	?
41R	15 November	1700	458.6–468.3	9.7	0.24	2.5	?
42R	15 November	1805	468.3–477.9	9.6	0.05	0.5	?
43R	15 November	1915	477.9–487.2	9.3	0.11	1.2	?
44R	15 November	2030	487.2–496.4	9.2	0.12	1.3	?
45R	15 November	2130	496.4–506.0	9.6	0.11	1.1	
46R	15 November	2240	506.0–515.7	9.7	0.08	0.8	
47R	15 November	2350	515.7–525.4	9.7	0.15	1.5	
48R	16 November	0011	525.4–534.6	9.2	0.64	7.0	
49R	16 November	0215	534.6–544.3	9.7	0.20	2.1	
50R	16 November	0320	544.3–553.9	9.6	0.11	1.1	
51R	16 November	0440	553.9–563.6	9.7	0.23	2.4	
52R	16 November	0615	563.6–573.3	9.7	0.21	2.2	Miocene-Oligocene
53R	16 November	0745	573.3–582.9	9.6	0.32	3.3	Miocene-Oligocene
54R	16 November	0855	582.9–592.6	9.7	0.05	0.5	Miocene-Oligocene
55R	16 November	1015	592.6–602.3	9.7	0.12	1.2	Miocene-Oligocene
56R	16 November	1135	602.3–612.0	9.7	0.21	2.2	Miocene-Oligocene
57R	16 November	1355	612.0–621.6	9.6	0.37	3.9	Miocene-Oligocene
58R	16 November	1510	621.6–631.3	9.7	0.20	2.1	Miocene-Oligocene
59R	16 November	1625	631.3–641.0	9.7	0.33	3.4	Miocene-Oligocene
60R	16 November	1735	641.0–650.3	9.3	0.04	0.4	Miocene-Oligocene
61R	16 November	1845	650.3–659.6	9.3	0.10	1.1	Miocene-Oligocene
62R	16 November	2000	659.6–669.2	9.6	0.05	0.5	Oligocene
63R	16 November	2115	669.2–678.5	9.3	0.76	8.2	Oligocene
64R	16 November	2230	678.5–688.1	9.6	1.53	15.9	Oligocene
65R	16 November	2330	688.1–697.8	9.7	0.23	2.4	Oligocene
66R	17 November	0015	697.8–707.5	9.7	0.89	9.2	Oligocene
67R	17 November	0200	707.5–717.1	9.6	0.42	4.4	Oligocene
68R	17 November	0315	717.1–726.8	9.7	0.38	3.9	Oligocene
69R	17 November	0500	726.8–736.4	9.6	2.98	31.0	
70R	17 November	0700	736.4–746.0	9.6	6.29	65.5	
71R	17 November	0925	746.0–755.6	9.6	4.08	42.5	
72R	17 November	1135	755.6–765.3	9.7	3.60	37.1	
73R	17 November	1300	765.3–770.1	4.8	2.32	48.3	
74R	17 November	1450	770.1–775.6	5.5	1.68	30.5	
75R	17 November	1650	775.6–784.8	9.2	2.02	21.9	
76R	17 November	1900	784.8–794.4	9.6	5.32	55.4	
77R	17 November	2100	794.4–799.1	4.7	3.52	74.9	
78R	17 November	2200	799.1–800.1	1.0	0.84	84.0	
79R	17 November	2350	800.1–804.1	4.0	3.65	91.2	
80R	18 November	0200	804.1–813.7	9.6	5.87	61.1	
81R	18 November	0445	813.7–823.4	9.7	8.74	90.1	
82R	18 November	0650	823.4–833.0	9.6	5.20	54.1	
83R	18 November	0920	833.0–842.7	9.7	4.89	50.4	
84R	18 November	1130	842.7–852.0	9.3	5.30	57.0	
Coring totals				749.6	87.25	11.6	
Washing totals				102.4	0.42		
Combined totals				852.0	87.67		

LITHOSTRATIGRAPHY

Sedimentary Units

Drilling of the Bougainville Guyot at Site 831 revealed that 727.5 m of carbonate overlies an andesite basement. The carbonate cap at Site 831 consists of 16.9 m of pelagic carbonate overlying 710.6 m of neritic carbonates. The latter proved extremely difficult to recover as evidenced by an average recovery rate of <5%. Such poor recovery complicates the process of delineating lithostratigraphic units. Moreover, it should be recognized that in many cores only a few carbonate cobbles (e.g., coral and mollusc fragments) were actually recovered, and such recovery may represent material that has fallen to the bottom of the hole from some indeterminable position. Lithostratigraphic units identified herein, therefore, may not fully represent the lithostratigraphy of the Bougainville Guyot. Given these cautions and the available data, the carbonate cap is best divided into three major units (Table 2 and Fig. 8).

Hole 831A

Unit I

Depth: 0–16.9 mbsf
Interval: Sections 134-831A-1H-1, 0 cm, to 134-831A-3H-CC, 15 cm
Thickness: 16.9–100.0 m
Age: Pleistocene

Unit I is composed of a Pleistocene sequence of brown (7.5Y 5/3), foraminiferal ooze with scattered, partially lithified grainstone clasts, that grades downward to a greenish gray

Table 2. Lithostratigraphic units, Holes 831A and 831B.

Interval	Unit	Subunit	Depth (mbsf)	Thickness (m)	Age
Sections 134-831A-1H-1, 0 cm, to 134-831A-3H-CC, 15 cm	I		0.0–16.9	16.9	Pleistocene
Sections 134-831A-5X-1, 0 cm, to 134-831A-13N-1, 27 cm	II	IIA	16.9–100.0	83.1	Pleistocene
Sections 134-831B-2R-CC, 0 cm, to 134-831B-19R-1, 8 cm	II	IIB	102.4–256.0	153.6	Pleistocene to Pliocene
Sections 134-831B-20R-CC, 0 cm, to 134-831B-29R-CC, 10 cm	II	IIC	256.0–352.3	96.3	Indeterminate
Sections 134-831B-30R-CC, 0 cm, to 134-831B-37R-CC, 3 cm	II	IID	352.3–429.6	77.3	Indeterminate
Sections 134-831B-38R-CC, 0 cm, to 134-831B-54R-CC, 7 cm	III	IIIA	429.6–592.6	163.0	38R–51R: Indeterminate 52R–54R: early Miocene
Sections 134-831B-55R-CC, 0 cm, to 134-831B-57R-CC, 0 cm	III	IIIB	592.6–621.6	29.0	early Miocene
Possible unconformity					
Sections 134-831B-58R-CC, 0 cm, to 134-831B-62R-CC, 0 cm	III	IIIC	621.6–669.2	47.6	late Oligocene
Sections 134-831B-63R-CC, 0 cm, to 134-831B-69R-1, 65 cm	III	IIID	669.2–727.5	58.3	late Oligocene

(5GY 5/1) to light yellowish brown (10YR 6/4) bioclastic foraminiferal ooze (Fig. 9). Bioclasts include a variety of small bivalves, gastropod fragments, occasional solitary corals, echinoid fragments, and pteropods. Pteropods are especially abundant and in portions of some cores, the sediment consists almost entirely of pteropods. Two volcanic ash layers, 4- and 22-cm thick, occur between 12 and 15 mbsf (Sections 134-831A-3H-5 and -3H-6). A bioclastic sed-lithic conglomerate sequence occurs from 0.4 to 3.0 mbsf in Unit I. The contact between Unit I and Unit II is marked by an abrupt faunal transition from pelagic microfossils of Unit I to neritic microfossils of Unit II (see "Biostratigraphy" section, this chapter).

Unit II

Hole 831A

Depth: 16.9–100.0 mbsf
Interval: Sections 134-831A-5X-1, 0 cm, to 134-831A-13N-1, 27 cm
Thickness: 83.1 m
Age: Pleistocene

Hole 831B

Depth: 102.4–429.6 mbsf
Interval: Sections 134-831B-2R-CC, 0 cm, to 134-831B-37R-CC, 3 cm
Thickness: 327.2 m
Age: Subunit IIB–Pliocene to Pleistocene; Subunit IIC–Indeterminate; and Subunit IID–Indeterminate

Unit II in Hole 831A consists of neritic carbonates that contain evidence of a wide diversity of shallow-water carbonate organisms including corals, molluscs (gastropods and pelecypods), coralline algae, echinoderms, bryozoans, and occasional large benthic foraminifers. Unit II is subdivided into four subunits based on fossil assemblages and qualitative estimates of the degree and type of cementation and dissolution. Subunit IIA occurs only in Hole 831A (Fig. 8).

Subunit IIA

Depth: 16.9–100.0 mbsf
Interval: Sections 134-831A-5X-1, 0 cm, to 134-831A-13N-1, 27 cm
Thickness: 83.1 m
Age: Pleistocene

Subunit IIA consists of white (10YR 8/2) coral and bioclastic grainstone and foraminiferal wackestone. Well-preserved corals include *Porites* and *Acropora,* with variable amounts of marine carbonate cement and internal sediment. Petrographic analysis indicates that some of the coral pores are fringed with acicular crystals, 60–120 microns (μm) in length. X-ray diffraction (XRD) analyses indicate that some of the corals observed in Subunit IIA contain minor amounts of calcite. The bioclasts in Subunit IIA occur mostly as fragments (<2 cm) and include echinoid spines, corals, foraminifers, and molluscs.

Hole 831B

Drilling at Hole 831B started by washing down 102.4 m (Fig. 8). Several well-preserved to partially calcitized pieces of large coral heads were recovered during the washing process. These neritic carbonate fragments are similar to those occurring in Subunit IIA in Hole 831A. We have chosen to define a new subunit at the top of the first rotary-drilled core in Hole 831B based on a change in sedimentary facies from wackestone and grainstone in Subunit IIA to rudstone and floatstone in Subunit IIB.

Subunit IIB

Depth: 102.4–256.0 mbsf
Interval: Sections 134-831B-2R-CC, 0 cm, to 134-831B-19R-1, 8 cm
Thickness: 153.6 m
Age: Pliocene to Pleistocene

Subunit IIB consists of coral rudstone and mollusc floatstone. We use a liberal definition of rudstone by including individual coral fragments without matrix under this term. Coral rudstone consists of individual fragments of white (10YR 8/2) *Acropora* and *Porites,* some with marine borings (*Lithophaga*?). XRD analyses indicate that several of the corals observed in Subunit IIB contain calcite, whereas others retain their original 100% aragonite mineralogy. An exceptionally well-preserved *Porites* head coral was recovered in Core 134-831B-18R (Fig. 10).

The mollusc floatstone is partially lithified and has abundant primary porosity and minor amounts of carbonate cement. Large fragments of a tridacnid and of a conch shell (*Strombus*?) have been identified in isolated cores (Fig. 11). Other bioclasts recognized in this unit include fragments of *Halimeda,* bryozoans, molluscs, echinoids, and coralline algae. Megascopic identification of marine cement is confirmed

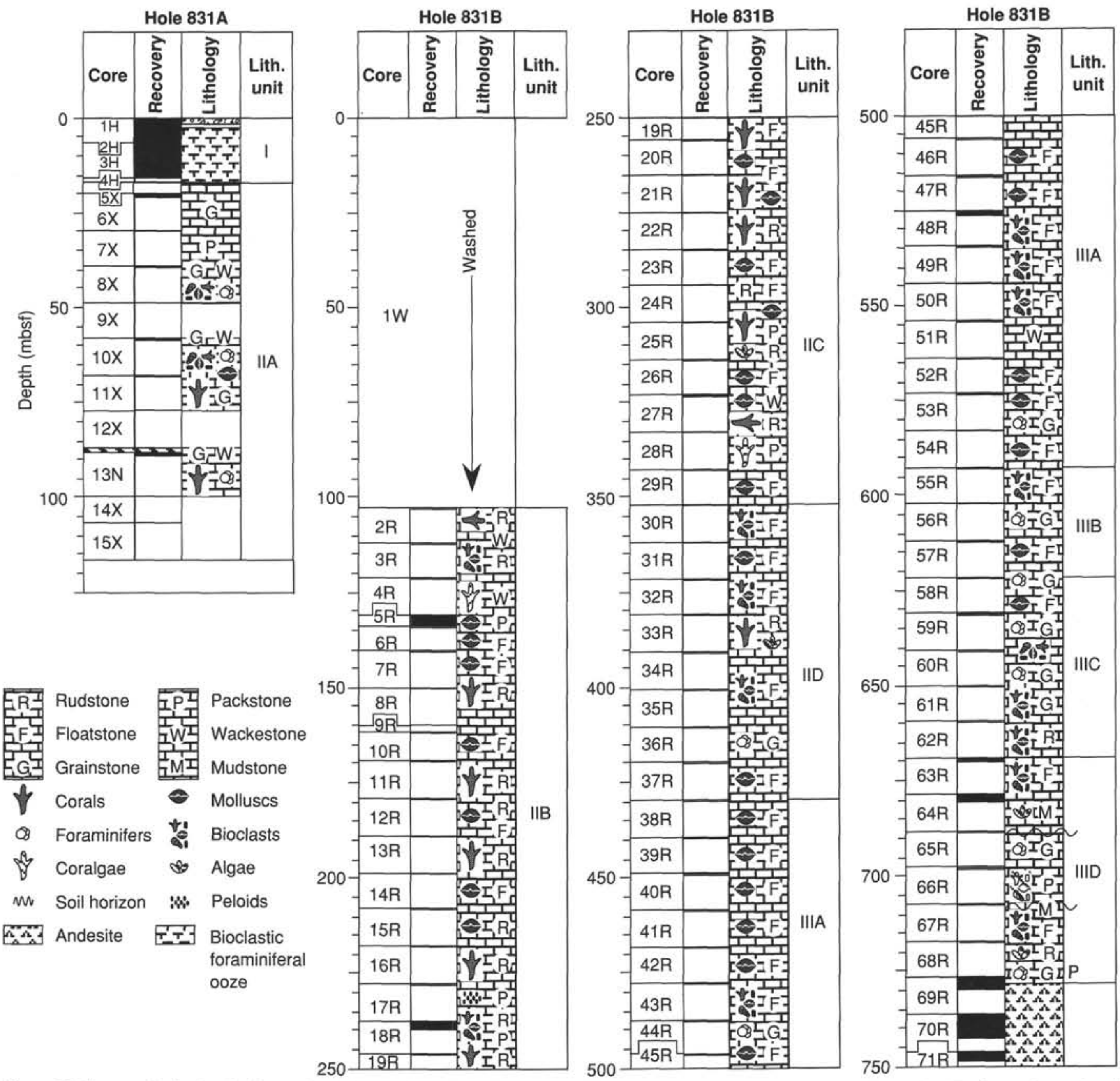

Figure 8. Diagram depicting the four major lithostratigraphic units of Holes 831A and 831B. The carbonate cap of Bougainville Guyot is restricted to Units I, II, and III.

by petrographic analyses, which document the occurrence of acicular crystals about 60 μm in length.

Subunit IIC

Depth: 256.0–352.3 mbsf
Interval: Sections 134-831B-20R-CC, 0 cm, to 134-831B-29R-CC, 10 cm
Thickness: 96.3 m
Age: Indeterminable

Subunit IIC consists of coral rudstone and mollusc floatstone (Fig. 12). Megascopic evidence of extensive carbonate dissolution (e.g., moldic and vuggy porosity) is present for the first time (Fig. 13). Minor amounts of carbonate cement are distributed along the edges of mollusc and coral molds, a cement morphology that is produced in both the marine and freshwater diagenetic environments. XRD analysis of whole-rock powder derived from a thin-section billet from Section 134-831B-25R-CC indicates that aragonite is present as a minor mineralogical constituent.

Large fragments, 3 × 5 cm, of well-preserved *Porites* head coral and very well-preserved tridacnid shells occur sporadically in this subunit. Petrographic analysis indicates that skeletal grains include fragments of corals, molluscs, bryozoans, echinoids, *Halimeda,* and coralline algae, and small benthic foraminifers and rare rotaliids. Vuggy and moldic porosity forms about 10% to 15% of the rock volume.

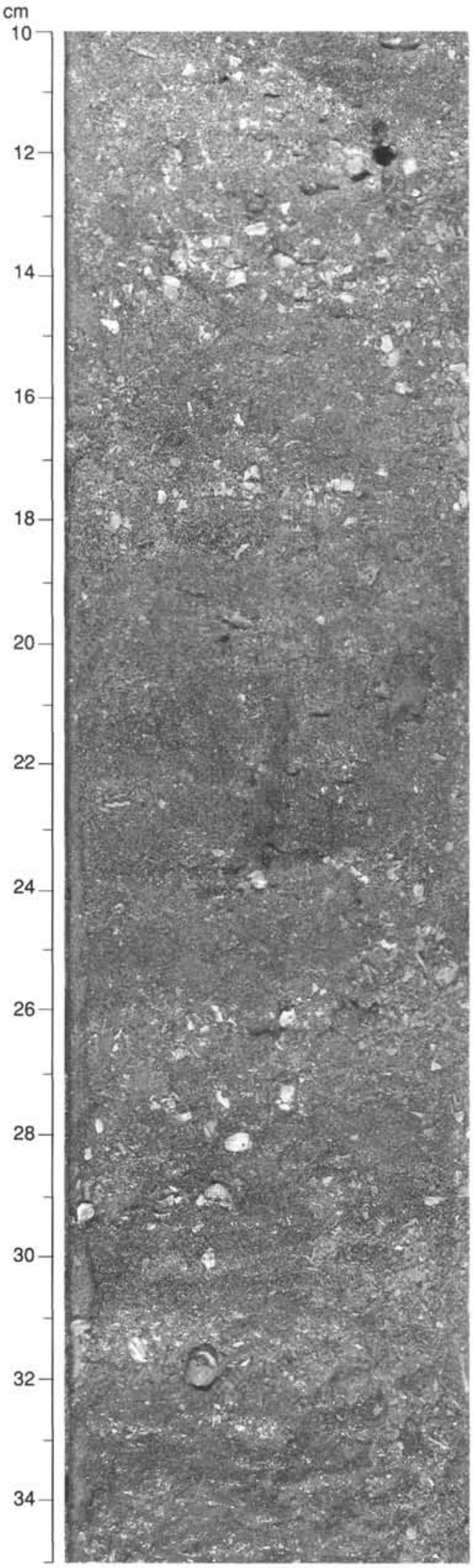

Figure 9. Photograph of interval 134-831A-3H-6, 10–35 cm, showing the bioclastic foraminiferal ooze that is the dominant lithology of Unit I.

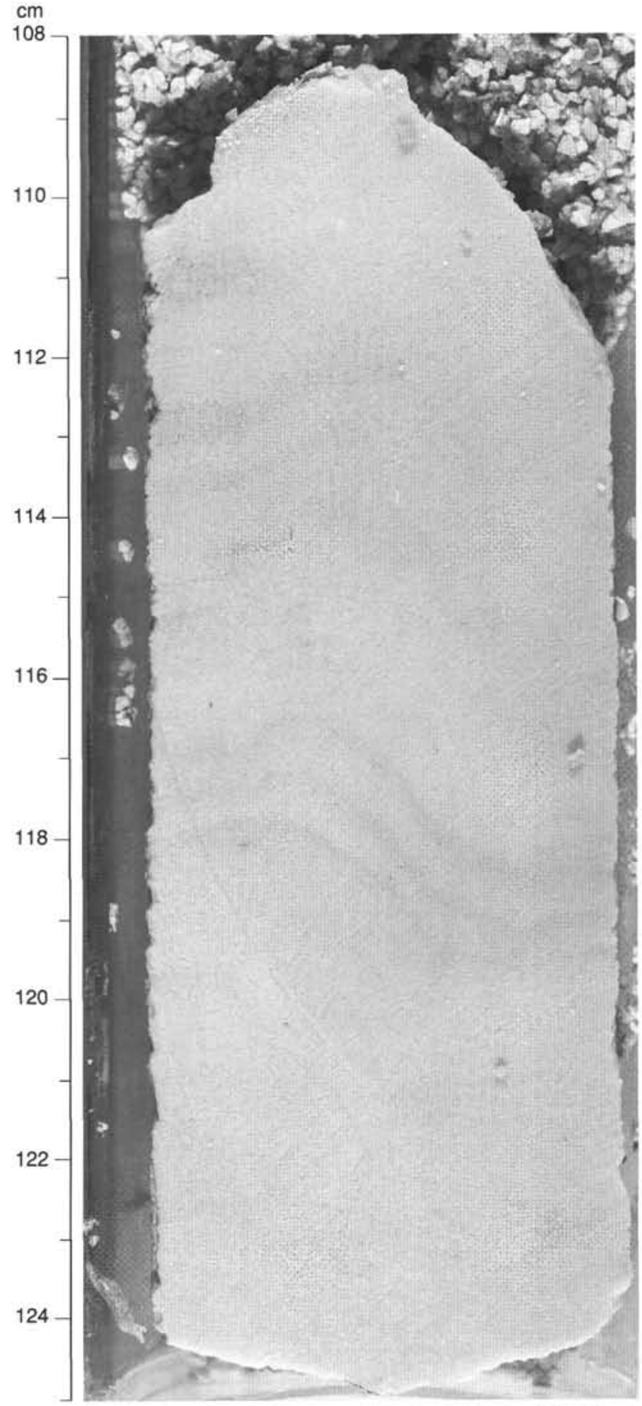

Figure 10. Photograph of interval 134-831B-18R-1, 108–125 cm, showing an exceptionally well-preserved specimen of *Porites* head coral that occurs within Subunit IIB.

Subunit IID

Depth: 352.3–429.6 mbsf
Interval: Sections 134-831B-30R-CC, 0 cm, to 134-831B-37R-CC, 3 cm
Thickness: 77.3 m
Age: Indeterminable

Subunit IID consists of a white (10YR 8/2), well-lithified, bioclastic floatstone with marine cement and abundant secondary carbonate cement. XRD analysis of whole-rock pow-

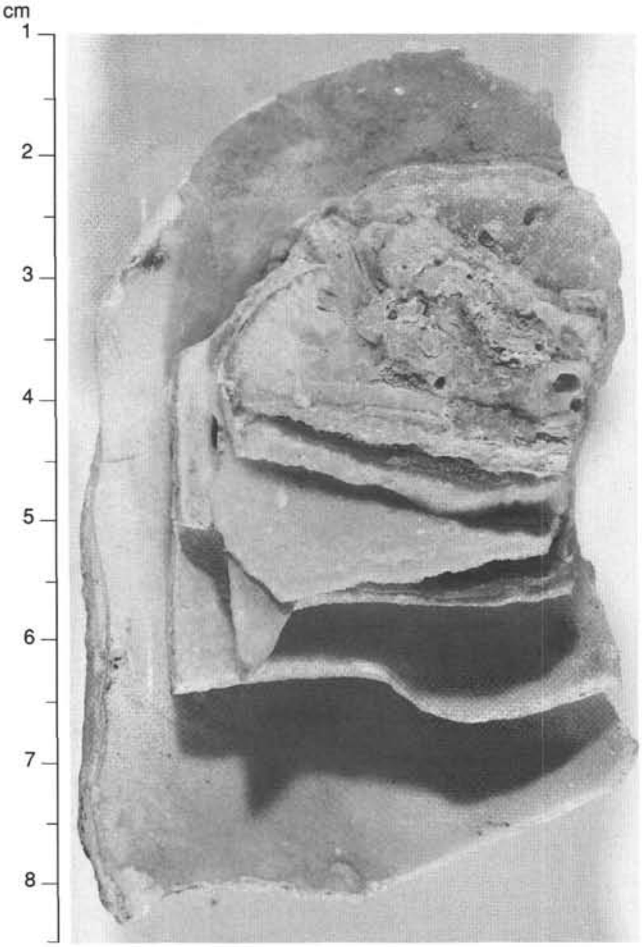

Figure 11. Photograph of interval 134-831B-15R-CC, 1–8.5 cm, showing a large mollusc shell fragment, possibly a conch (*Strombus*?), that was recovered in Subunit IIB.

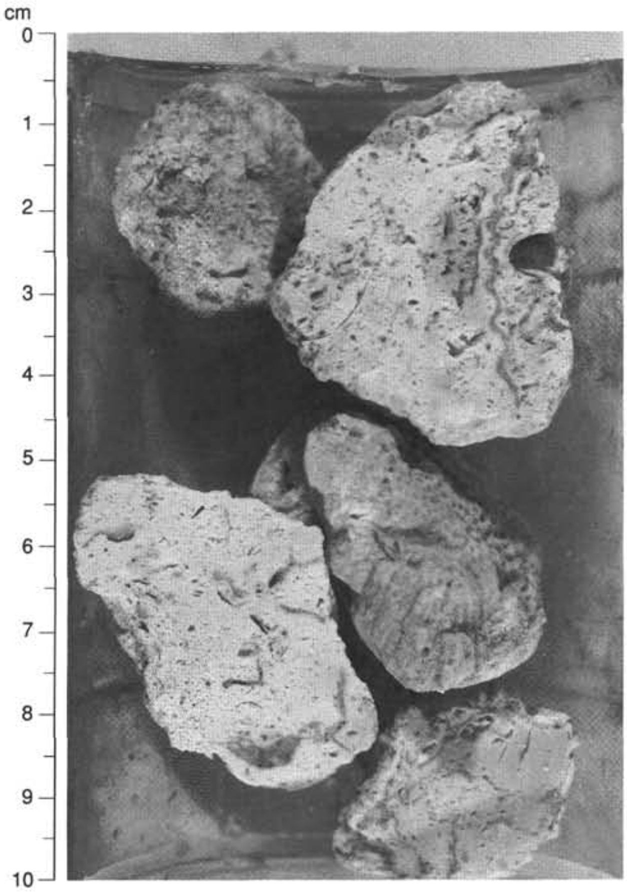

Figure 12. Photograph of interval 134-831B-29R-CC, 0–10 cm, showing one coral rudstone sample (at 4.5–7.5 cm, right hand side of core) and four pieces of mollusc floatstone; the dominant lithology of Subunit IIC.

der derived from a thin-section billet from Section 134-831B-31R-CC indicates that the majority of the sample is calcite but a small percentage of aragonite is also present. In contrast, a sample from Section 134-831B-36R-CC contains only calcite.

Petrographic analyses confirm the abundance of carbonate cement and indicate that intergranular pore space is typically filled with a mosaic of sparry calcite cement crystals, 20–70 μm in size (Fig. 14). Moreover, calcite cement crystals tend to increase in size with increasing distance away from the pore wall.

Unit III

Depth: 429.6–727.5 mbsf
Interval: Sections 134-831B-38R-CC, 0 cm, to 134-831B-69R-1, 65 cm
Thickness: 297.9 m
Age: Indeterminate from Cores 134-831B-38R to -51R; early Miocene from Cores 134-831B-52R to -57R; late Oligocene from Cores 134-831B-58R to -69R

Unit III consists of neritic carbonates containing an abundance of molluscs (gastropods and pelecypods) and large benthic foraminifers. The transition from Unit II to Unit III coincides with a distinct facies change. Unit II is dominated by a coral- and mollusc-rich facies, whereas Unit III is dominated by a mollusc- and foraminifer-rich facies (Fig. 15). Moreover, the transition from Unit II to Unit III coincides with a sharp increase in the degree of carbonate dissolution and cementation (Fig. 13). Unit III is subdivided into four subunits based on fossil assemblages and qualitative estimates of the degree and type of cementation and dissolution.

Subunit IIIA

Depth: 429.6–592.6 mbsf
Interval: Sections 134-831B-38R-CC, 0 cm, to 134-831B-54R-CC, 7 cm
Thickness: 163 m
Age: Indeterminate from Cores 134-831B-38R to -51R; early Miocene from Cores 134-831B-52R to -54R

Subunit IIIA consists of white (10YR 8/2) bioclastic floatstone that is highly altered, extensively dissolved, and has abundant secondary carbonate cement (Fig. 13). Subunit IIIA contains numerous molds of gastropods, 0.5 to 2 cm long (Fig. 16). Many of the molds are rimmed with coarse-grained calcite cement. This subunit also has other minor to pervasive calcite cements, and some carbonates of this subunit have zones of light brownish gray (10YR 6/2) depositional or diagenetic mottling. XRD analysis of whole-rock powder derived from a thin-section billet from Section 134-831B-53R-CC indicates complete calcitization of the sample.

Petrographic analysis indicates that micritized skeletal grains are common; they include foraminifers (e.g., miliolids, peneropolids, other rotaliids, biserial forms, and a few planktonic forms), pelecypods, gastropods, and coralline algae. In parts of this subunit, intergranular pore spaces, shell molds, and foraminifer chambers are filled with microspar, 10–30 μm in size.

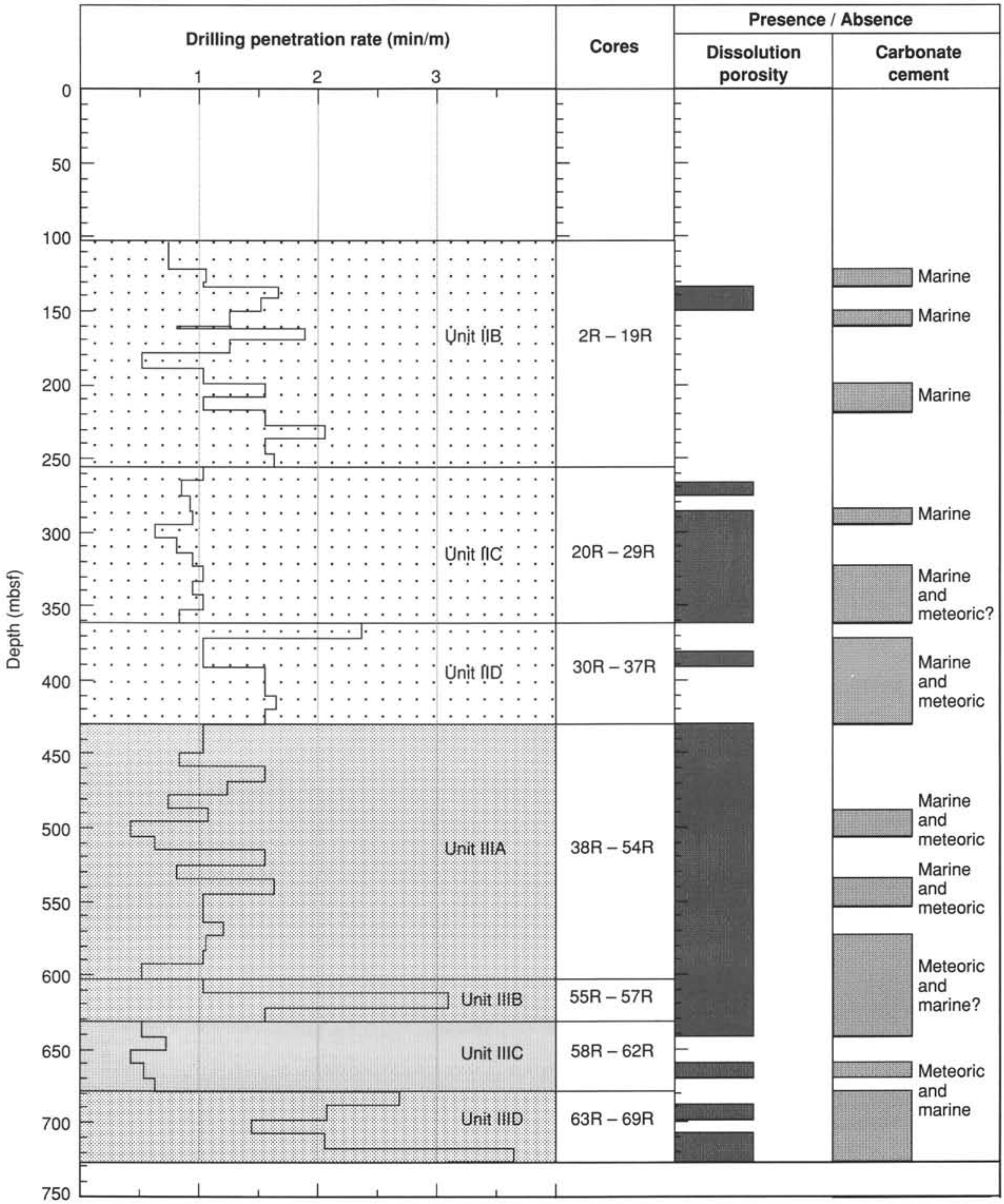

Figure 13. Diagram illustrating the correlation of drilling penetration rate (minutes per meter of core penetrated), lithostratigraphic units, cores, and the presence or absence of carbonate dissolution and cementation.

Subunit IIIB

Depth: 592.6–621.6 mbsf
Interval: Sections 134-831B-55R-CC, 0 cm, to 134-831B-57R-CC, 0 cm
Thickness: 29.0 m
Age: early Miocene

Subunit IIIB consists of white (10YR 8/2), well-cemented bioclastic floatstone and foraminiferal grainstone that has abundant vuggy and moldic porosity (Fig. 13). Some mollusc molds are partially filled with sparry calcite cement. Very pale brown (10YR 7/3) mottled intervals sporadically occur in this unit and may be the result of burrowing. Drilling penetration rate (minutes per meter of core penetrated) is significantly greater than the rates indicated for Subunits IIIA and IIIC (Fig. 13). Petrographic analysis indicates that intergranular spaces of the foraminiferal grainstone are filled with sparry

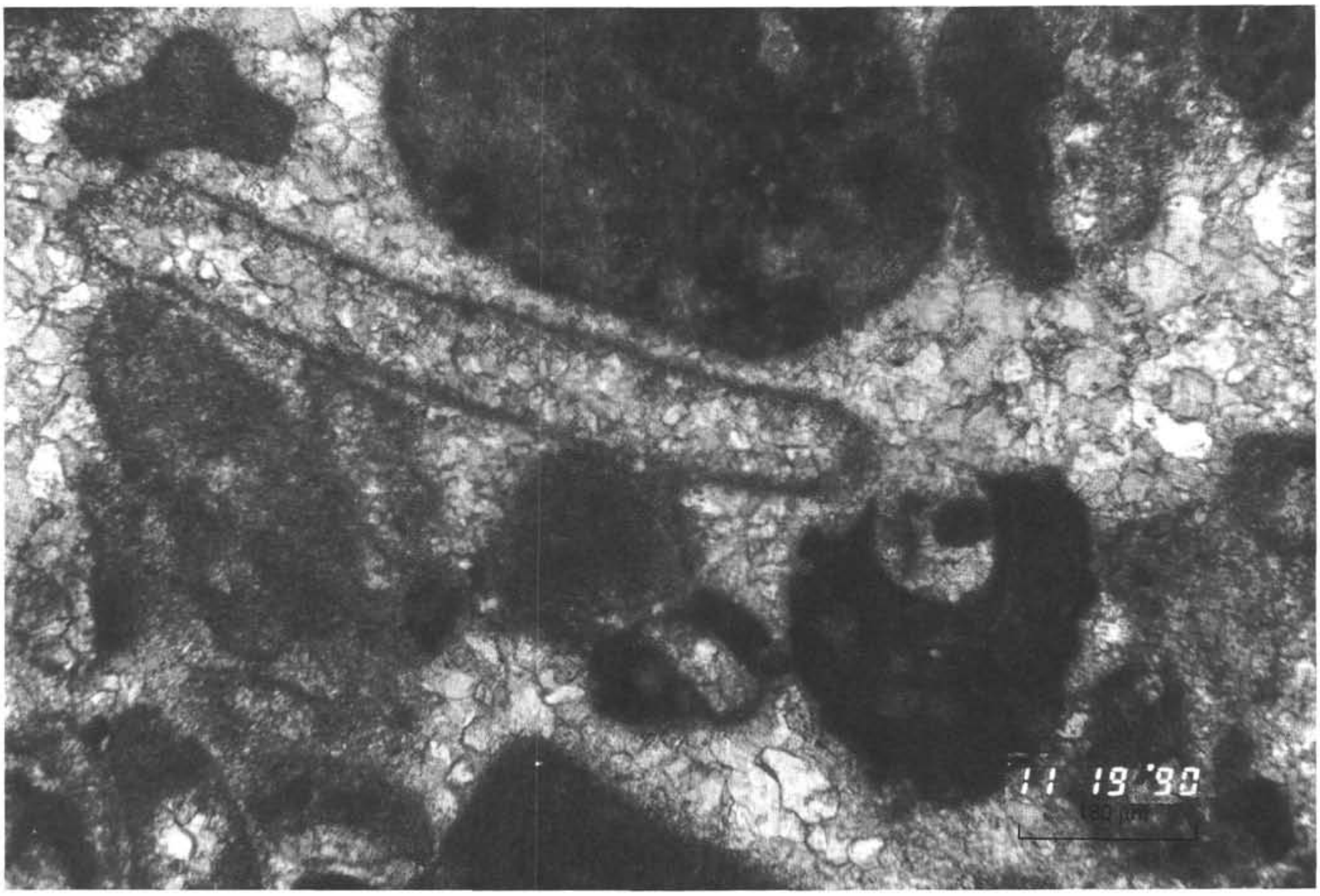

Figure 14. Photomicrograph of interval 134-831B-36R-CC, 7–8 cm, showing a mosaic of inter- and intragranular calcite cement crystals, micritized skeletal grains, red algae, and peloids from a grainstone in Unit IID. Scale bar is 180 μm. Plane light.

mosaic cement and dentate fringing cement, 50–150 μm in size, and peloidal micritic cement.

Subunit IIIC

Depth: 621.6–669.2 mbsf
Interval: Sections 134-831B-58R-CC, 0 cm, to 134-831B-62R-CC, 0 cm
Thickness: 47.6 m
Age: late Oligocene

Subunit IIIC consists of white (10YR 8/2) and very pale brown (10YR 7/1) bioclastic and foraminiferal grainstone which has minor amounts of moldic porosity (Fig. 17). Drilling penetration rate (minutes per meter of core penetrated) abruptly decreases relative to stratigraphically adjacent subunits (Fig. 13).

Petrographic analysis indicates that the foraminiferal grainstone comprises about 70% grains, 20% sparry calcite cement, and 10% moldic porosity. Grains are 400 μm to 2 mm in size. Most of the intergranular pore space is filled with sparry mosaic cement, with a crystal size of 20–100 μm; a few open intergranular pores are lined with dentate crystals, 50–70 μm in size (Fig. 18).

Subunit IIID

Depth: 669.2–727.5 mbsf
Interval: Sections 134-831B-63R-CC, 0 cm, to 134-831B-69R-1, 65 cm
Thickness: 58.3 m
Age: late Oligocene

Subunit IIID consists of white to gray (10YR 8/2 to 10YR 7/2), very well-lithified bioclastic and algal packstone and foraminiferal grainstone (Fig. 19). The dense bioclastic packstone has pale brown (10YR 7/3) mottling and distinct burrows. Petrographic analysis of a sample from this facies indicates that intergranular space is filled with sparry mosaic cement (50–150 μm) and micrite.

The algal packstone is light gray (10YR 7/2) and laminated. Most of the primary porosity has been occluded by marine cement. In some instances this facies has abundant veins of chlorite. Petrographic analysis of a sample from this facies indicates that it contains about 40% coralline algae, including both encrusting and branching forms. Foraminifers (mainly rotaliids), echinoids, molluscs, and micritic grains are also present; some grains are preserved only as micritic rims infilled with microspar cement crystals, 10–20 μm in size. Intergranular space is filled with microspar of similar size and micrite. Moldic and vuggy porosity account for about 15% of the rock.

Petrographic analysis shows that the light brown (7.5YR 6/4) foraminiferal grainstone consists of well-sorted grains 0.5–1 mm in size. The grains are mainly miliolid and rotaliid foraminifers and fragments of coralline algae, with minor mollusc and echinoid fragments. Many of the foraminifers are micritized, and molluscs are preserved only as micritic rims infilled with spar. Intergranular spaces are filled with sparry mosaic cement, with crystal size ranging from 10–50 μm. XRD analysis of a sample from this facies (Section 134-831B-63R-CC) indicates that the sample has been completely calcitized.

Two soil horizons occur within this unit. The first soil horizon occurs at 688.1 mbsf and is a reddish brown (2.5YR 5/4) silty clay (sensu stricto Terra Rosa; Fig. 20). The second soil horizon occurs at 707.6 mbsf and is a very pale brown

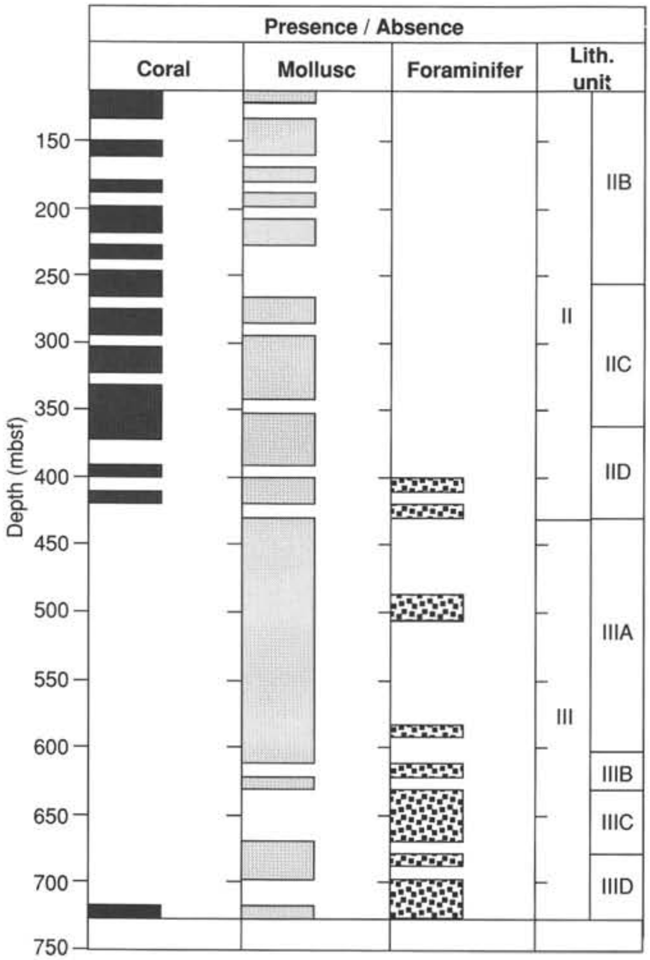

Figure 15. Sedimentary facies distribution of Hole 831B as indicated by the presence or absence of coral-rich, mollusc-rich, or foraminifer-rich facies.

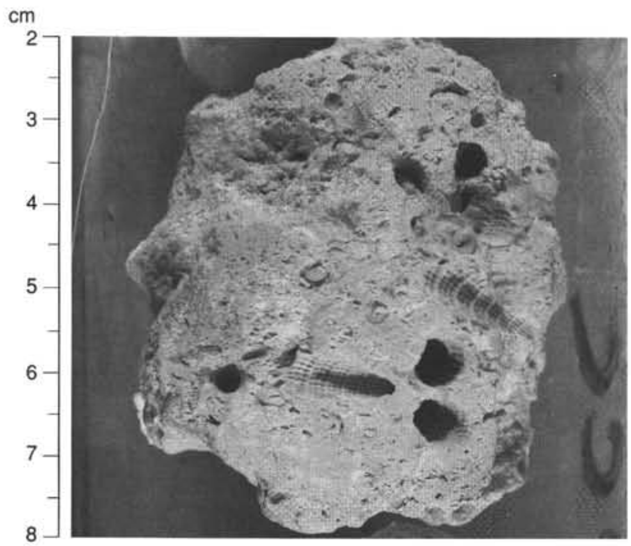

Figure 16. Photograph of interval 134-831B-51R-CC, 2–8 cm, showing the moldic porosity after gastropod shells that is characteristic of the mollusc floatstone of Subunit IIIA.

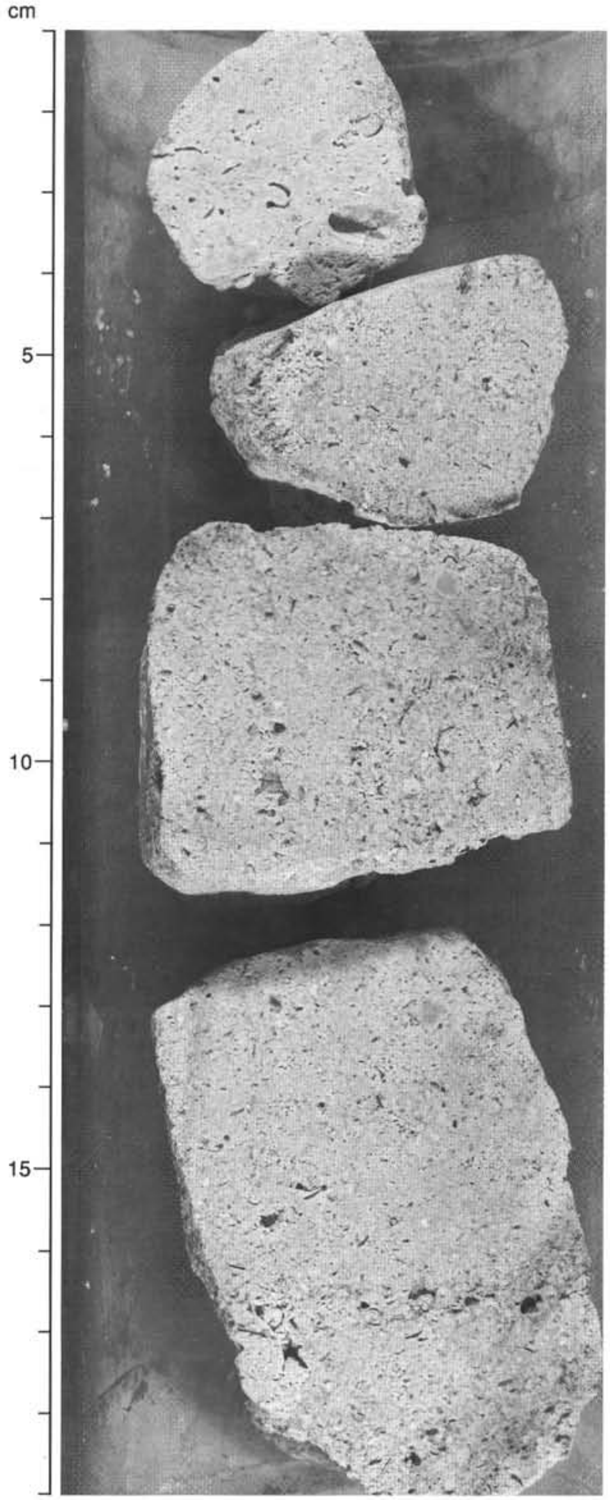

Figure 17. Photograph of bioclastic grainstone from interval 134-831B-58R-CC, 1–19 cm, showing the bioclastic and foraminiferal grainstone that is the dominant lithology of Subunit IIIC.

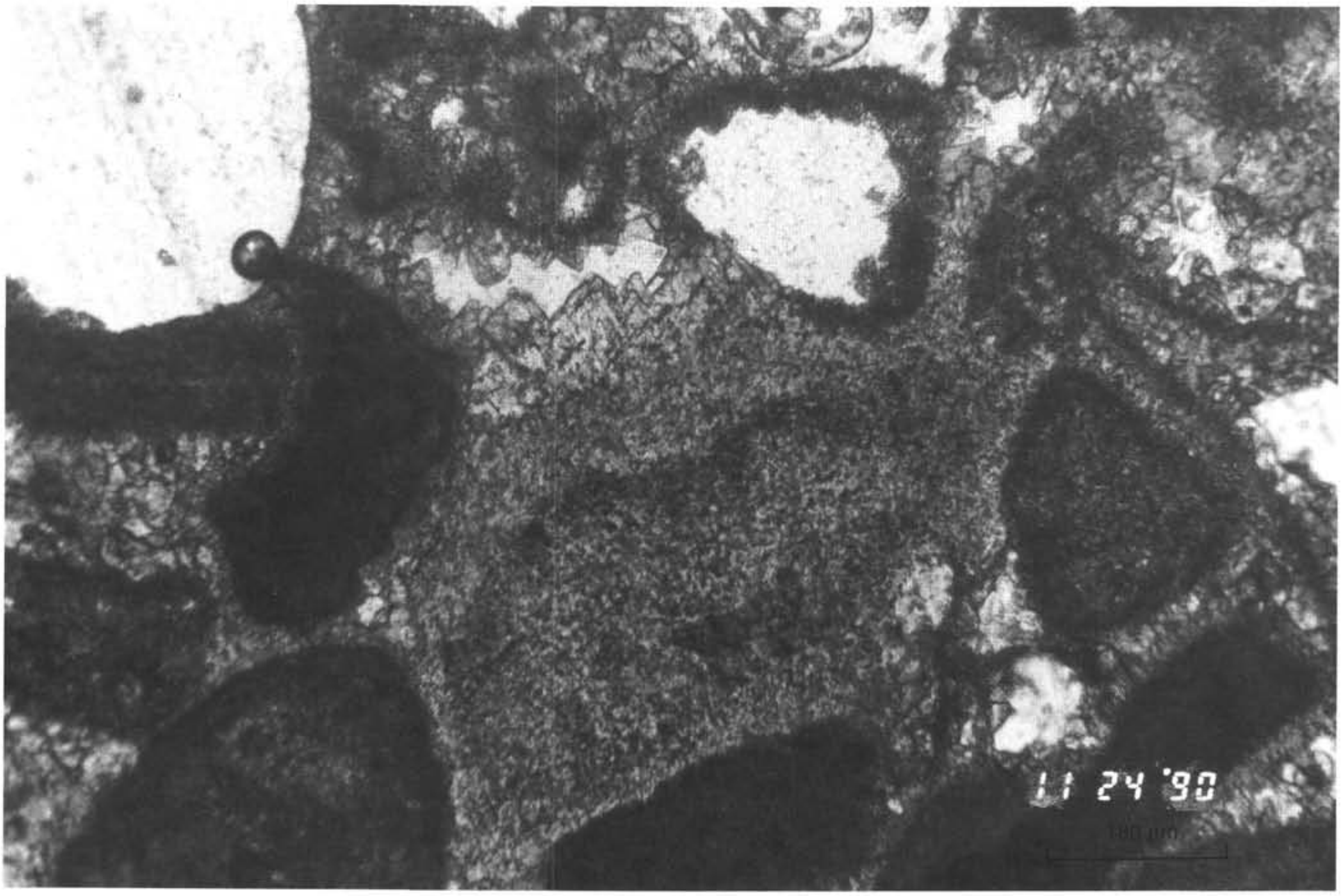

Figure 18. Photomicrograph of interval 134-831B-61R-CC, 8–10 cm, showing an echinoderm grain with syntaxial overgrowth of calcite cement, open pore space, micritized skeletal grains, and drusy mosaic of calcite cement crystals. Scale bar is 180 μm. Plane light.

(10YR 8/3 to 7/4) foraminiferal wackestone with clay with streaks of red (10R 5/6) and light yellowish brown (10YR 6/4).

The contact between the carbonate cap of the guyot and its andesite basement occurs at 727.5 mbsf in Section 134-831B-69R-1 (Fig. 21). The contact consists of 65 cm of very dense, well-cemented fragments of carbonate rock, 2 to 10 cm long, overlying a weathered andesite basement (see "Igneous Petrology" and "Igneous Geochemistry" sections, this chapter). We are fairly confident that the carbonate to andesite transition is stratigraphically in place, or very nearly so, despite the fact that we did not recover this transition as a continuous piece of core.

Unit IV

Depth: 727.5–852.0 mbsf
Interval: Sections 134-831B-69R-1, 65 cm, to 134-831B-84R-4, 142 cm
Thickness: 124.5 m
Age: Indeterminate

Lithostratigraphic Unit IV consists of andesite breccias. A discussion of this unit can be found in the "Igneous Geochemistry" section (this chapter).

Conclusions

Conclusions regarding the geology of the 727.5 m of carbonate overlying andesite basement at the Bougainville Guyot are limited by poor core recovery. Nonetheless, from the carbonates that were recovered several fundamental conclusions can be made:

1. The Bougainville Guyot has a thin veneer (16.9 m) of pelagic carbonate overlying a thick sequence (710.6 m) of neritic carbonates.
2. The 710.6 m of neritic carbonates are best subdivided into two primary sedimentary facies: (1) an overlying coral- and mollusc-rich facies (Unit II; 16.9–429.6 mbsf), and (2) an underlying mollusc- and foraminifer-rich facies (Unit III; 429.6–727.5 mbsf). These facies are consistent with deposition in the lagoon of an atoll.
3. The neritic carbonate cap is best divided into three diagenetic rock types based on a qualitative assessment of the degree and type of cementation and dissolution. The first includes Subunits IIA and IIB and is characterized by the presence of marine-water carbonate cements and minor dissolution. The second diagenetic rock type 2 includes Subunits IIC and IID and is characterized by the presence of marine-water and possibly freshwater carbonate cements and moderate dissolution. The third includes all of Unit III and is characterized by pervasive alteration of original mineralogy to calcite, major dissolution of skeletal allochems, and abundant freshwater carbonate cements.

BIOSTRATIGRAPHY

A summary of the preliminary biostratigraphic results of Site 831, from which we recovered predominantly shallow-water carbonate deposits, is presented in Figure 22. The application of nannofossil and planktonic foraminiferal biostratigraphy to the sedimentary succession in this hole is limited by the nature of the deposits and poor core recovery.

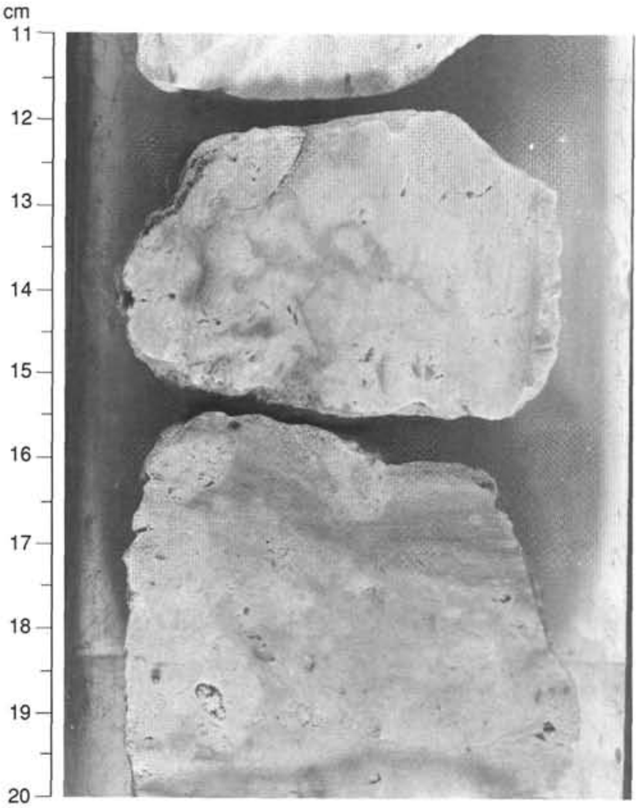

Figure 19. Photograph of interval 134-831B-63R-CC, 11–20 cm, showing the dense, well-cemented texture and pale brown mottling of bioclastic packstone from Subunit IIID.

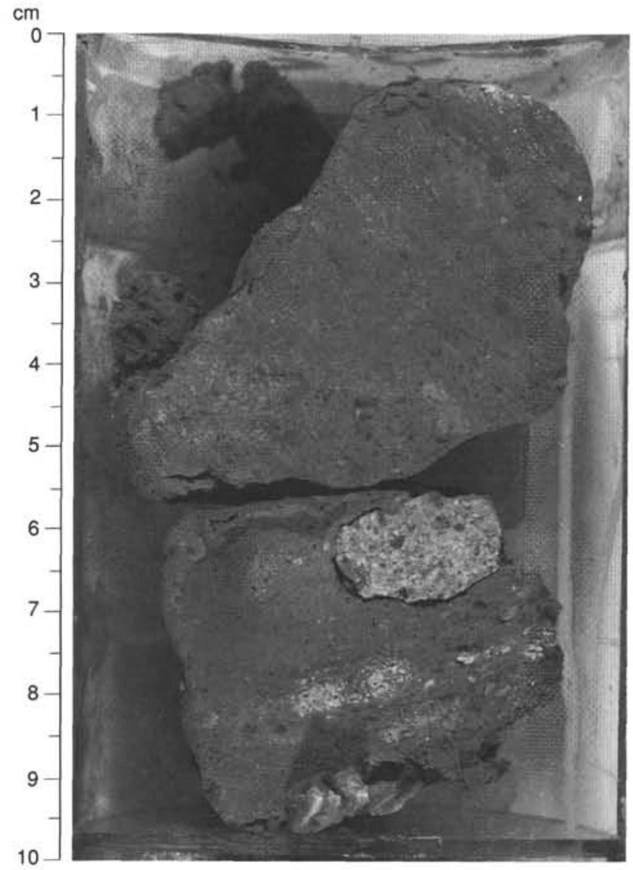

Figure 20. Photograph of interval 134-831B-65R-CC, 0–10 cm, showing the oxidized soil horizon (sensu stricto Terra Rosa) that is present near the base of Subunit IIID.

These groups of microfossils could be used for stratigraphic interpretation of deposits in only the upper 20.0 mbsf of Hole 831A.

The larger foraminiferal assemblage was utilized to subdivide the carbonate deposits, particularly the succession from 16.9 mbsf (Hole 831A) to 246.4 mbsf (Hole 831B), and from 563.6 to 727.5 mbsf in Hole 831B. Larger foraminifers were analyzed in hand specimens and occasional thin sections. Some larger foraminiferal specimens were highly micritized and this hindered, to some extent, the identification of species. This type of alteration is quite evident in the carbonate section below 621.6 mbsf (Sample 134-831B-58R-CC). The contact of the carbonate sequence with the basement was recorded at 727.5 mbsf, and the drilling of Site 831 terminated within the basement rocks at 852.0 mbsf.

Smaller benthic foraminifers varying in abundance and preservation are observed at Site 831. Relatively abundant and well-preserved forms occur from the seafloor to 6.4 mbsf in Hole 831A, and a few moderately preserved specimens are recorded in Sample 134-831A-3H-CC. Rare, poorly preserved specimens predominate in the interval between 20.0 mbsf (Sample 134-831A-5X-CC) and 246.4 mbsf (Sample 134-831B-18R-CC). Below 246.4 mbsf at Site 831, the succession consists of indurated carbonate sediments that contain mainly shallow-water forms. The paleodepths for the interval between 20.0 mbsf and 727.5 mbsf are inferred generally from the lithofacies and biofacies.

Nannofossils

Nannofossils were recovered in only three samples from this site. Samples 134-831A-1H-CC and 134-831A-3H-CC contained a middle Pleistocene flora typified by the presence of *Gephyrocapsa oceanica, Rhabdosphaera claviger, Gephyrocapsa caribbeanica, Calcidiscus leptoporus,* and small gephyrocapsids. Sample 134-831A-2H-CC contained only *G. caribbeanica* and *C. leptoporus* in an otherwise rare nannofossil assemblage. All of these samples are tentatively placed in nannofossil Zone CN14. All subsequent samples were either barren or lacked age-diagnostic specimens.

Radiolarians

Rare radiolarians, moderately preserved, were found only in two samples from Core 134-831A-1H.

Planktonic Foraminifers

Core-catcher samples recovered from the upper 20.0 mbsf of Hole 831A (Samples 134-831A-1H-CC to -5X-CC) are Pleistocene or Holocene (Zone N22) in age, based on the occurrence of *Globorotalia truncatulinoides*. Some prominent species in this interval include *Globorotalia menardii, G. tumida, G. crassaformis, Neogloboquadrina dutertrei, Globigerinoides conglobatus, G. sacculifer, Globigerinoides ruber, Candeina nitida, Globigerinella aequilateralis,* and *Orbulina universa*. Planktonic foraminifers are very rare in sediment samples below 20.0 mbsf (Sample 134-831A-5X-CC) in Hole 831A.

Benthic Foraminifers

Larger Benthic Foraminifers

The core-catcher samples between 29.6 mbsf (Sample 134-831A-6X-CC) and 246.4 mbsf (Sample 134-831B-18R-CC)

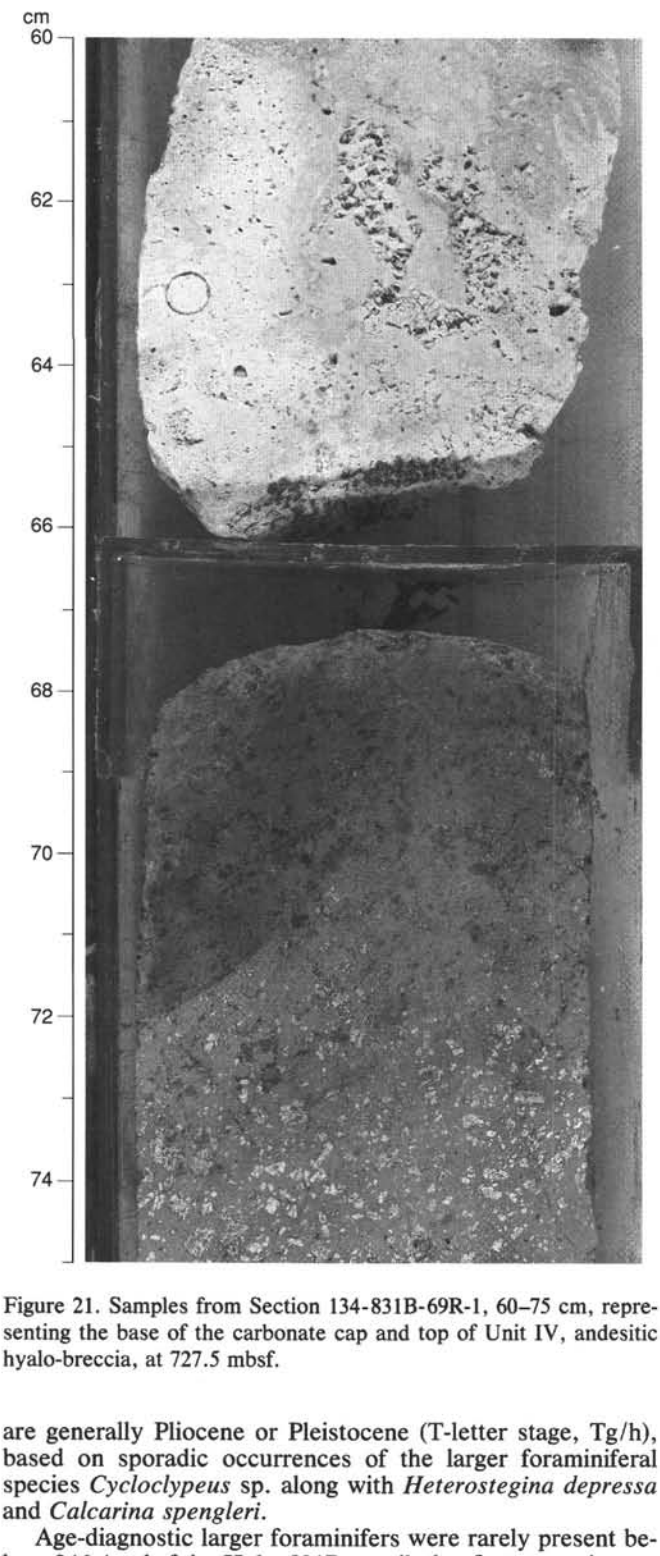

Figure 21. Samples from Section 134-831B-69R-1, 60–75 cm, representing the base of the carbonate cap and top of Unit IV, andesitic hyalo-breccia, at 727.5 mbsf.

are generally Pliocene or Pleistocene (T-letter stage, Tg/h), based on sporadic occurrences of the larger foraminiferal species *Cycloclypeus* sp. along with *Heterostegina depressa* and *Calcarina spengleri*.

Age-diagnostic larger foraminifers were rarely present below 246.4 mbsf in Hole 831B, until the first conspicuous assemblage was encountered at 563.6 mbsf (Sample 134-831B-52R-CC). The interval between 563.6 and 621.6 mbsf (Sample 134-831B-57R-CC) is lower Miocene (T-letter stage, Te5), based on the occurrence of *Austrotrillina howchini* (Fig. 23). A late Oligocene (T-letter stage, upper Te1–4) age is suggested for the interval between 621.6 mbsf (Sample 134-831B-58R-CC) and 727.5 mbsf (Sample 134-831B-69R-1, 66 cm) by the presence of *Spiroclypeus margaritatus* (Fig. 24). *Austrotrillina striata*, *Borelis* sp. (Figs. 25 and 26), *Austrotrillina howchini*, and *Sorites* sp. occur throughout this entire upper Oligocene to lower Miocene sequence.

Smaller Benthic Foraminifers

Deposition in the middle bathyal zone (500–2000 mbsl) is suggested for the uppermost part (from 0 to 6.4 mbsf) of Hole 831A on the basis of rare specimens of the deep-water species *Pyrgo murrhina*. This species occurs in intermediate waters or the middle bathyal zone (van Morkhoven et al., 1986). The presence of *Hoeglundina elegans* in Sample 134-831A-3H-CC indicates outer sublittoral zone (80–150 mbsl) deposition for the interval between 6.4 and 15.9 mbsf of Hole 831A. Inner sublittoral zone (0–30 mbsl) species that occur throughout the entire section from the top to 246.4 mbsf at Site 831 include *Amphistegina radiata*, *A. madagascariensis*, and *Calcarina spengleri*.

The carbonate succession below 246.4 mbsf at Site 831 is deposited under inner or outer sublittoral conditions, based on the occurrence of smaller and larger benthic foraminiferal assemblages in thin sections. Corals and larger foraminifers, generally restricted to the photic zone (0–150 mbsl) because of their symbionts (cf. Boersma, 1978), are common at various intervals throughout the sequence. The thin section from Sample 134-831B-56R-CC contains a foraminiferal assemblage (Fig. 27) apparently similar to that interpreted by Sartorio and Venturini (1988) as being deposited on an inner shallow platform.

Samples from Cores 134-831A-1H to -5X provide a rich foraminiferal fauna that consists of planktonic foraminifers (60% to 90%), and smaller and larger benthic foraminifers (10% to 40%). The relative proportion of foraminifers with respect to the entire suite of bioclasts varies from 40% to 90%. Other elements present as bioclasts include pteropods (up to 15% in Sample 134-831A-3H-CC), coral and bivalve fragments (up to 85% in the fraction >700 μm in Sample 134-831A-1H-CC), and *Gorgonia* spicules (up to 2% in all the samples). The planktonic foraminiferal assemblage shows a marked decrease in the proportion of keeled vs. unkeeled forms from Sample 134-831A-3H-CC to Sample 134-831A-5X-CC. Among the keeled species are *Globorotalia truncatulinoides*, *G. tumida*, and *G. menardii*. These species at present live below 100 mbsl in the water column (adult stages, cf. Bé, 1977). The implication of this change in the foraminiferal assemblage is that the lagoon of the guyot was shallower at the time of deposition of sediments below Sample 134-831A-3H-CC, and became deeper later.

Benthic foraminifers from Samples 134-831A-1H-CC through 134-831A-5H-CC include a high proportion of shallow-water forms such as smaller miliolids, *Amphistegina* sp. and *Heterostegina* sp., forms that at present live in association with coral reef communities whose water depth is restricted to the photic zone. Other smaller benthic foraminifers occurring in these samples are *Lenticulina* sp., *Spirillina* sp., *Globocassidulina* sp., *Cibicides* sp., *Hoeglundina elegans*, *Pyrgo murrhina*, *Uvigerina hispida*, and *Sphaeroidina bulloides*. The last three species occur in very low proportions and are indicative of paleodepths deeper than the upper middle bathyal zone (~600 mbsl).

The above evidences indicate that:

1. The shallow-water carbonate platform (coral reef, represented by Core 134-831A-6X) was drowned, and then outer sublittoral sediments (represented by Core 134-831A-5X) accumulated with very few keeled planktonic foraminifers, indicating paleodepths no deeper than 100 mbsl.
2. Subsequently, major subsidence and pelagic sedimentation occurred in the interval from Core 134-831A-5X to

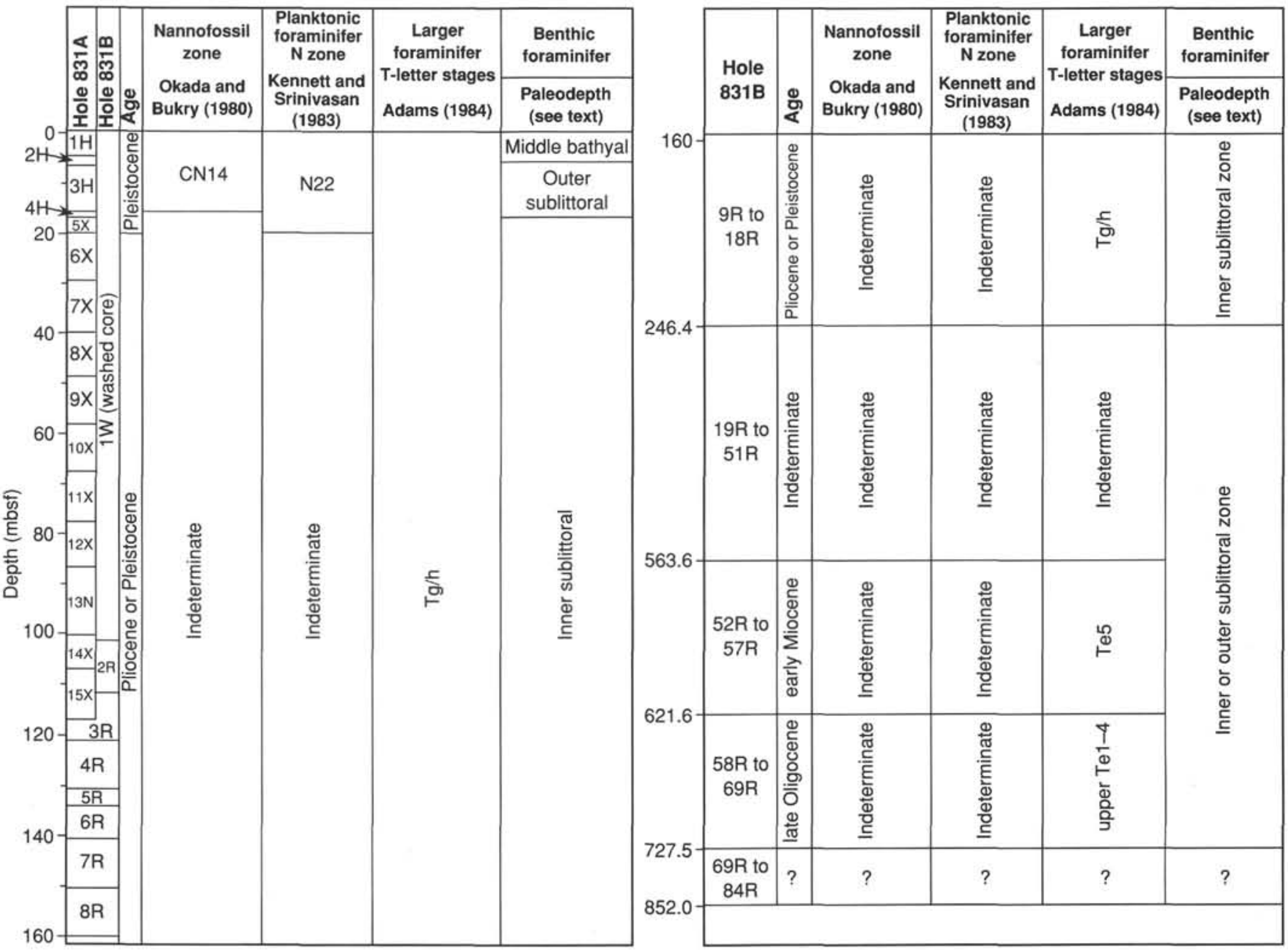

Figure 22. Biostratigraphic summary of Site 831.

-3H, with an increasing percentage of planktonic foraminifers (many of them keeled), pteropods, and smaller benthic deep-water forms. Progressive subsidence seems reasonable as the apparent proportion of these pelagic components increases toward Core 134-831A-1H, indicating paleodepths that range from outer sublittoral to middle bathyal. The occurrence of shallow-water elements in all of these samples suggests reworking from the reef forming the former atoll.

Summary

The core-catcher samples recovered from the upper 20.0 mbsf of Hole 831A are Pleistocene, and within the interval between 29.6 mbsf in Hole 831A and 246.4 mbsf in Hole 831B are generally Pliocene or Pleistocene in age. Continuing downhole, the age of samples between 246.4 and 563.6 mbsf are indeterminate. An age of early Miocene (approximately 21.8–23.6 Ma) is suggested for the carbonate succession between 563.6 and 621.6 mbsf. The sequence from 621.6 to 727.5 mbsf of Site 831 is late Oligocene (approximately 23.6–28.2 Ma) in age.

The Pleistocene sediments from 0 to 6.4 mbsf and from 6.4 to 15.9 mbsf were deposited in the middle bathyal zone and outer sublittoral zone, respectively. Sediments between 16.9 and 246.4 mbsf were deposited under inner sublittoral conditions, whereas the sediments below 246.4 mbsf were deposited under inner or outer sublittoral conditions. The coral reef platform evidently grew on a guyot submerged to bathyal depths during middle Pleistocene time (nannofossil Zone CN14).

IGNEOUS PETROLOGY

Two conspicuous beds of volcanic ash (4 cm and 22 cm thick) are interbedded with foraminiferal and pteropod oozes in the upper part (lithostratigraphic Unit I) of Hole 831A (see "Lithostratigraphy" section, this chapter). The thicker layer occurs at 14.4 mbsf and is a silt-sized deposit incorporating a few bioclasts (<5%) of foraminifers and sponge spicules. The main component is a pale brown glass (53%), which is often clear but sometimes dusted with very fine opaque mineral grains. The glass shards (<0.1 mm) tend to have a cuspate form, which is attributed to fracturing across vesicles, or they occur in fasciculate clusters. Opaque mineral grains make up about 25% of the total, which is a surprisingly high figure that may have been enhanced as a consequence of some reworking, winnowing, or fractionation during subaerial or submarine settling. There is also the possibility that some of the grains classified as opaque under smear-slide observation may be material such as small scoriaceous fragments from the matrix of volcanic rocks, rather than actual opaque minerals. The other mineral constituents are plagioclase (6%, 0.02–0.1 mm in diameter) and clinopyroxene (1%, <0.1 mm in diameter); chlorite, celadonite, and iron oxide minerals make up the remainder.

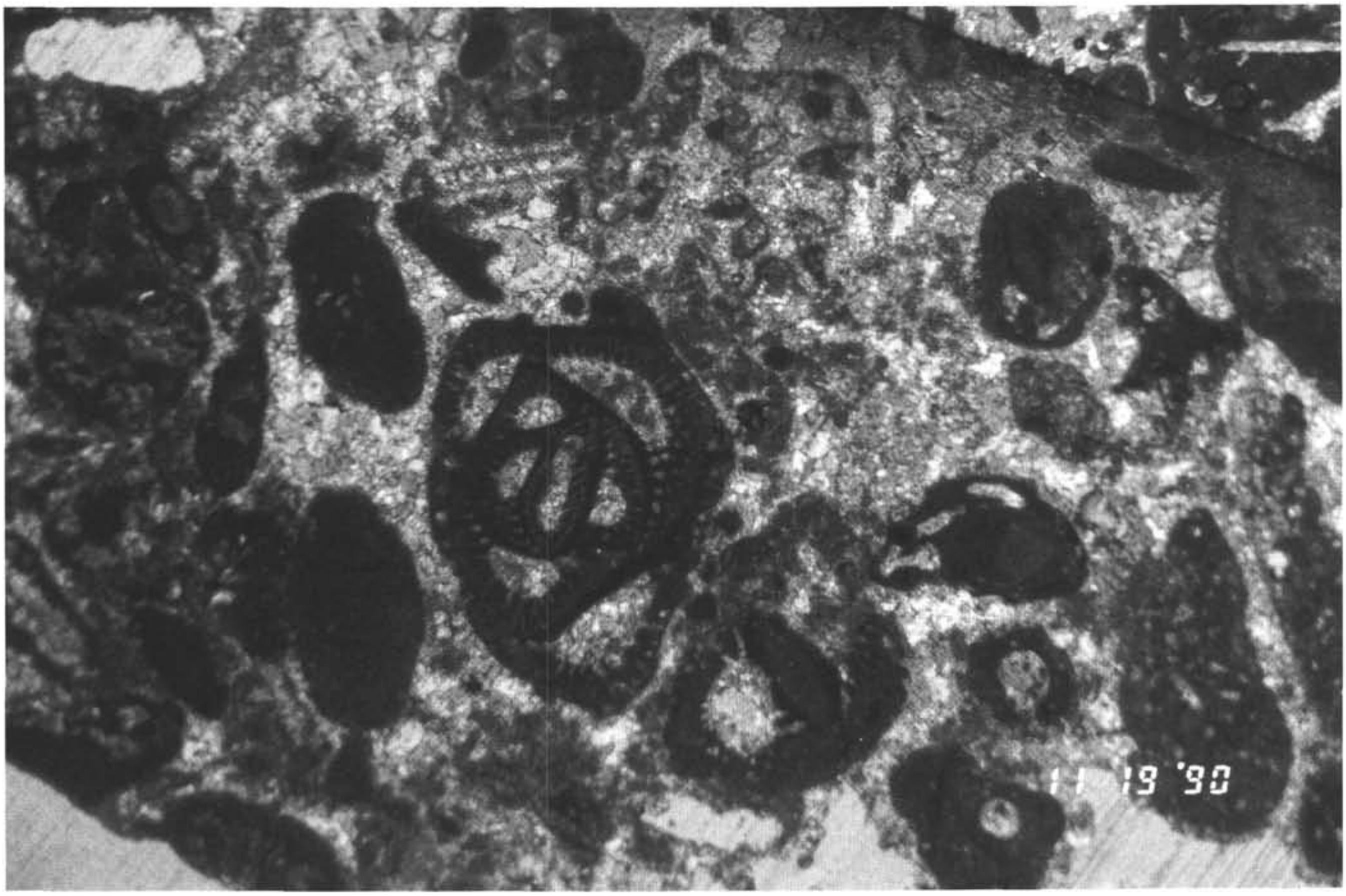

Figure 23. Photomicrograph of *Austrotrillina howchini*. Sample 134-831B-69R-CC, 24–26 cm, magnification ×50, axial view.

At 727.5 mbsf in Hole 831B the carbonate cap, described earlier in this chapter, rests on a pale orange-brown (7.5YR 6/8) to pale red-brown (10R 6/4) bole, which marks the weathered surface of the volcanic rocks. The latter were penetrated, with an average 56% recovery, through a total thickness of 124.5 m to the bottom of the hole at 852 mbsf. The entire sequence, designated as lithostratigraphic Unit IV, is composed of andesitic hyalo-breccias. Broadly speaking, it consists of two-pyroxene andesite clasts or blebs in a matrix of lithic fragments, crystals, and glass. The relative proportions of these components and also the color of the rock as a whole are subject to considerable variation. The term hyalo-breccia is preferred at this stage as a nonspecific term denoting the presence of glass in significant quantities. Some of this glass has been transformed to palagonite, so that the term palagonite breccia is applicable in many instances. However, it should be noted that the term palagonite is generally used for the alteration of basaltic glass or sideromelane, whereas the glass in these rocks is andesitic. "Hyaloclastite" is another possible descriptive prefix, but it is not entirely appropriate since the breccias lack the abundant clear glass clasts and shards implied by this term (e.g., Fisher and Schmincke, 1984). In the breccias of Hole 831B the glass is more continuous in its distribution around the clasts; also, the fragments broken from the margins of the clasts and incorporated within the glass or its alteration products are to some extent microcrystalline and often turbid. The term "clast" is used in this account as the general name for the more coherent lithic pieces found within the breccia matrix, but their form is such that the term "bleb" or even "globule" is more suitable in many instances. Several of the larger fragments referred to as clasts were recovered as isolated pieces, so that their contact relations were not visible. It is possible that these, too, could be parts of larger blebs.

Five subunits have been distinguished within the sequence of andesitic hyalo-breccias. It should be stressed that these do not necessarily mark sharp lithological breaks; in fact, the subunits have many characteristics in common and are to a large extent gradational in their nature. They fall into two groups (Subunits IVA, IVC, and IVE on the one hand and Subunits IVB and IVD on the other), which suggests a cyclicity of eruptive or depositional conditions. The essential features of the five subunits are as follows:

Subunit IVA (727–741 mbsf)

The strongly oxidized horizons at the contact with the carbonate cap (Fig. 21) pass down into light brown (2.5YR 6/6) and brownish gray (2.5YR 5/2) breccias and then into similar coarse clastic rocks in pastel shades of olive gray (5Y 4/3) and yellow-green gray (10Y 7/2). At one or two horizons (e.g., 737.75 mbsf) the primary hyalo-breccia has been reworked as thin beds of grit and sandstone. Clasts of dark gray andesite (10Y 3/1) become larger and progressively more abundant (20%) toward the bottom.

Subunit IVB (741–789 mbsf)

Subrounded to wispy andesitic blebs (gray; 5B 5/1) are enclosed within a pale green (10G 7/2) matrix. Most of these blebs have a conspicuous corona that is described from

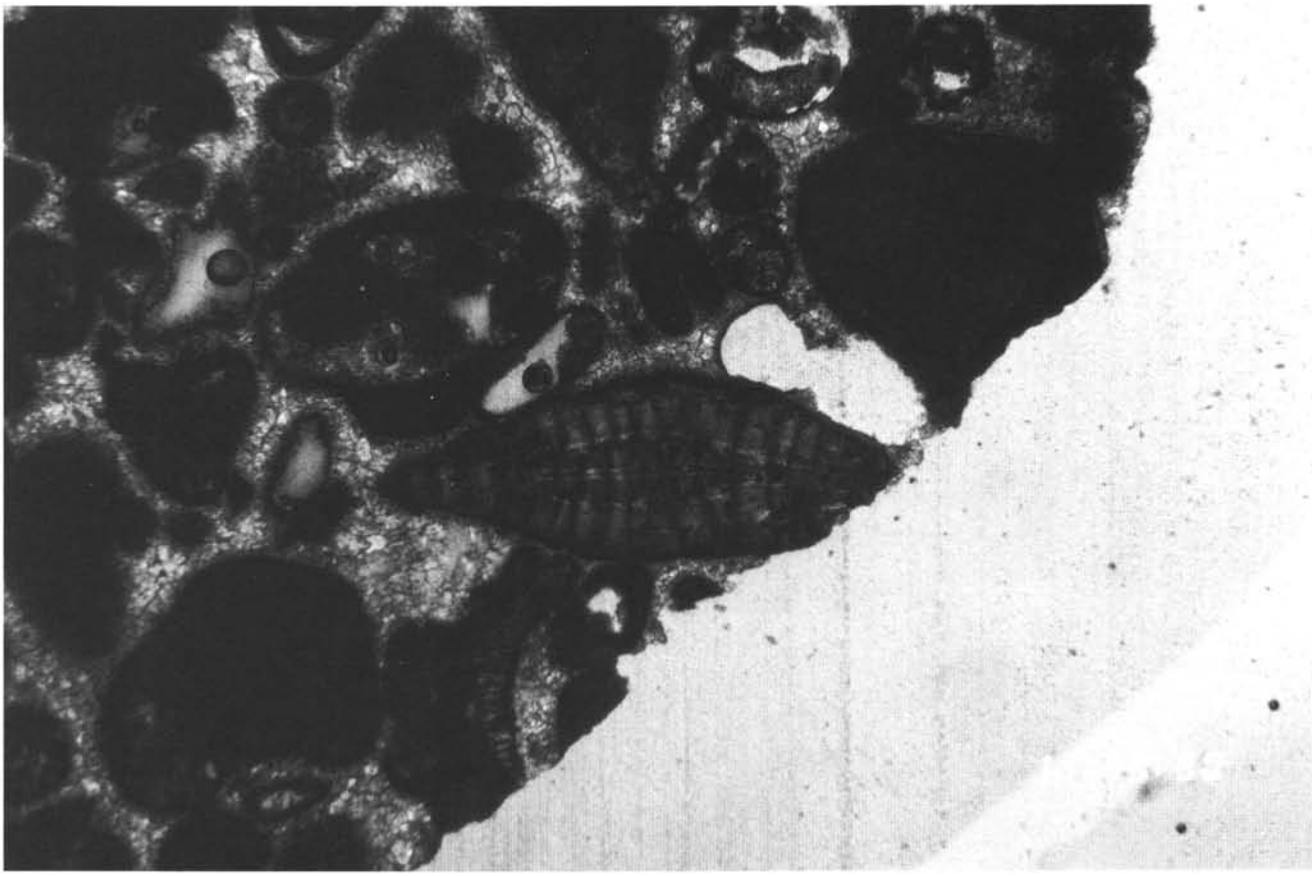

Figure 24. Photomicrograph of *Spiroclypeus margaritatus*. Sample 134-831-58R-CC, 6–8 cm, magnification ×50, axial view.

thin-section examination later. They range between 0.5 and 8 cm in diameter and make up about 50% of the rock.

Subunit IVC (789–822 mbsf)

Coarse breccias including pale reddish brown (10R 5/4) fragments are occasionally interbedded with grits and sandstones. The breccias become progressively less sorted toward the lower part of the subunit, and the incidence of reddish brown clasts increases. They are set in a variegated matrix ranging between weak red (2.5YR 5/2) and gray (2.5Y 5/0). There are also beds of gray, clast-rich breccias (798–802 mbsf) in which coronas or reaction rims are absent or poorly developed. The clasts make up about 25% of the whole rock and range in size from about 1 cm to 15 cm in diameter; they are commonly about 2 cm across. The clasts are sometimes subangular or subrounded but are often rounded or wispy in outline, with indistinct boundaries. Frequently, there is a marginal zone or halo (2–4 mm wide). In some instances the fresh interior of the clast has a thin (<0.5 mm) white (N9) rim that is surrounded by another zone of very light greenish gray (10Y 7/1) discoloration, above a fairly sharp contact with the breccia matrix. The evidence clearly suggests a reaction between the clasts and matrix. The latter consists of smaller andesitic lithics of similar composition, to the larger clasts with crystals of plagioclase and clinopyroxene, together with altered glass.

Subunit IVD (822–838 mbsf)

This consists almost exclusively of well-defined gray (2.5Y 5/0) blebs with distinct coronas or reaction rims in a grayish green (5G 5/2) matrix (Fig. 28). Near the bottom of the subunit (837 mbsf) the blebs or clasts become more diffuse with irregular or wispy outlines: they make up 40%–50% of the total rock. The blebs are fresh andesite of a similar petrographic type to that described previously. Again, there has evidently been a reaction between the blebs and the matrix. Fractures in the matrix tend to be filled with grayish green (5G 5/2) minerals, probably celadonite and zeolites.

Subunit IVE (838–852 mbsf)

Reddish (weak red; 10R 4/3) lava fragments appear and the matrix becomes a paler shade of greenish gray (5G 6/1). The matrix of this subunit is distinguished from that of the one above in that pervasive altered glass is absent. Instead, sand-sized fragments of lava with varying degrees of oxidation are abundant. The color of the fragmented lava varies from weak red (10R 4/3) through light brownish gray (10YR 6/2) to dark gray (2.5YR 4/0). These breccias pass downward into poorly consolidated grits and a cross-bedded sandstone at 851.7 mbsf.

Selected Petrographic Descriptions

Andesitic Clasts

Typical of the more crystalline andesitic clasts is Sample 134-831B-76R-5, 109–110 cm, from Subunit IVC. It is a porphyritic andesite with phenocrysts of plagioclase (30%, 0.2–6 mm in diameter), which vary from euhedral to subhedral in form and have very sharply defined oscillatory zoning. Next in abundance are clinopyroxene phenocrysts (6%, 0.05–2 mm in diameter) with subhedral morphology. Orthopyroxenes tend to be more euhedral but are a little less abundant

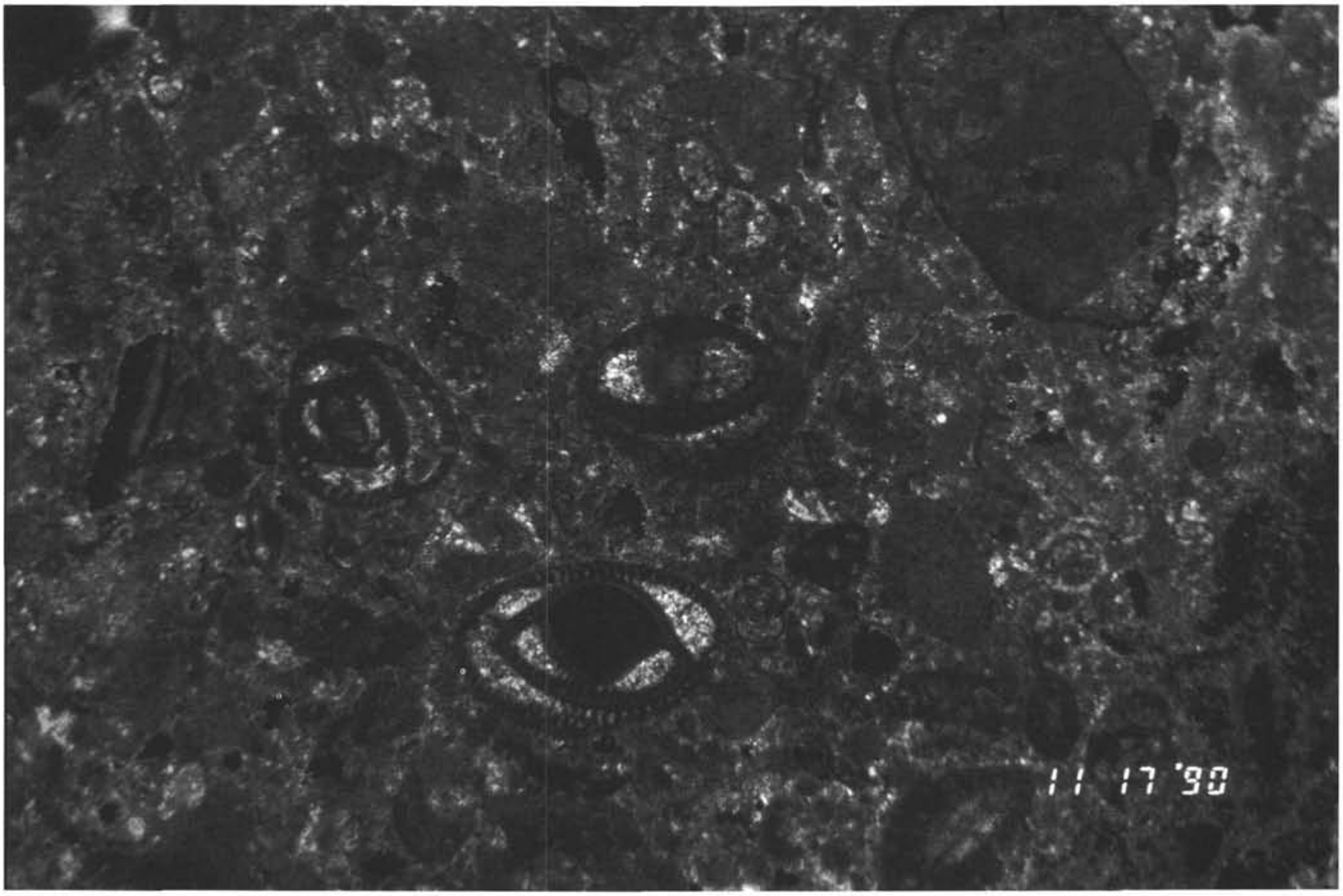

Figure 25. Photomicrograph of *Austrotrillina striata*. Sample 134-831B-56R-CC, 14–16 cm, magnification ×50, axial view.

(4%, 0.1–1.5 mm in diameter). Opaque mineral phenocrysts are subhedral and rather sparse (1%, 0.1–1 mm in diameter). The groundmass is a fine-grained assemblage of plagioclase laths (25%), anhedral pyroxenes (20%), and opaque mineral grains (14%). Some samples show moderately well-developed flow structure, defined by the plagioclase laths. With some variations, clasts of this type are common, especially in Subunits IVA, IVC, and IVE. Plagioclase invariably makes up between 25% and 30% of the total volume of the rock. There is a little variation in the relative abundances of clinopyroxene and orthopyroxene phenocrysts but the former is usually dominant and orthopyroxene is occasionally absent (e.g., Sample 134-831B-70R-1, 123–125 cm). Pale brown to dark brown scoriaceous glass may make up as much as 20% of some rocks (e.g., Sample 134-831B-70R-3, 34–36 cm) but it is often devitrified, or altered to chlorite and clay minerals, as in the highly oxidized lava fragment (Sample 134-831B-70R-3, 34–36 cm), from near the top of Unit IV. Elsewhere, the glass tends to be replaced by palagonite and its alteration products, which also form the matrix of the clasts.

Andesitic Blebs

In Subunits IVB and IVC the larger pieces within the breccia are best referred to as blebs in view of their globular form. In the hand specimen the blebs show a composite rim or corona consisting, from the inside outward, of a thin pale brown rim (0.3 mm across), a white zone (0.6–0.8 mm across), and a pale gray outermost zone (<2 mm across), before passing into the grayish green (5G 5/2) matrix. Sample 134-831B-83R-2, 106–109 cm, comes from a section which may be regarded as the type-example of this material. In thin section the phenocryst assemblage closely resembles that found in the other andesite clasts and blebs. Plagioclase phenocrysts (30%, 0.4–2 mm in diameter), the dominant component, are conspicuously euhedral; they have characteristic oscillatory zoning and contain bands of small inclusions of crystals and glass. Clinopyroxene (4%, 0.2–1 mm in diameter) is subhedral and appreciably more abundant than the orthopyroxene (1%, 0.2–0.5 mm in diameter). About 50% of the volume of a bleb is composed of a remarkably clear, fresh, pale brown glass containing crystallites. The blebs constitute about 45% of the whole rock and are set in a matrix of streaky gray to yellow glass, which is altered to palagonite, and contains a phenocryst assemblage similar to that of the blebs. In plane-polarized light it is evident that a darker zone encircles each bleb, from which it is separated by a fracture about 0.1 mm wide, filled by zeolite minerals (Fig. 29). This darker rim is a chilled margin since the crystallites, discernible under crossed nicols, are significantly smaller than those in the glass of the bleb's interior. The chilled relationship is confirmed in another example (Sample 134-831B-82R-2, 41–43 cm), where a very distinct but darker margin remains attached to the interior. The fracture dividing the rind from the main part of the bleb is thought to be the result of differential cooling and delayed contraction of the interior, as opposed to the chilled rim.

The blebs and their chilled rinds are enclosed within swirling and streaky glass, variably transformed to yellowish palagonite and its alteration products, which are mainly zeolites, clay minerals, and iron oxide minerals. Cutting the

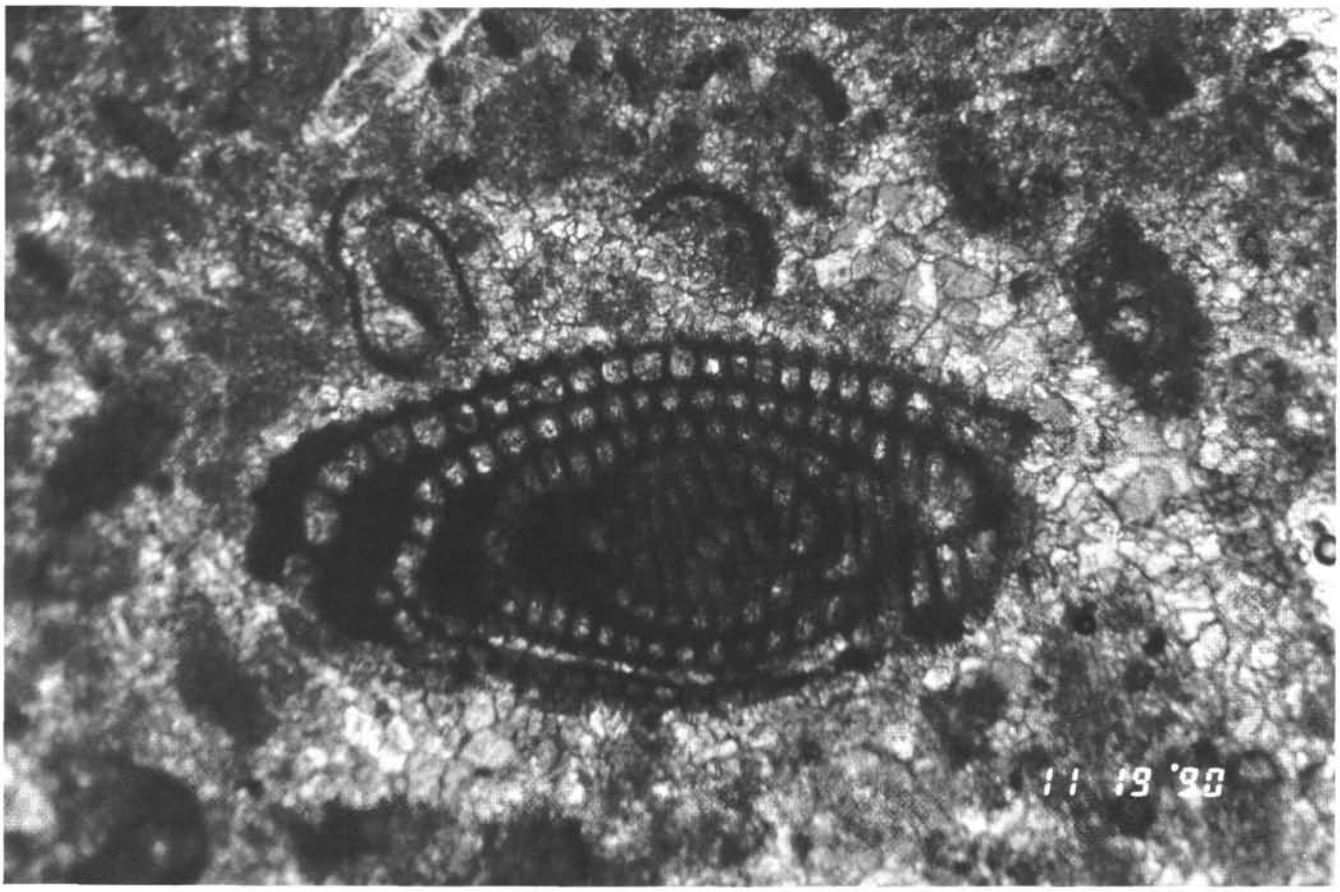

Figure 26. Photomicrograph of *Borelis* sp., Sample 134-831B-56R-CC, 14–16 cm, magnification ×200, axial view.

matrix are veins of clearer, partially palagonitized glass containing disrupted plagioclase phenocrysts. The latter range from dispersed slivers and sharp clasts to instances where the crystals show incipient disintegration around glass-filled fractures. It would seem that the breakup of the plagioclases was related to the invasion of melt along the intervening fractures. The shattered feldspars are evidently responsible for the white zones, which are often observed around clasts and blebs, in the hand specimen. These are sometimes immediately adjacent to the chilled margin, or peripheral fracture, but may also occur several millimeters away, as a zone in the banded palagonite of the breccia matrix (Fig. 30).

Discussion

The andesitic hyalo-breccias are interpreted as having been emplaced during a protracted series of submarine eruptions, before the late Oligocene (see "Lithostratigraphy" section, this chapter). Their formation is believed to be analogous to that of pillow lavas and their associated hyaloclastite deposits. Detailed differences in the features exhibited are most likely due to the greater viscosity of the andesitic melt. While basaltic pillow breccias are relatively common, the occurrence of their andesitic counterparts appears to be rather rare.

As it was extruded, the lava evidently developed miniature pillows, which formed chilled margins on contact with seawater. Many of the small pillows or blebs were probably destroyed during this process; the chilled rinds spalled off and were incorporated into the glassy matrix of the hyalo-breccia. This interaction did not produce the kind of glass shards and cuspate splinters found in typical basaltic hyaloclastites; instead, the disintegrating glassy crust held together in larger fragments. However, around most blebs there are zones of shattered feldspar crystals; the plagioclase phenocrysts are thought to have disintegrated as a consequence of the quenching. The vitrophyric blebs that survived represent the cores of the miniature pillows that were insulated from the violent interaction with seawater by the protective rinds and accumulating glass.

The blebs (e.g., in the type-example of Section 134-831B-83R-2) are nonvesicular, and vesicles are also very limited in the enclosing glassy matrix. This implies that the water depth was sufficient to prevent significant degassing and vesiculation. The precise depth is open to question, since vesiculation will also depend on the volatile content of the magma and the viscosity of the melt. However, the minimum depth was probably of the order of a few hundred meters (see Fisher and Schmincke, 1984). The globular and sometimes wispy form of the blebs indicates that the magma was still reasonably fluid or plastic; this is consistent with the lack of vesicles and thus the retention of volatiles, which would depress the solidus and moderate the viscosity.

The miniature pillows and glassy breccia probably formed on the slopes of a submarine andesitic volcano, as part of an apron of such material. Some of the lithologies recovered from Hole 831B, especially some of the more chaotic breccias, may have been deposited by avalanches or debris flows of hyalo-breccia material, moving down the unstable slope. The oxidized clasts and more vesicular fragments, found in Subunits IVA, IVC, and IVE, suggest a shallower-water origin and

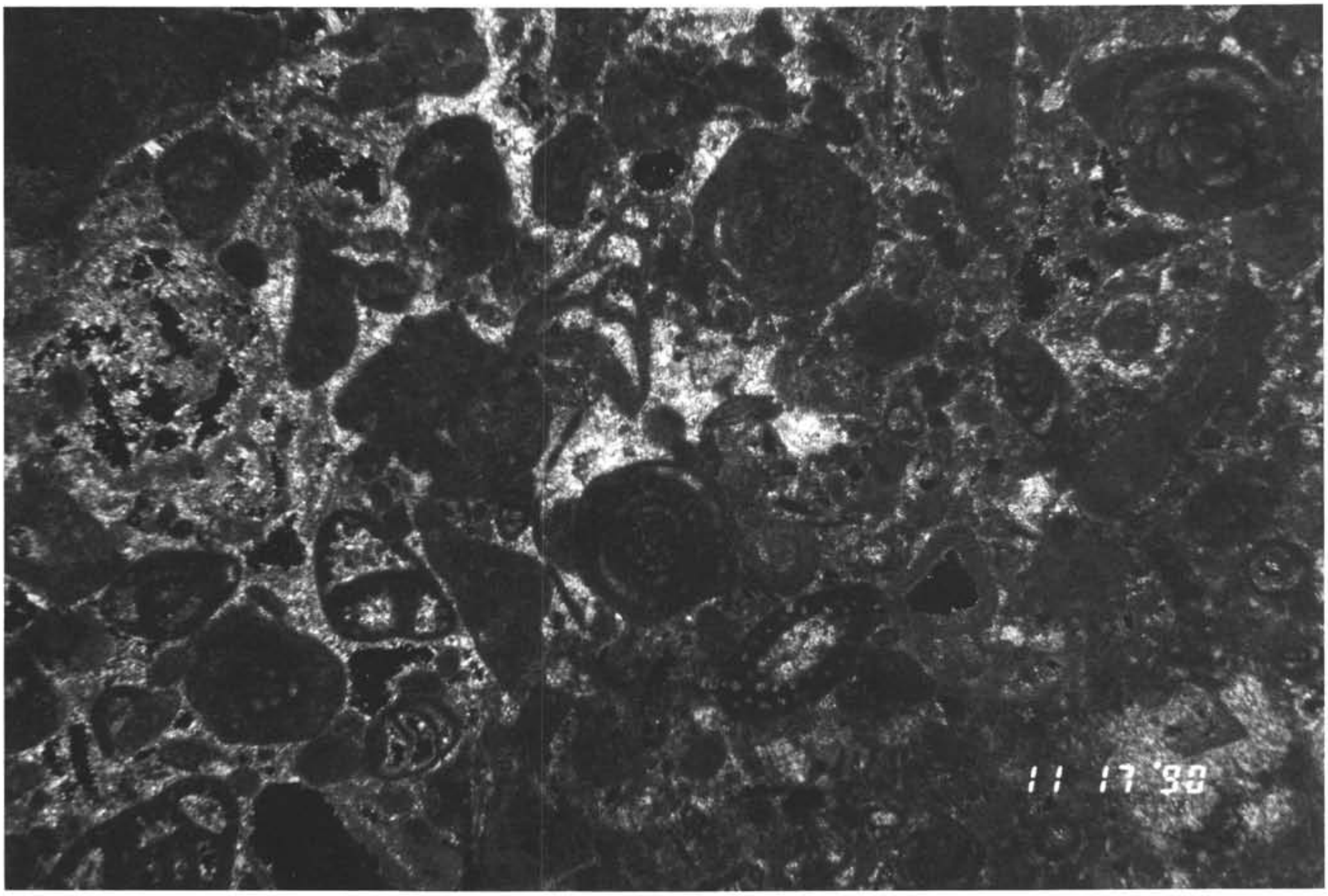

Figure 27. Photomicrograph of an assemblage consisting predominantly of miliolines and smaller rotaliids. Sample 134-831B-56R-CC, 14–16 cm, magnification ×50.

there may, on occasion, have been an input of subaerial material. The subunit lithologies thus seem to indicate changes in depositional conditions in response to varying water depth. There may have been changes in sea level that were sufficient to bring the erupting magma to a depth where vesiculation became possible. This could have been achieved by fluctuations about a critical depth and need not imply very large changes in sea level. Material of subaerial or shallow-water provenance may have been transported downslope by gravity flows. However, the strongly oxidized beds of Subunit IVA, and in particular the development of a bole, point to a phase of emergence and subaerial weathering prior to the deposition of the overlying reef limestone during the late Oligocene.

On the basis of their petrographic characteristics the two-pyroxene andesites are of calc-alkaline or perhaps island-arc tholeiite affinity. In either case they point unequivocally to an island-arc origin for the Bougainville Guyot.

IGNEOUS GEOCHEMISTRY

This section covers the geochemistry of volcanic ashes interbedded with the Pleistocene foraminiferal and pteropod oozes of lithostratigraphic Unit I, and the andesitic hyalo-breccias of lithostratigraphic Unit IV, beneath the carbonate cap of the Bougainville Guyot that was drilled at Site 831. Major and trace element analyses were performed using X-ray fluorescence (XRF) (see "Explanatory Notes" chapter, this volume) and the results are compiled in Table 3.

Pleistocene Volcanic Ashes (Lithostratigraphic Unit I)

The two ash layers analyzed are of basaltic andesite to andesite composition (55.7 and 57.6% SiO_2). Their major element chemistry conforms to that of typical calc-alkaline lavas (e.g., TiO_2, 0.9%; MgO, 2.8%–3.0%) but Al_2O_3 abundance is rather low (cf. Jakes and White, 1972). In contrast, K_2O is high (1.7%–1.8%), placing the ashes just within the field of the calc-alkaline series (Fig. 31) on the basis of the K_2O vs. SiO_2 classification of Taylor et al. (1981). Although the major element chemistry of these pyroclastic rocks gives a general indication of their compositional affinities, caution must be exercised in their interpretation. For example, there may well have been some winnowing of finer and less-dense constituents during subaerial transport. In addition, there is the possibility of some fractionation and reworking during submarine settling. The most obvious tendencies will be for early separation of denser ferromagnesian and Fe-Ti oxide minerals from the proximal part of the ash cloud. In contrast, finer and lighter constituents, such as the residual glass, will be concentrated in the more distal deposits. Also, an apparently single but rather thick (22-cm) ash layer, such as the lower of the two considered here, may be a composite product of more than one eruptive event. For these reasons the analyses obtained do not necessarily conform in detail to the original magmatic composition.

The trace element abundances of the ashes are much as to be expected in calc-alkaline magmas of this SiO_2 range (cf. Jakes and White, 1972). The only features worthy of special

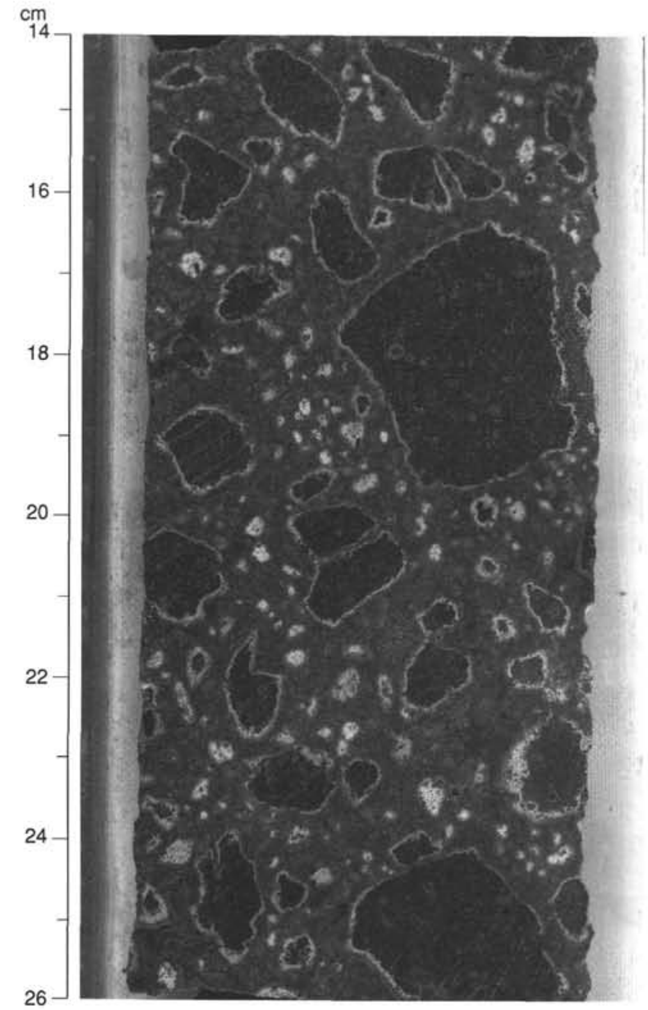

Figure 28. Hyalo-breccia from Subunit IVD (interval 134-831B-83R-2, 14–26 cm), showing andesitic blebs and coronas.

mention are the slightly high concentration of Sr (426–461 parts per million, or ppm) and the high concentration of Ba (456–505 ppm). The mid-ocean ridge basalt (MORB)-normalized patterns for selected minor and trace elements are shown in Figure 32. The patterns for the two ashes are very similar and show the characteristic calc-alkaline or subduction-related features of enrichment in large ion lithophile (LIL) elements relative to the high field strength (HFS) elements. Both samples also show conspicuous negative Nb anomalies. The patterns resemble those from Epi and Emae islands (Dupuy et al., 1982), examples of which are shown in Figure 32 for comparison. The ashes have clearly been erupted from one of the volcanoes of the Central Chain in the New Hebrides Island Arc during the Pleistocene to Holocene.

Andesitic Breccias (Lithostratigraphic Unit IV)

Major Element Geochemistry

Analyses were confined to clasts or blebs, which are usually remarkably fresh, as evident from petrographic examination (see "Igneous Petrology" section, this chapter). This is also supported by the generally low values (0.42%–1.57%) for loss on ignition (LOI), apart from two instances where the LOI is somewhat high (Samples 134-831B-70R-1, 125–129 cm, and -81R-1, 72–76 cm). SiO_2 ranges from 58.0% to 61.9%, with an average of 60.4%, placing these rocks firmly in the middle of the andesite range. There is no systematic variation of SiO_2 or any of the other oxides with stratigraphic position in lithostratigraphic Unit IV.

Concentrations of Al_2O_3 (16.1%–17.3%) are also characteristic of calc-alkaline andesites but are not particularly high considering that most of the analyzed samples have approximately 30% plagioclase phenocrysts. Concentrations of Fe_2O_3 (4.7%–7.6%), MgO (2.0%–4.8%), CaO (6.5%–7.8%), and TiO_2 (0.6%–0.9%) are all within the usual range of variation for calc-alkaline lavas. The abundance of Na_2O varies from 3.0% to 4.2%, which is again within the expected range for such lavas. However, the low K_2O abundance (0.32%–0.68%) is the most significant feature of the major element chemistry. A plot of K_2O vs. SiO_2 (Fig. 31) demonstrates that all of the andesites plot entirely within the low-potassium tholeiite series of Taylor et al. (1981). In this respect they resemble the island-arc tholeiite (IAT) series of the South Sandwich Islands and Saint Kitts in the Lesser Antilles (Wilson, 1989). One of the most unusual features of the Hole 831B lavas is that they do not appear to show any evidence of a positive correlation between K_2O and SiO_2. If anything, the reverse is the case, but there are insufficient analyses to confirm this.

Trace Elements

Twelve trace elements were analyzed on the shipboard XRF (Table 3). At 1–2 ppm, Nb is close to its detection limit but can certainly be regarded as <3 ppm. The low Ce figures (14–22 ppm) must be regarded as unreliable and the Ba concentrations (26–64 ppm) should be considered as having a large error. Our conclusions are dependent on the low Nb but place no particular dependence on Ce or Ba. There is nothing particularly remarkable about most of the trace element abundances. Some, such as Sr (273–342 ppm), Y (18–28 ppm), Zn (36–69 ppm), Cu (15–36 ppm), and Ni (16–36 ppm), are in the usual range for IAT and many calc-alkaline suites (cf. Jakes and White, 1972). At the level of 3 to 6 ppm, Rb clearly suggests IAT affinity. The variability of Cr, Ni, and V is undoubtedly related to the fractionation or accumulation of ferromagnesian and oxide phases. The most notable feature of the trace elements is the unusually high concentration of Zr (149–198 ppm), which is outside the normal range for either IAT or calc-alkaline lavas with similar SiO_2 contents.

LIL elements (e.g., K and Rb) do not show the usual positive correlation with SiO_2 contents or with HFS-incompatible elements such as Zr. This is illustrated in Figure 33, which shows the unexpected, albeit rather weak, negative correlation between K_2O and Zr, and the stronger negative correlation between MgO and Zr. The characteristic positive correlations between TiO_2 and Zr, and between Na_2O and Zr, are shown for comparison. All except the K_2O vs. Zr trend are relationships that may be accounted for by fractional crystallization. Note that one of the andesites (Sample 134-831B-84R-4, 137–141 cm) in Figure 33, tends to plot off the main trend (e.g., it falls below the array for both TiO_2 and MgO vs. Zr). It may be significant that this clast comes from the lowest part of the sequence (Subunit IVE), where a substantial influx of shallow-water or possibly subaerial constituents is suspected (see "Igneous Petrology" section, this chapter).

MORB-normalized trace element patterns (Pearce, 1983) are depicted in Figure 34 for four representative andesites covering the range of distributions seen in the volcanic rocks of Hole 831B. The patterns are remarkably similar and their most obvious features are as follows:

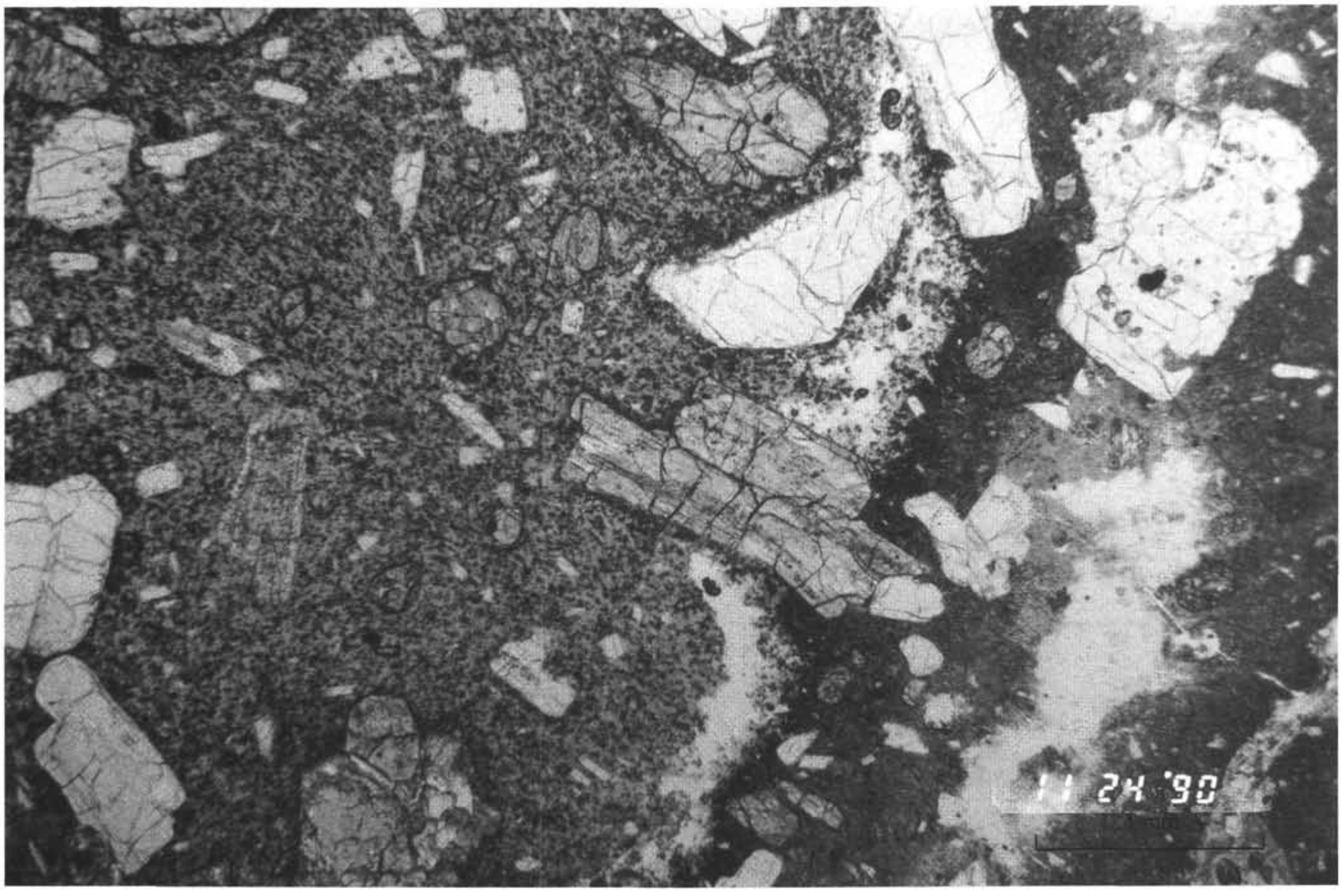

Figure 29. Photomicrograph of Sample 134-831B-83R-2, 106–109 cm, showing andesitic bleb (left) separated by a zeolite-filled fracture from its chilled margin and the palagonitic matrix (plane-polarized light).

1. A conspicuous Nb anomaly, which is characteristic of subduction-related magmas.

2. Minimal enrichment in LIL elements (K, Rb, and Ba) relative to HFS elements. Strong enrichment in LIL elements is typical of IAT and calc-alkaline suites, and is usually attributed to transport of these elements by means of fluids or partial melts derived from the subducting slab (Pearce, 1983).

3. There is an unusual enrichment in Zr relative to Ti and Y. Depletion in Ti in these relatively evolved rocks may be achieved by fractionation of titanomagnetite but this is not suggested by Figure 33. The Zr/Y ratio should be unaffected by fractionation. High Zr, in relation to both Ti and Y, therefore appears to be a source characteristic.

4. The general shape of the patterns is quite unlike that for usual calc-alkaline or IAT andesites. Apart from the Nb trough and Zr peak, there is a gently falling gradient from the LIL to the HFS elements, which is reminiscent of enriched MORB. In fact, the patterns could almost be regarded as MORB-like spectra on which Nb and Zr anomalies have been superimposed. The plot of Cr vs. Y (Fig. 35) offers supporting evidence for this contention in that the andesites from Hole 831B overlap the boundary between IAT and MORB.

Conclusions

The major element chemistry of the Hole 831B rocks indicates that the Bougainville Guyot lavas are low-potassium andesites belonging to the IAT series. Nevertheless, the trace element chemistry is unusual. It suggests a decoupling of the process of LIL enrichment from Nb depletion. The latter may be due to retention of Nb in phases such as ilmenite and sphene at the site of magma generation in the subducting oceanic crust (Saunders et al., 1980). Lack of LIL element enrichment points to a close affinity with MORB, though the overall increase in the abundance of these trace elements may be ascribed to fractionation or a lower degree of partial melting.

The conclusion is that these andesites have a subduction-related origin but probably belong to a very early stage of island-arc development, before any significant enrichment of the source region in LIL elements. Nevertheless, even at this stage it was apparently possible to generate the typical arc signature of the negative Nb anomaly, which is attributed to processes independent of LIL enrichment. There are some similarities in trace element characteristics between the andesites of Hole 831B and the basaltic rocks of Hole 828A on the North d'Entrecasteaux Ridge (see Fig. 34). Both display features transitional between MORB and IAT, but the Hole 828A lavas have closer affinities with MORB, whereas the Bougainville Guyot rocks seem to have a stronger subduction zone affinity.

SEDIMENT AND FLUID GEOCHEMISTRY

Results

Only two pore-fluid samples were collected at Site 831 because of the limited core recovery within the sedimentary section. These samples were measured for the normal suite of solute concentrations (see "Explanatory Notes" chapter, this

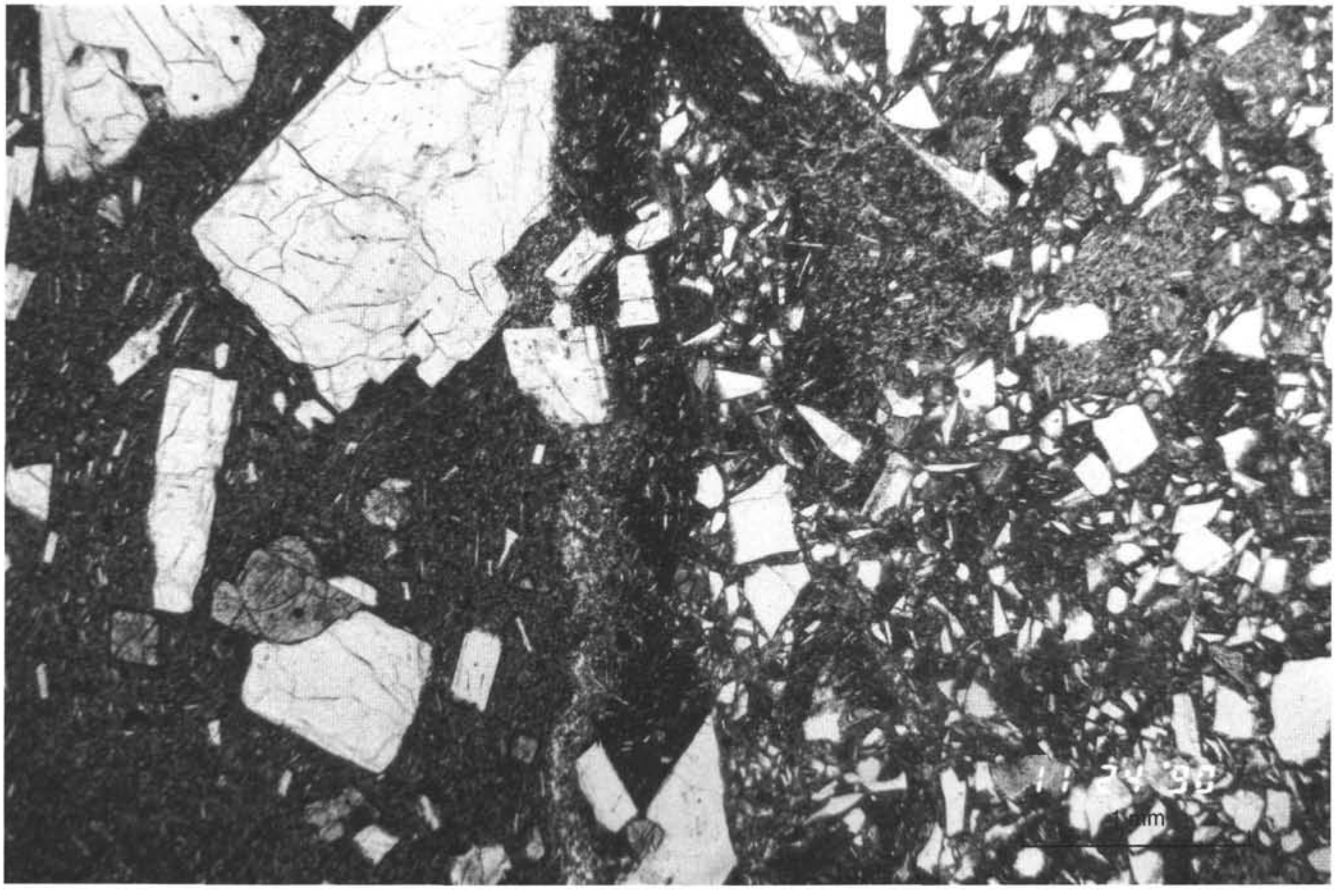

Figure 30. Photomicrograph of Sample 134-831B-70R-4, piece 4, 77–80 cm, showing andesite bleb (left) with chilled margin (center) and zone of shattered plagioclase in palagonitic matrix (plane-polarized light).

volume) and their values are reported in Table 4. Most solutes exhibit approximately seawater concentrations with the exception of calcium, magnesium, and sulfate. The deepest sample, from a depth of 135.4 mbsf, is slightly enriched in calcium and depleted in magnesium, possibly reflecting carbonate diagenesis (see "Lithostratigraphy" section, this chapter). This sample also is slightly depleted in sulfate, reflecting sulfate reduction.

From these data, the $CaCO_3$ and organic carbon data were calculated. The carbon data are reported in Table 5. The organic carbon contents are low which probably accounts for the minor amount of sulfate reduction.

PALEOMAGNETISM

Drilling at Site 831 recovered only 20 m of sediment, the pelagic carbonate of lithostratigraphic Unit I, (see "Lithostratigraphy" section, this chapter) in which recovery was sufficient to permit magnetic measurements using the cryogenic magnetometer. Below lithostratigraphic Unit I is a 727-m section of neritic carbonate (lithostratigraphic Units II and III) in which recovery consisted mostly of fragments of carbonate rocks; paleomagnetic measurements were not made in these units. Underlying the neritic carbonate is lithostratigraphic Unit IV, a section of andesite breccia 125 m thick, that contains clasts of andesite in a glassy matrix, much of which has altered to palagonite (see "Igneous Petrology" section, this chapter). A total of 90 discrete samples were taken from the clasts and matrix of the breccia. The quality of paleomagnetic data depends strongly on lithology, thus the discussion of paleomagnetism at Site 831 is organized on the basis of lithostratigraphy.

Paleomagnetism of Pelagic Carbonate

We recovered pelagic carbonate from Cores 134-831A-1H to -3H (0–15.9 mbsf); Cores 134-831A-2H and -3H were oriented using the multishot technique, although both were disturbed by drilling. The natural remanent magnetization (NRM) of archive halves from Cores 134-831A-1H to -3H measured in the cryogenic magnetometer exhibits moderate to steep upward inclinations (−60° to −80°). Alternating field (AF) demagnetization to 10 mT (Fig. 36) removes a soft component of magnetization, as indicated by a change in inclination to values ranging from −30° to −50°. Declinations vary substantially within individual sections of Cores 134-831A-2H and -3H, even after orientation using multishot data, indicating that the recovered material rotated within the core liner.

AF demagnetization at 20 mT of five samples from Cores 134-831A-1H to -3H isolated a characteristic component of remanence whose mean inclination is −41.36°. Thus, the inclinations of both archive halves and discrete sample indicate normal polarity, consistent with deposition during the Brunhes Chron.

Paleomagnetism of Andesite Breccia

Seventy of the 90 samples taken from the clasts and matrix of the andesite breccia in Cores 134-831B-69R to -84R (726.8–852.0 mbsf) were AF-demagnetized aboard the *JOIDES Reso-*

Table 3. Shipboard XRF analyses of rocks from Holes 831A and 831B.

Number	1	2	3	4	5	6	7	8	9	10	11	12
Hole, core, section	831A-3H-5	831A-3H-6	831B-70R-1	831B-70R-3	831B-71R-2	831B-74R-2	831B-76R-5	831B-77R-3	831B-80R-3	831B-81R-1	831B-82R-2	831B-84R-4
Sample interval (cm)	98–100	50–52	125–129	31–34	70–74	78–82	110–112	139–141	110–115	72–76	43–46	137–141
Rock type	Ash layer	Ash layer	Andesite	Andesite	Andesite	Andesite	Andesite	Andesite	Andesite	Andesite	Andesite	Andesite
Major elements (wt%)												
SiO_2	57.56	55.74	61.56	60.67	61.32	61.62	59.37	60.87	58.01	59.42	59.34	61.89
TiO_2	0.89	0.91	0.92	0.85	0.82	0.81	0.80	0.89	0.76	0.71	0.74	0.63
Al_2O_3	15.12	15.08	17.07	16.08	16.23	16.38	16.39	17.29	16.93	16.06	16.64	16.92
Fe_2O_3(t)	10.50	10.80	6.11	6.66	6.43	6.48	6.29	5.01	6.51	7.61	6.54	4.73
MnO	0.21	0.20	0.06	0.12	0.11	0.12	0.15	0.14	0.13	0.15	0.12	0.06
MgO	2.79	3.03	1.97	3.55	3.62	3.39	4.00	3.51	4.80	4.85	4.31	2.63
CaO	6.61	7.16	6.72	6.47	6.54	6.48	6.95	7.80	7.83	7.39	7.61	7.70
Na_2O	3.20	2.91	4.19	3.86	3.89	3.98	3.76	4.21	3.29	2.97	3.46	3.91
K_2O	1.81	1.70	0.32	0.62	0.56	0.47	0.39	0.38	0.59	0.63	0.69	0.54
P_2O_5	0.33	0.32	0.14	0.13	0.13	0.13	0.12	0.12	0.10	0.13	0.12	0.10
Total	98.99	97.83	99.05	98.99	99.63	99.85	98.21	100.20	98.94	99.90	99.55	99.08
LOI	1.07	0.62	2.38	0.42	0.85	0.64	1.02	1.57	1.35	4.71	1.19	1.22
Mg#	0.34	0.36	0.39	0.51	0.53	0.51	0.56	0.58	0.59	0.56	0.57	0.52
Trace elements (ppm)												
Ti	5306	5455	5515	5066	4886	4826	4796	5306	4556	4226	4436	3747
Nb	4	5	1	2	2	2	1	2	1	1	2	1
Zr	144	147	198	183	184	187	184	177	154	149	158	160
Y	26	28	24	25	27	28	25	27	21	18	23	18
Sr	461	426	291	281	279	284	275	273	300	342	300	322
Rb	28	30	3	6	5	5	4	3	4	6	4	6
Zn	109	110	36	47	55	52	44	38	69	45	48	49
Cu	153	103	15	34	33	36	35	27	36	24	46	19
Ni	17	6	16	19	19	19	22	27	30	36	24	28
Cr	16	10	35	31	37	29	35	52	66	58	71	96
V	273	210	142	150	150	152	142	152	151	126	160	171
Ce	34	32	22	17	25	26	18	18	21	14	24	15
Ba	456	505	44	63	64	53	52	55	34	26	52	55

Note: Fe_2O_3(t) = total iron as Fe_2O_3; LOI = loss on ignition; Mg# = MgO/(MgO + FeO_{total}) mol%.

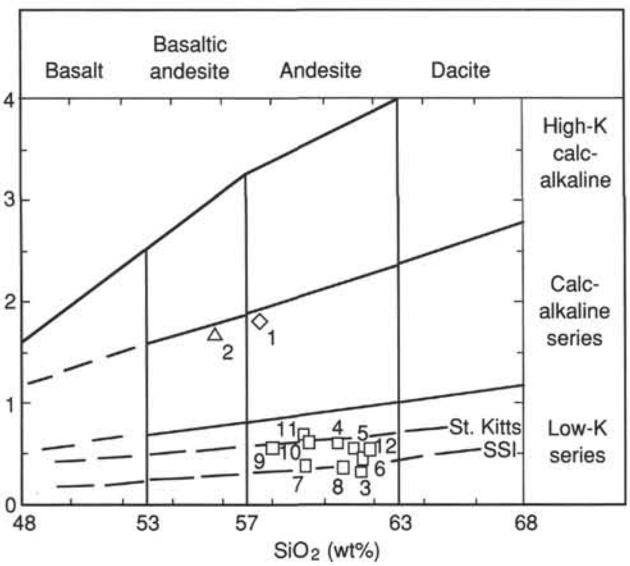

Figure 31. Classification of Site 831 volcanic rocks on the basis of K_2O vs. SiO_2 (after Taylor et al., 1981). Ash layers: diamond represents Sample 134-831A-3H-5, 98–100 cm; triangle is Sample 134-831A-3H-6, 50–52 cm. Squares represent samples of andesites from Hole 831B. Numbers refer to the listing in Table 3. Trends for Saint Kitts and South Sandwich Islands (SSI) from Wilson (1989).

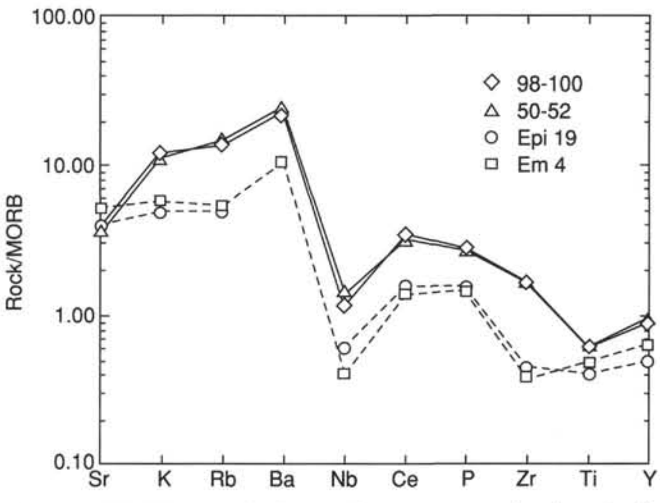

Figure 32. MORB-normalized trace element patterns for the volcanic ashes of Hole 831A, with comparative spectra for Epi and Emae (Em), from Dupuy et al. (1982). In the legend, the first two samples are from Hole 831A and the numbers refer to their centimeter intervals. The full sample numbers are quoted for these intervals in Table 3.

lution. The maximum demagnetization field ranged from 40 to 100 mT, depending on the coercivity of the sample. Typical AF-demagnetization diagrams are shown in Figure 37. In general, after removal of a soft component of magnetization that may result from drilling, samples from clasts are characterized by a single stable component of remanence whereas several samples from the matrix display two components of magnetization. Histograms showing the frequency of occurrence of median destructive fields (MDF's) (Fig. 38) indicate that the magnetization of the matrix is carried by material whose coercivity is lower than that of the clasts. Figure 39 illustrates the rather random distribution of paleomagnetic directions from both clasts and matrix. The dispersion in declinations results from the lack of orientation of the cores, the random orientation of pieces of core within the liners, and the unoriented nature of clasts within the breccia. Figure 40

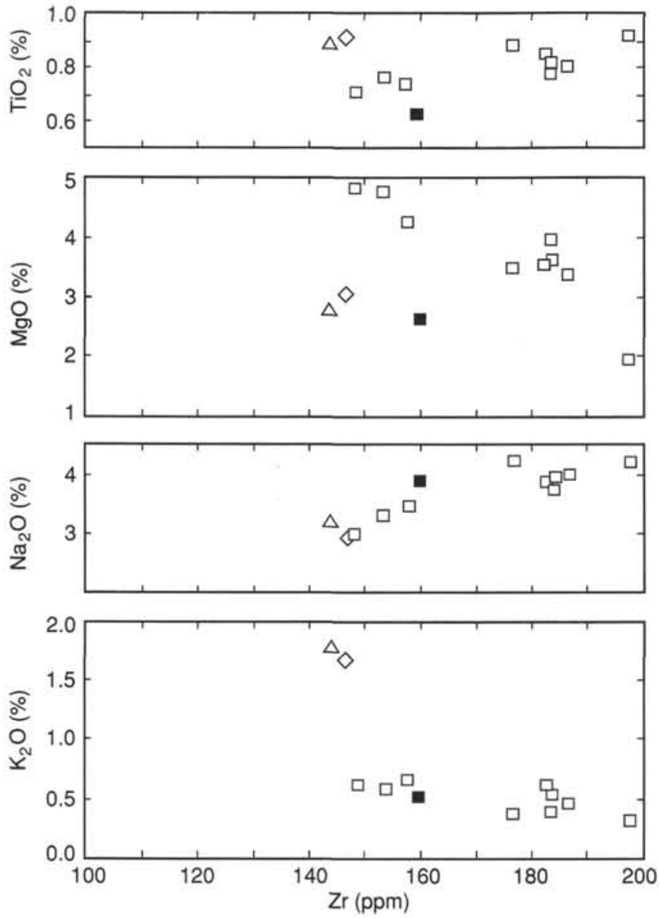

Figure 33. Plots of TiO_2, MgO, Na_2O, and K_2O vs. Zr for the two volcanic ashes of Hole 831A (symbols as in Fig. 31) and the andesites of Hole 831B (squares). The filled square represents the slightly anomalous Sample 134-831B-84R-4, 137–141 cm, from Subunit IVE.

illustrates the change in inclination as a function of depth, which is also random for samples from both clasts and matrix.

Eight samples of andesite breccia were thermally demagnetized aboard ship (Fig. 37). The unblocking temperatures are high (about 570°C) and suggest that the magnetization of the breccia is carried by magnetite, consistent with the coercivity of the material based on the results of AF demagnetization.

Magnetic Susceptibility

The poor recovery and fragmented nature of the neritic carbonate recovered at Site 831 precluded the measurement of magnetic susceptibility in lithostratigraphic Units II and III. Magnetic susceptibility of the andesite breccia of lithostratigraphic Unit IV ranges from 0.005 to 0.02 SI (Fig. 41). In general, the magnetic susceptibility of the zones of breccia containing reddish brown fragments of andesite in a red, brown, or gray matrix (Subunits IVA, IVC, and IVE; see "Igneous Petrology" section, this chapter) is higher than that in zones of breccia characterized by gray clasts in a greenish palagonitic matrix (Subunits IVB and IVD).

SEDIMENT ACCUMULATION RATES

The biostratigraphic information from Holes 831A and 831B does not permit us to calculate accurate sediment accumulation rates for the following reasons:

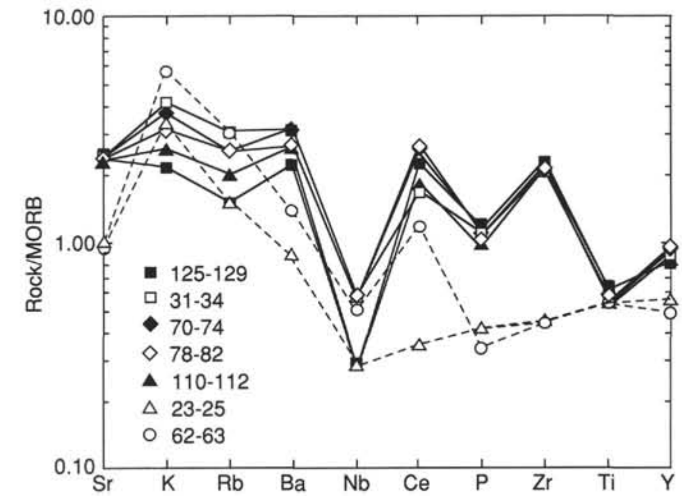

Figure 34. MORB-normalized trace element patterns for the andesitic blebs and clasts of Hole 831B and comparative distributions for basaltic rocks of Hole 828A. Solid lines are for Hole 831B and centimeter intervals for individual samples are given in the legend. For full sample specification refer to Table 3. The Hole 828A specimens (dashed lines) are as follows: 23–25 (Sample 134-828A-15N-1, 23–25 cm); 62–63 (Sample 134-828A-15N-2, 62–63 cm). The normalizing values are from Pearce (1983).

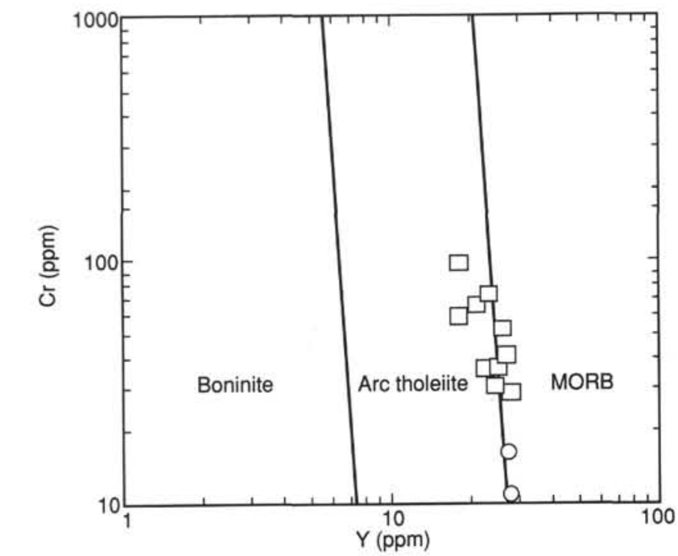

Figure 35. Plot of Cr vs. Y for the andesites of Hole 831B, illustrating the transitional affinities between MORB and island-arc tholeiite (fields from Fryer, Pearce, Stokking, et al., 1990).

1. The Pleistocene record between the seafloor and 20 mbsf was determined by the presence of *Globorotalia truncatulinoides,* whose first occurrence is registered at the base of Core 134-831A-3H. In Core 134-831A-4H no recovery was obtained, and in Core 134-831A-5H this species was not found in spite of the occurrence of an otherwise typical Pleistocene assemblage. Uncertainty remains as to whether or not this earliest occurrence in Sample 134-831A-3H-CC could correspond to its first appearance datum (FAD) elsewhere. If this is the case, and if we accept a Pleistocene age for the whole interval (between Cores 134-831A-1H and -5H), then a sediment accumulation rate ranging from 7.4 m/m.y. to ~10

Table 4. Pore-fluid chemistry, Site 831.

Interval (cm)	Depth (mbsf)	pH	Salinity (‰)	Sodium (mM)	Chloride (mM)	Potassium (mM)	Magnesium (mM)	Calcium (mM)	Sulfate (mM)	Alkalinity (mM)	Phosphate (μM)	Ammonia (μM)	Silica (μM)
134-831A-1H-2, 145–150	3.0	7.7	35	559.1	469	10.4	55.8	10.7	28.5	3	0.9	4.5	210
134-831B-5R-3, 145–150	135.4	7.7	37	559	470	10.6	53.3	11.4	27.8	3	0.3	26.6	134

m/m.y. would result from a calculation using values of 1.9 and 2.7 m.y., respectively, for the FAD of *G. truncatulinoides* (cf. Hills and Thierstein, 1989). Nonetheless, the marked facies change at 16.9 mbsf (from pelagic to shallow-water carbonates) would suggest an earlier appearance of this species not recorded in the sequence of Hole 831A. Hence, the figures calculated here could represent minimum values.

2. The Pliocene and/or Pleistocene record found between 20 and 246.4 mbsf (Samples 134-831A-5X-CC to 134-831B-18R-CC) is poorly defined and only suggested by the occurrence of some benthic foraminiferal genera of wide stratigraphic range and without recognized datum values. Furthermore, the underlying interval (246.4–563.6 mbsf) is barren, leaving open the question of the lower Pliocene contact and preventing any reliable estimation.

3. The lower Miocene interval between 563.6 and 621.6 mbsf (Samples 134-831B-52R-CC to -57R-CC), and the upper Oligocene interval between 621.6 mbsf and 727.5 mbsf (Samples 134-831B-58R-CC to -69R-1, 66 cm), were determined by the occurrence of smaller and larger benthic foraminifers assigned to Zones Te5 and upper Te1–4, respectively. In the absence of data above 563.6 and below 727.5 mbsf to constrain these zones, any attempt to calculate sediment accumulation rates would be quite tentative.

Table 5. Sediment carbon contents, Site 831.

Core, section, interval (cm)	Depth (mbsf)	Total carbon (wt%)	Inorganic carbon (wt%)	TOC (wt%)	$CaCO_3$ (wt%)
134-831A-					
1H-1, 10–13	0.1		6.22		51.8
1H-1, 90–93	3.9	8.53	8.54	0.00	71.1
2H-1, 80–83	5.2		9.70		80.8
2H-2, 59–61	6.5	9.53	9.47	0.06	78.9
3H-1, 52–54	6.9		9.49		79.1
2H-3, 59–61	8.0		9.76		81.3
2H-4, 59–61	9.5		9.88		82.3
3H-3, 52–54	9.9	8.92	8.89	0.03	74.1
2H-5, 59–61	11.0		9.62		80.1
2H-6, 59–61	12.5		10.22		85.1
3H-5, 53–55	12.9		8.02		66.8
2H-7, 54–56	13.9		12.02		100.1
3H-6, 52–53	14.4		2.82		23.5
3H-7, 42–44	15.8		9.71		80.9
6X-1, 25–26	20.3		11.64		97.0
8X-CC, 13–15	39.2		11.63		96.9
10X-CC, 10–13	58.1		11.70		97.5
13N-1, 17–20	88.2		11.63		96.9
134-831B-					
5R-1, 55–56	131.5		11.67		97.2
6R-CC, 14–17	134.0		11.69		97.4
5R-3, 55–56	134.5	11.72	11.69	0.03	97.4
30R-CC, 0–14	352.3	11.56	11.85	0.00	98.7
40R-CC, 20–23	449.1	11.75	11.94	0.00	99.5
49R-CC, 0–20	534.6	12.04	11.95	0.09	99.5
59R-CC, 20–32	631.5	12.12	11.95	0.17	99.5
63R-CC, 10–13	670.3	11.97	11.97	0.00	99.7
65R-CC, 4–7	688.1		0.22		1.8
67R-1, 4–7	707.5		10.19		84.9
69R-1, 82–84	727.6		0.03		0.2
69R-2, 70–72	728.9	0.14	0.04	0.10	0.3
69R-3, 25–27	729.6		0.07		0.6
70R-2, 12–14	737.8	0.15	0.07	0.08	0.6
71R-1, 90–92	746.9	0.15	0.07	0.08	0.6
72R-1, 50–53	756.1	0.01	0.03	0.00	0.2

Note: TOC = total organic carbon.

PHYSICAL PROPERTIES

Full APC and XCB cores from Hole 831A were measured using the gamma-ray attenuation porosity evaluator (GRAPE) and the *P*-wave logger (PWL) on the multisensor track. Measurements of index properties (Table 6) and sonic velocities using the Hamilton Frame (Table 7) were made on most cores from the pelagic carbonate sediments of lithostratigraphic Unit I (0–16.9 mbsf in Hole 831A; see "Lithostratigraphy" section, this chapter) that cover the guyot cap and from the volcanic breccia of lithostratigraphic Unit IV (726.5–852 mbsf in Hole 831B; see "Igneous Petrology" section, this chapter) that comprises the basement rocks. Because of poor recovery, few measurements could be made in the carbonate rock of lithostratigraphic Units II and III (see "Lithostratigraphy" section, this chapter). Thermal conductivity was measured in lithostratigraphic Units I and IV (Table 8) and 2-min GRAPE measurements were made on pieces of volcanic breccia from lithostratigraphic Unit IV. Only four shear-strength measurements could be made at Site 831 (Table 9) in the surface sediments on the guyot; therefore, shear strength is not discussed below. All measurements were performed in accordance with the procedures described in the "Physical Properties" section of the "Explanatory Notes" chapter (this volume).

Index Properties

Index property values are listed in Table 6. The variation of index properties as a function of depth below seafloor is illustrated in Figure 42. At Site 831, porosity ranges from 0% to 73.9%, water content ranges from 0% to 90.8%, and bulk density ranges from 1.59 to 3.26 Mg/m^3. Index properties can be separated into three zones: the soft pelagic sediments that cover the guyot cap (lithostratigraphic Unit I, 0–16.9 mbsf); the hard corals that comprise lithostratigraphic Units II and III (16.9–727.5 mbsf); and the volcanic breccia or lithostratigraphic Unit IV (727.5–852.0 mbsf), which forms the base of the guyot. In lithostratigraphic Unit I in Hole 831A (0–16.9 mbsf), water content ranges from about 45% to 90% and porosity varies from about 50% to 75%. Bulk density varies between 1.55 and 1.81 Mg/m^3. The wide range of index properties indicates that very little compaction has occurred in the pelagic sequence of lithostratigraphic Unit I.

In intervals of partially lithified grainstone and wackestone found in Subunit IIA (Cores 134-831A-6X, -8X, -10X, and -13N) (see "Lithostratigraphy" section, this chapter), porosity and water content drop sharply and bulk density shows a concomitant increase. Water content drops to 20%, porosity to 30%, and bulk density is above 2.00 Mg/m^3. Because of poor recovery, few index properties were measured in the neritic carbonate rocks of lithostratigraphic Unit II (Subunits IIB, IIC, and IID; 102.4–429.6 mbsf in Hole 831B) and Unit III (429.6–727.5 mbsf in Hole 831B). Water content is very low, ranging from 0% to 10.6%, porosity decreases from 24.5% at 134 mbsf to 0% at 697.8 mbsf, and bulk density ranges from 2.04 Mg/m^3 to as high as 3.26 Mg/m^3. However,

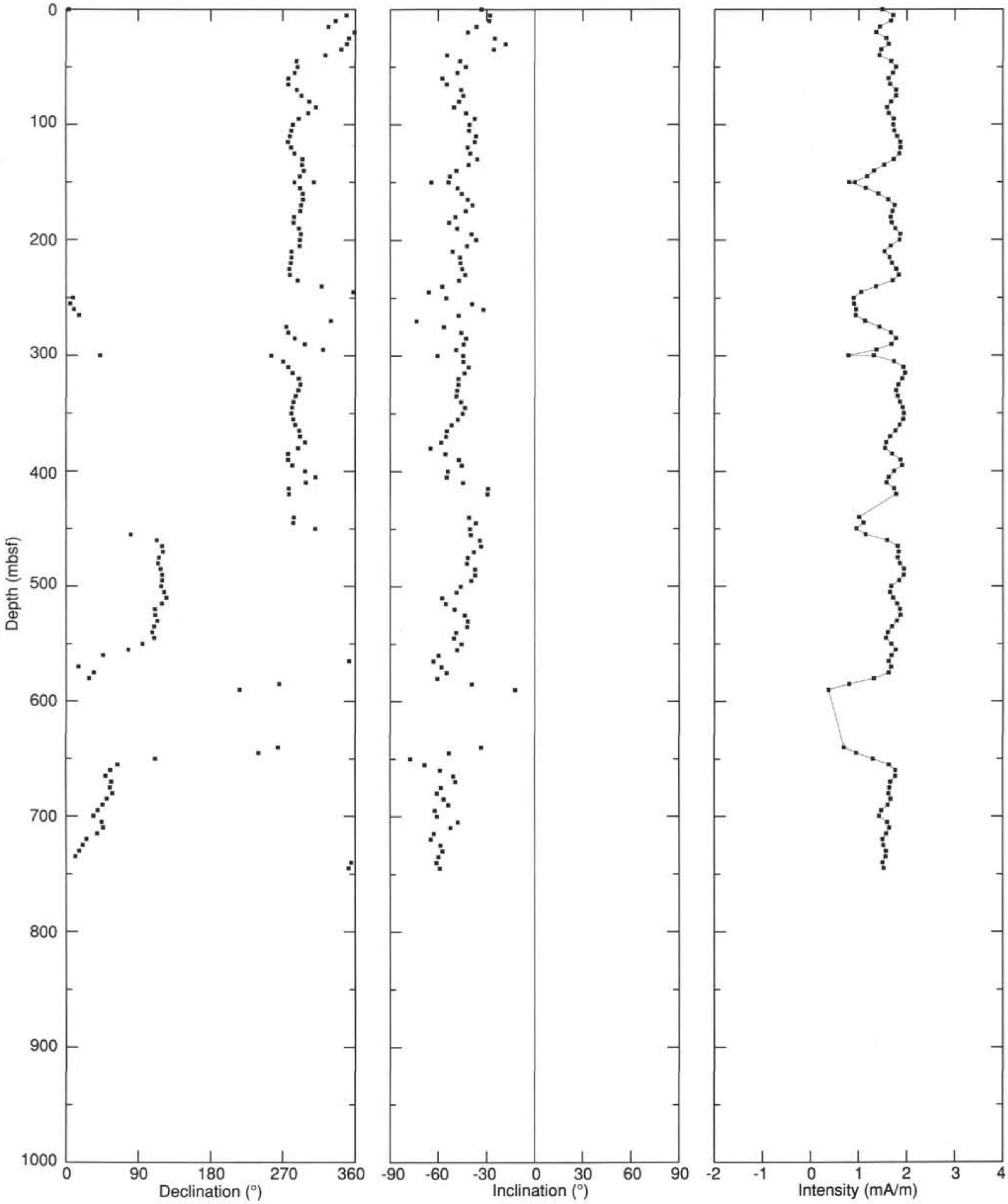

Figure 36. Plot of the remanent magnetization after AF demagnetization at 10 mT as a function of depth for Cores 134-831A-1H to -3H. Below about 10 mbsf, cores are disturbed by drilling and the data are unreliable. Core 134-831A-1H was not oriented. Declinations from Cores 134-831A-2H and -3H have been corrected using data from the multishot orientation technique.

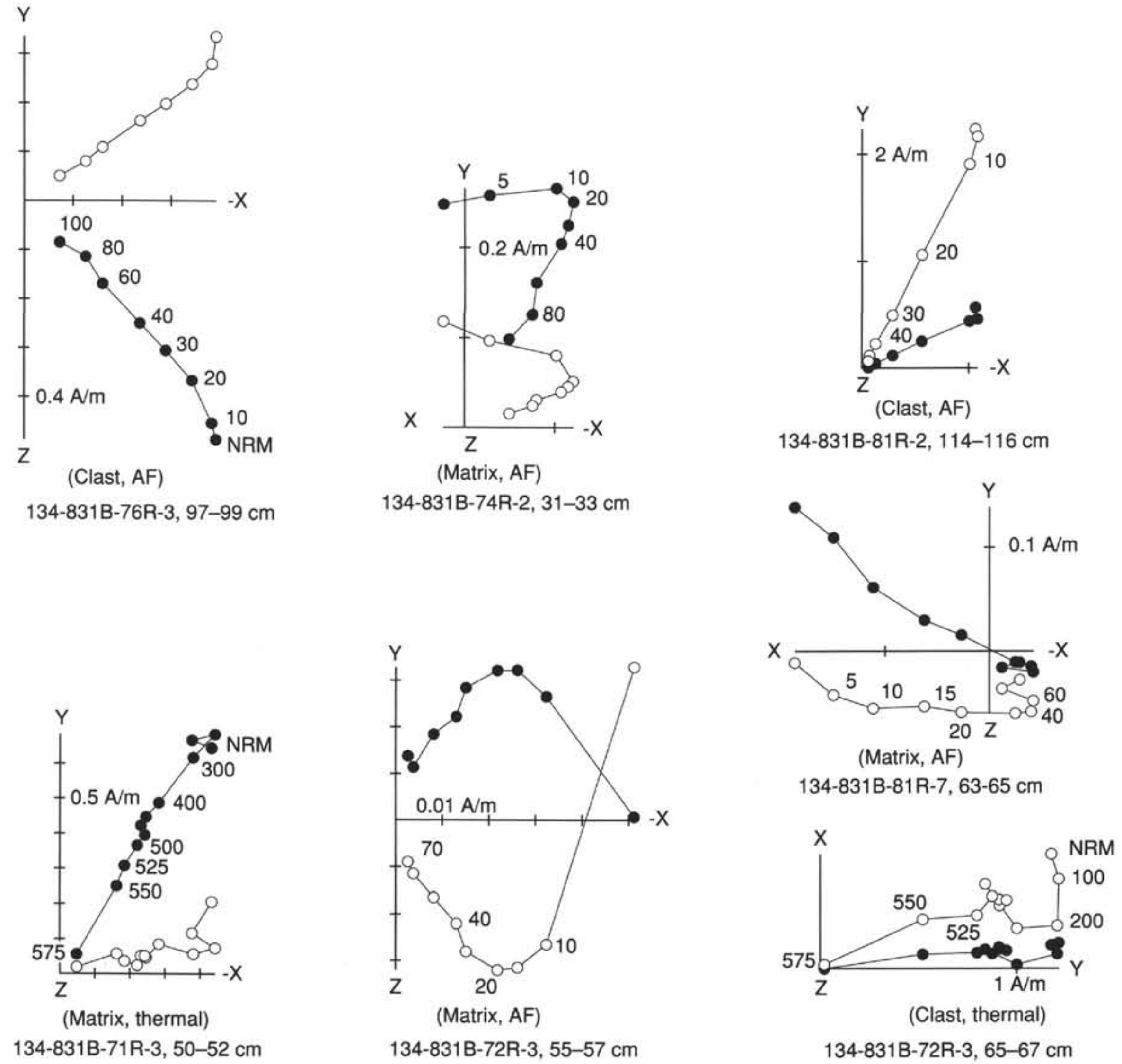

Figure 37. Orthogonal plots of AF and thermal demagnetization data for six samples from the andesite breccia of lithostratigraphic Unit IV. Open circles correspond to projections onto the vertical plane and filled circles correspond to projections onto the horizontal plane.

index properties near soil horizons in lithostratigraphic Unit III differ from those in the overlying and underlying intervals. In a red, oxidized soil horizon at 688 mbsf, porosity and water content are relatively high (57.7% and 45%) and bulk density is only 1.90 Mg/m^3. A sample of pale brown mudstone (Sample 134-831B-67R-1, 4 cm; 707.5 mbsf) overlying a soil horizon has a water content of 11.8%, a porosity of 25.5%, and a bulk density of 2.46 Mg/m^3 (Table 6 and Fig. 42).

Index properties vary widely in the andesite breccia of lithostratigraphic Unit IV (727.5–852.0 mbsf). Water content ranges from 1.2% to 20.2%, porosity varies from 3.2% to 36.1%, and bulk density ranges from 2.19 to 2.95 Mg/m^3 (Table 6 and Fig. 42). Porosity and water content values are higher in Subunits IVA (727–741 mbsf), IVC (789–822 mbsf), and IVE (838–852 mbsf), which have been oxidized, reworked, and occasionally interbedded with grits and sandstones (see "Igneous Petrology" section, this chapter). Bulk density was also measured in Unit IV rocks using the 2-min GRAPE procedure (see "Explanatory Notes" chapter, this volume). However, the 2-min GRAPE data are not discussed here because they disagree with pycnometer data and appear to be low, sometimes by as much as 0.5 Mg/m^3.

Sonic Velocity

Sonic velocities were measured using the PWL and the Hamilton Frame in the top 20 mbsf of Hole 831A; only Hamilton Frame measurements were obtained for Hole 831B. Because Hamilton Frame data exist for both holes, only these data are discussed here (Table 7 and Fig. 42). Vertical and horizontal velocities at Site 831 range from 1596 to 5837 m/s and show very little anisotropy. Velocities were usually measured in three directions because the poorly recovered cores often consisted of small, unoriented coral cobbles.

Vertical and horizontal velocities increase from 1596 m/s in the pelagic carbonate of lithostratigraphic Unit I (0–16.9 mbsf) to 2000 m/s or more in the partially consolidated packstone and wackestone in the upper part of lithostratigraphic Unit II (Subunit IIA, 16.9–100 mbsf). In the carbonate rock fragments of lithostratigraphic Units II and III (102.4-727.5 mbsf), sonic velocities range from 3000 to 5000 m/s, although a value of

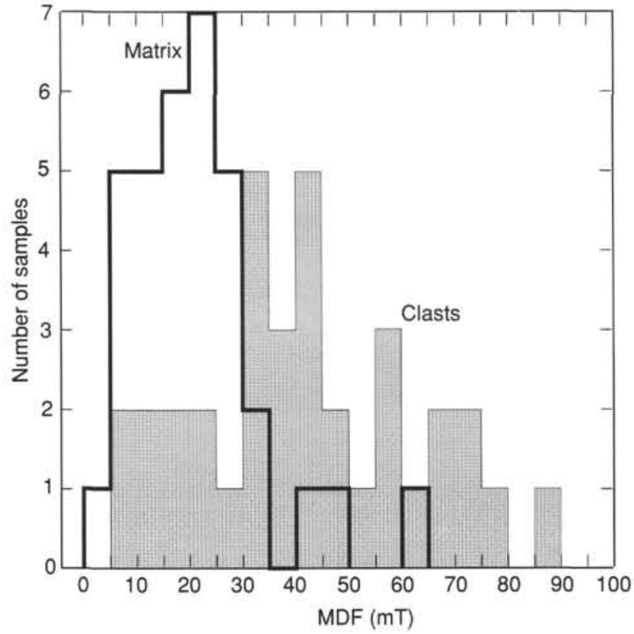

Figure 38. Histogram showing the frequency of occurrence of MDF's of samples from clasts and matrix of andesite breccia, Hole 831B.

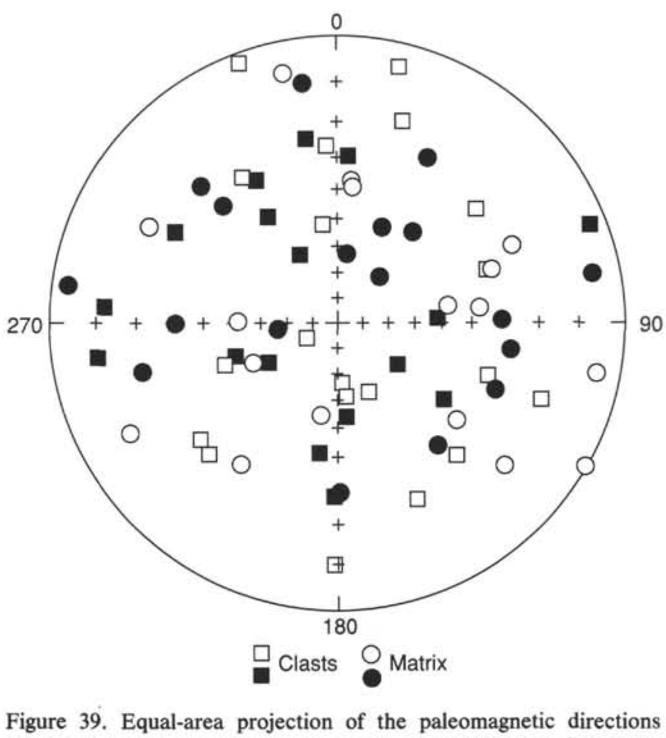

Figure 39. Equal-area projection of the paleomagnetic directions observed in discrete samples from clasts and matrix of andesite breccia from Hole 831B after AF demagnetization at 10 mT.

5728 m/s was obtained at 670 mbsf in a laminated algal packstone.

The contact between the carbonate of lithostratigraphic Unit III and the volcanic rocks of Unit IV at 725 mbsf is marked by an increase in scatter in the velocity data (Fig. 42). Sonic velocities in the andesite breccia vary from 2500 to 5800 m/s. Velocities are higher, ranging from 3800 to 5500 m/s, in zones containing unaltered andesite clasts in a palagonitic matrix (Subunits IVB and IVD; see "Igneous Petrology"

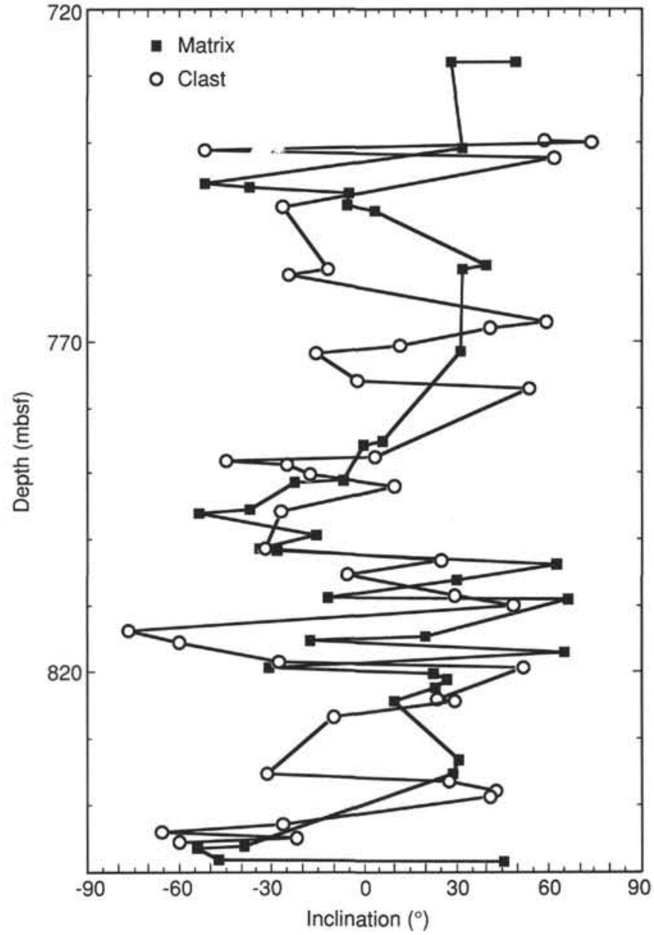

Figure 40. Inclination (after demagnetization at 200°C or 10 mT) as a function of depth from clasts and matrix of andesite breccia in Hole 831B.

section, this chapter). However, in zones containing andesite breccia with oxidized fragments and some reworked clasts (Subunits IVA, IVC, and IVE), sonic velocities decrease slightly, and are generally in the range of 2500–5000 m/s (Fig. 42).

Thermal Conductivity

At Site 831 a total of only eight thermal conductivity measurements were completed in both Holes 831A and 831B (Table 8), owing to the low core recovery. Six of these measurements were made on the andesite breccia of the basement using the "half-space" method, which is described in the "Explanatory Notes" chapter (this volume).

The highest thermal conductivity value recorded on Leg 134 was 2.40 W/(m · K), in foraminiferal grainstone with secondary carbonate cement at the base of the carbonate section (698.8 mbsf) of the Bougainville Guyot. One measurement was also made in each of the five subunits of andesite breccia in the basement rocks (lithostratigraphic Unit IV). Thermal conductivity decreases slightly in Subunit IVC (822.5 mbsf; 1.37 W/[m · K]) and Subunit IVE (843.6 mbsf; 1.13 W/[m · K]), which consist of andesite breccia with oxidized fragments and some reworked clasts. The lower thermal conductivity values correlate with index properties measurements, which show these two subunits to have higher water content than the other three subunits in the basement rocks (Fig. 42).

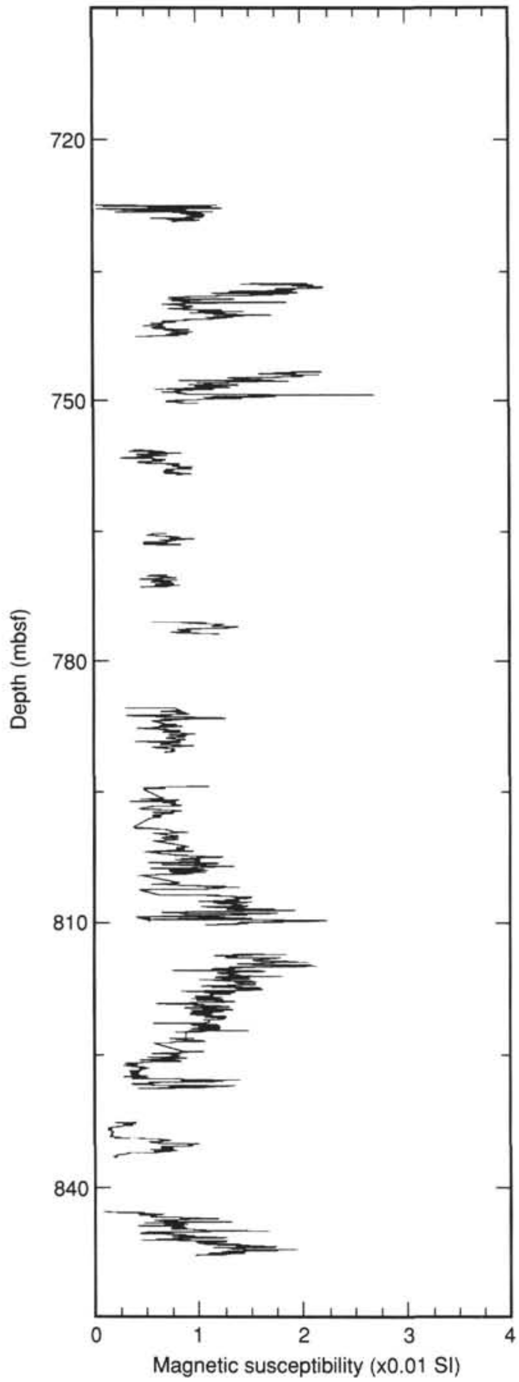

Figure 41. Magnetic susceptibility as a function of depth in Hole 831B.

DOWNHOLE MEASUREMENTS

Logging Operations

A complete set of high-quality logging data was collected at Hole 831B. Logging tools used consisted of the standard Schlumberger set of geophysical, formation microscanner (FMS), and geochemical strings, followed by the susceptibility and magnetometer tools and finally by the digital borehole televiewer (BHTV). Except for a leak in the logging cable that occurred during the FMS run, logging operations went smoothly. The maximum depth the tools reached decreased from one run to another, as a result of hole filling from debris falling from unstable parts of the hole. The first logging run reached 818 mbsf whereas the final logging run reached 741 mbsf.

Log Quality

Logging data recorded at Hole 831 are generally of good quality. The hole diameter is generally less than 15 in., although zones of larger diameters exist between 150–190 mbsf, 250–260 mbsf, 370–385 mbsf, 625–660 mbsf, and 685–700 mbsf. The hole is quite elliptical in cross-section, as determined by the BHTV and FMS logs. The elliptical hole resulted in considerable cycle-skipping in the sonic logs. The data were reprocessed to eliminate cycle-skipping but are still of only low to moderate quality. More thorough reprocessing of the data using a semblance-analysis technique on the waveforms will be done and the results will be presented in the *Scientific Results* volume. Resistivity, sonic, and caliper logs correlate well with each other and indicate the positions of alternating soft and hard layers in both carbonates and basement rocks. As at Sites 829 and 830, references made to geochemical content are qualitative only; geochemical data will be reprocessed during shore-based studies and presented in the *Scientific Results* volume. The very low values in geochemical logs (except for iron) in the upper part of Hole 831B (0–82 mbsf) result from logging through the pipe.

Logging Results

The well logs from the standard Schlumberger tools (run 1 and 3) are briefly analyzed here with respect to the lithostratigraphy (see "Lithostratigraphy" section, this chapter). Lithostratigraphic Units II, III, and IV are readily distinguished in the logs. The most useful logs for lithostratigraphic correlation at this hole are gamma ray, uranium, potassium, calcium, and photoelectric effect (PEF).

Lithostratigraphic Unit II is characterized by a high and variable gamma-ray and uranium logs. The gamma-ray values of pure carbonate are usually low, and the logs from Hole 831B show that most of the gamma rays in the unit are produced by uranium. The uranium content in Unit II is generally 2–4 ppm but some zones have values up to 10 ppm. Uranium is often biogenically scavenged from seawater, and corals are more efficient at this than molluscs. The zones of very high uranium concentration may represent remobilization of already concentrated uranium from corals at times of reef emergence. No other logs show as striking correlation with the abundance of corals as do the gamma-ray and uranium logs. There often are local increases in the resistivity values in the areas of higher gamma rays but the increases in resistivity extend below the depths of the gamma-ray increases.

The transition between lithostratigraphic Units II and III at 425 mbsf is characterized by a net decrease in gamma-ray and uranium values in Unit III. In comparison with lithostratigraphic Unit II, Unit III has a generally higher calcium yield from the geochemical logs. We must repeat, however, that this is based on the preliminary *normalized* geochemical results. The geochemical results will be reprocessed to elemental abundances and published in the *Scientific Results* volume. Although uranium content diminishes drastically from lithostratigraphic Unit II to Unit III (typically 1–2 ppm), spectral gamma-ray logs in Unit III are still driven primarily by uranium. The uranium content increases and becomes more variable with depth in Unit III. Compared to the upper part of Unit III, a more radioactive and more resistive layer is identified between 520 and 620 mbsf, most likely indicating the presence of corals. Note also that both the velocity and the quality of the sonic logs decrease in this interval compared

Table 6. Index properties data, Site 831.

Sample (cm)	Depth (mbsf)	Unit	Wet-bulk density (Mg/m^3)	Dry-bulk density (Mg/m^3)	Grain density (Mg/m^3)	Porosity Wet (%)	Porosity Dry (%)	Water content Wet (%)	Water content Dry (%)
134-831A-									
1H-1, 10	0.10	I	1.66	0.97	2.78	67.9	66.4	41.8	71.9
1H-3, 90	3.90	I	1.78	1.16	2.74	60.1	58.8	34.6	52.9
2H-1, 80	5.20	I	1.88	1.21	2.72	65.8	60.0	35.8	55.9
2H-2, 59	6.49	I	1.65	0.94	2.69	69.8	67.0	43.2	76.1
3H-1, 52	6.92	I	1.81	1.19	2.70	59.8	57.8	33.9	51.3
2H-3, 59	7.99	I	1.66	0.96	2.75	68.3	66.5	42.2	73.0
2H-4, 59	9.49	I	1.73	1.05	2.64	66.8	63.0	39.5	65.2
3H-3, 52	9.92	I	1.78	1.11	2.75	64.8	61.8	37.4	59.6
2H-5, 59	10.99	I	1.77	1.11	2.79	64.7	62.3	37.5	59.9
2H-6, 59	12.49	I	1.81	1.14	2.78	65.0	61.6	36.9	58.4
3H-5, 52	12.92	I	1.59	0.83	2.79	73.9	71.5	47.6	90.8
2H-7, 55	13.95	I	1.71	1.13	2.28	55.8	53.2	33.5	50.4
3H-6, 52	14.42	I	1.55	1.06	2.80	47.5	55.8	31.4	45.7
3H-7, 43	15.83	I	1.72	1.01	2.67	69.2	65.0	41.3	70.3
6X-1, 25	20.25	IIA	2.07	1.62	2.75	44.4	43.2	21.9	28.1
8X-CC, 13	39.23	IIA	2.33	2.00	2.79	32.6	31.4	14.3	16.7
10X-CC, 10	58.10	IIA	2.42	2.13	2.83	28.1	27.3	11.9	13.5
13N-1, 17	88.17	IIA	2.37	2.08	2.73	28.0	27.0	12.1	13.8
134-831B-									
5R-1, 55	131.45	IIB	2.04	1.58	2.76	45.1	44.3	22.6	29.2
6R-CC, 14	134.04	IIB	2.62	2.37	2.80	24.5	22.6	9.6	10.6
5R-3, 55	134.45	IIB	2.08	1.61	2.75	45.7	44.1	22.6	29.1
30R-CC, 0	352.30	IID	2.66	2.43	2.73	22.6	20.4	8.7	9.5
40R-CC, 20	449.10	IIIA	2.69	2.61	2.67	8.1	7.7	3.1	3.2
49R-CC, 0	534.60	IIIA	3.07	3.01	3.06	5.9	5.7	2.0	2.0
59R-CC, 20	631.50	IIIC	2.80	2.76	2.77	3.8	3.7	1.4	1.4
63R-CC, 10	670.34	IIID	3.26	3.24	3.24	1.5	1.5	0.5	0.5
65R-CC, 4	688.14	IIID	1.90	1.31	2.72	57.7	54.7	31.0	45.0
66R-1, 4	697.84	IIID	2.77	2.77	2.77	0.0	0.0	0.0	0.0
67R-1, 4	707.54	IIID	2.46	2.20	2.71	25.5	24.0	10.6	11.8
69R-1, 82	727.62	IVA	2.35	2.14	2.56	20.7	20.0	9.0	9.9
69R-2, 70	728.89	IVA	2.63	2.49	2.69	14.0	13.2	5.4	5.7
69R-3, 25	729.61	IVA	2.47	2.26	2.30	21.1	17.8	8.7	9.6
70R-1, 66	737.06	IVA	2.80	2.60	2.73	19.1	16.8	7.0	7.5
70R-2, 12	737.83	IVA	2.89	2.66	2.70	22.2	18.5	7.9	8.6
70R-3, 12	739.27	IVA	2.66	2.63	2.63	3.2	3.1	1.2	1.2
70R-4, 102	741.54	IVB	2.44	2.25	2.64	18.9	18.2	7.9	8.6
71R-1, 90	746.90	IVB	2.66	2.57	2.57	9.1	8.4	3.5	3.6
71R-3, 75	749.69	IVB	2.58	2.42	2.70	15.2	14.6	6.0	6.4
72R-1, 50	756.10	IVB	2.39	2.18	2.66	20.2	19.9	8.7	9.5
72R-3, 47	759.07	IVB	3.05	2.85	2.86	19.3	16.3	6.5	6.9
73R-1, 87	766.17	IVB	2.50	2.32	2.62	17.3	16.5	7.1	7.7
73R-2, 101	767.81	IVB	2.66	2.62	2.66	3.2	3.2	1.3	1.3
74R-1, 47	770.57	IVB	2.52	2.29	2.59	22.8	20.7	9.3	10.2
75R-2, 100	778.10	IVB	2.60	2.49	2.66	10.7	10.3	4.2	4.4
76R-2, 63	786.93	IVB	2.26	1.96	2.60	29.8	28.5	13.5	15.6
77R-1, 90	795.30	IVC	2.20	1.96	2.36	24.1	22.7	11.2	12.6
77R-3, 90	797.65	IVC	2.69	2.57	2.68	12.4	11.6	4.7	4.9
78R-1, 60	799.70	IVC	2.69	2.56	2.66	12.4	11.5	4.7	4.9
79R-2, 4	801.34	IVC	2.99	2.86	2.87	12.1	10.9	4.1	4.3
79R-3, 115	803.86	IVC	2.60	2.52	2.53	7.2	6.8	2.8	2.9
80R-1, 44	804.54	IVC	2.38	2.12	2.76	25.7	25.3	11.1	12.5
80R-3, 40	807.35	IVC	2.19	1.83	2.75	36.1	35.4	16.8	20.2
80R-5, 45	810.27	IVC	2.28	1.97	2.74	30.5	30.0	13.7	15.9
81R-2, 36	814.86	IVC	2.61	2.31	2.84	29.3	26.7	11.5	13.0
81R-4, 49	817.65	IVC	2.82	2.51	2.76	29.4	24.6	10.7	12.0
81R-6, 66	820.72	IVC	2.80	2.74	2.74	5.7	5.4	2.1	2.1
82R-2, 75	825.65	IVD	2.64	2.41	2.76	22.0	20.2	8.5	9.3
82R-4, 75	828.65	IVD	2.69	2.53	2.72	15.6	14.5	5.9	6.3
83R-2, 95	835.38	IVD	2.36	2.07	2.74	28.3	27.5	12.3	14.0
83R-4, 102	838.13	IVE	2.76	2.64	2.73	12.5	11.5	4.6	4.8
84R-2, 98	845.14	IVE	2.95	2.65	3.56	29.7	28.7	10.3	11.5
84R-4, 102	848.10	IVE	2.58	2.31	2.97	26.6	25.7	10.6	11.8

with the upper part of Unit III. Some of the lithostratigraphic subunits defined in Unit III are reflected in the logs. For example, the uranium calcium content is higher in Subunit IIIB than in Subunit IIIC. Compared to adjacent Subunits IIIA and IIIC, Subunit IIIB is also identified by higher resistivity and velocity as well as by a smaller hole diameter, all of which indicate a more cemented formation. Subunit IIIA is not a clear single subunit as defined by the logs but can be subdivided according to the very low uranium content with little variation between 425 and 520 mbsf compared to the higher and more variable values below 520 mbsf. Several peaks in calcium are observed in geochemical logs of Subunits

Table 7. Hamilton Frame sonic velocity data, Site 831.

Sample (cm)	Depth (mbsf)	Unit	Vertical velocity (m/s)	Wave type[a]	Horizontal velocity (1) (m/s)	Wave type[a]	Horizontal velocity (2) (m/s)	Wave type[a]
134-831A-								
1H-1, 10	0.10	I	1596	C	1607	C		
1H-3, 90	3.90	I	1625	S			1635	S
2H-1, 80	5.20	I	1664	S			2086	S
6X-1, 1	20.01	IIA	2577	C				
8X-CC, 13	39.23	IIA	1895	S			1953	S
10X-CC, 10	58.10	IIA	1953	C			2164	C
13N-1, 17	88.17	IIA	1961	C			1933	C
2R-CC, 0	102.40	IIB	2856	S	4046	C	4130	C
16R-CC, 0	217.80	IIB	4973	C	4723	C		
18R-1, 110	238.30	IIB	3854	C			4041	C
22R-CC, 0	275.20	IIC	4556	C	4008	S	5094	C
27R-CC, 0	323.40	IIC	4515	S			4502	S
30R-CC, 0	352.30	IID	4503	C			4408	C
33R-CC, 0	381.30	IID	4986	C	4661	C	4836	C
36R-CC, 0	410.30	IID	4792	C	5213	C	5270	C
40R-CC, 20	449.10	IIIA	4107	C	3926	C	4143	C
44R-CC, 0	487.20	IIIA	4882	C	4868	C		
47R-CC, 0	515.70	IIIA	4017	C	4013	C	4017	C
49R-CC, 0	534.60	IIIA	4164	C	4410	C	4583	C
53R-CC, 20	573.50	IIIA	4154	C	4107	C	4171	C
56R-CC, 0	602.30	IIIB	4224	C	3635	C	3631	C
59R-CC, 20	631.50	IIIC	4603	C	4897	C	5075	C
63R-CC, 10	670.34	IIID	5765	C	5728	C	5702	C
65R-CC, 18	688.28	IIID	4622	C				
66R-1, 4	697.84	IIID	4825	C				
69R-1, 82	727.62	IVA	3062	C	2993	C		
69R-2, 70	728.89	IVA	4408	C	3774	C		
69R-3, 25	729.61	IVA	3965	C	4078	C		
70R-1, 66	737.06	IVA	3480	C	3161	C		
70R-2, 80	738.51	IVA	3541	C				
70R-3, 12	739.27	IVA	5670	C	5513	C		
70R-4, 102	741.54	IVB	3775	C	3943	C		
71R-1, 90	746.90	IVB	3929	C	4122	C		
71R-3, 75	749.69	IVB	5230	C	5454	C		
72R-1, 50	756.10	IVB	3803	C			3657	C
72R-3, 47	759.07	IVB	4151	C			4199	C
73R-1, 87	766.17	IVB	4162	S			3966	C
73R-2, 101	767.81	IVB	5560	S	3555	S	3392	S
74R-1, 47	770.57	IVB	3936	C	4050	C		
75R-2, 100	778.10	IVB	5333	C			3115	S
76R-2, 63	786.93	IVB	3521	C			2945	C
77R-1, 90	795.30	IVC	3256	C			3196	C
77R-3, 90	797.65	IVC	5145	C			4792	C
78R-1, 60	799.70	IVC	3522	C	3600	C		
79R-2, 4	801.34	IVC	4129	C	3952	C		
79R-3, 115	803.86	IVC	5837	C	5667	C		
80R-1, 44	804.54	IVC					4383	C
80R-3, 40	807.35	IVC	3080	C			2946	C
80R-5, 45	810.27	IVC	3183	C			3148	C
81R-2, 36	814.86	IVC	3548	C			3392	C
81R-4, 49	817.65	IVC	3341	C			3265	C
81R-6, 66	820.72	IVC	4355	C			3638	C
82R-2, 75	825.65	IVD	4045	C			3862	C
82R-4, 75	828.65	IVD	5121	C			5278	C
83R-2, 95	835.38	IVD	4126	C	4014	C		
83R-4, 102	838.13	IVE	4718	A			4307	C
84R-2, 97	845.13	IVE	3165	C			3712	C
84R-4, 107	848.15	IVE	2539	C	2742	C	2725	C

[a] C = compressional (*P*-wave) and S = shear (*S*-wave).

IIIC and IIID (for example, at 675–685 mbsf and 698–704 mbsf) and correlate with an increase in resistivity and low contents of chlorine and hydrogen. These peaks reflect the existence of brown silty clay in Core 134-831B-65R and the yellowish brown wackestone with clay in Core 134-831B-66R. The presence of other peaks with the same signature in the logs at 572–577 mbsf and 610–615 mbsf suggests that the clays are thicker and more abundant than indicated in the cores.

Of all the logs related to physical properties, the PEF shows best the Unit III–Unit IV contact between carbonates and the andesite breccia. PEF is inversely related to the electron density in the formation, which is itself proportional to the formation density (to a first approximation). The decrease in the PEF log observed at 733 mbsf indicates a change to a much higher density lithology. At this transition, uranium decreases drastically and potassium increases, which globally results in a decrease of gamma ray. Geochemical logs show that andesite breccia contains higher yields of iron and silicon and lower yields of calcium than in the overlying carbonate rocks. Geophysical logs of the andesite breccia indicate higher resistivity and velocity values than are recorded in the overlying carbonate sequence. The geophysical

Table 8. Thermal conductivity data, Site 831.

Core, section interval (cm)	Depth (mbsf)	Unit	Value (W/[m · K])
134-831A-			
1H-2, 75	2.25	I	0.9658
1H-3, 75	3.75	I	1.0866
134-831B-			
66R-CC, 1	698.76	IIID	2.4000
70R-1, 35	736.75	IVA	1.4900
71R-2, 88	748.35	IVB	1.4200
81R-7, 93	822.49	IVC	1.3700
83R-2, 1	834.44	IVD	1.6500
84R-1, 90	843.60	IVE	1.1300

Table 9. Shear-strength data, Site 831.

Sample (cm)	Depth (mbsf)	Unit	Undrained shear strength[a] (kPa)
134-831A-			
1H-1, 5	0.05	I	6.6
1H-3, 92	3.92	I	56.5
2H-1, 77	5.17	I	24.2
6R-1, 25	20.25	I	9.5

[a] Values determined by Wykeham-Farrance spring vane- shear apparatus.

logs show a more gradual change in physical properties between Unit III and Unit IV than the abrupt change in the geochemical logs.

FMS Results

Because of the relatively small diameter of the hole, the contact between the four FMS pads with the borehole wall was generally good, resulting in 600 m of reliable FMS data. Most of the data were processed aboard the *JOIDES Resolution*. The processed FMS data are presented in microfiche at the back of this volume. A second FMS pass was run from 763 to 552 mbsf to double the coverage of the hole. Because of rotation of the tool in the hole, double coverage was not possible in some intervals. An example FMS image in which both passes were successful is presented in Figure 43. A change in resistivity marks the contact between carbonate and andesite breccia at 733.5 mbsf. The images show high resistivity contrasts and indistinctly outlined vuggy features that correspond to the vuggy porosity of the recovered cores. Resistivity is much more uniform in the andesite breccia—the contrast is less, and round resistive features are distinctively seen in a more conductive matrix. The contact between lithostratigraphic Units III and IV is sharp and localized, as was observed in the cores (see "Lithostratigraphy" section, this chapter).

BHTV Results

BHTV logging was performed from the bottom of the hole at 740 mbsf to the end of the drill pipe at 90 mbsf. Most of the open hole was logged twice with the second run also starting at the bottom of the borehole.

The carbonate-andesite breccia contact between lithostratigraphic Units III and IV is quite distinct. The borehole cross-section increases continuously from 800 mm^2 in the breccia at 725 mbsf to 950 mm^2 at 720 mbsf in the carbonate (Fig. 44).

Only a few planar structures intersected the borehole between 730 and 90 mbsf (Fig. 45). These structures had dips between 30° and 60° and most were in the lower part of the hole. No structures were observed in the interval from 420 to 520 mbsf. Azimuths of the dip directions are widely scattered and no preferred orientation is obvious (Fig. 45).

The shapes of borehole cross-sections observed in the BHTV data vary from circular to pear-shaped to highly ellipsoidal (Fig. 46). The change in cross-sectional shape apparently does not result from changes in borehole deviation. Deviation ranges only between 2° and 4°, whereas the changes in cross-sectional shape may reflect change in some physical properties or other lithology.

Fractures and changes in the cross-sectional shape of the borehole observed on BHTV data can be correlated with individual increases and zones of increased gamma rays (Fig. 47). Figure 47 shows the spectral gamma-ray log with these features marked numerically as follows:

1. Individual peaks or intervals of increased gamma rays are associated with a fracture or an interval bounded with a fracture (number 1 in Fig. 47).
2. An increase in gamma rays is associated with a change in the cross-sectional shape of the borehole (number 2 in Fig. 47).

Heat Flow

Two runs of the water sampler temperature probe (WSTP) temperature tool were performed at Site 831, both of which were successful. The data reduction techniques used at this site were the same as at previous sites. The thermal conductivity values are reported in the "Physical Properties" section (this chapter) (Table 8).

The individual temperature measurements are discussed below. Determination of the mudline reference temperature was a problem because of the shallow depth of this site (similar to Site 830). The water column has a significant vertical temperature gradient, so stopping the probe at a different depth gives a different reference temperature. Temperature run 9X in Hole 831A (Fig. 48), done at a depth of 48.6 mbsf, displays an adequate temperature decay curve. The reduction to equilibrium temperature is plotted in Figure 49. Run 13X in Hole 831A at 87.0 mbsf is illustrated in Figure 50. The temperature probe was all the way in the sediment as shown by the considerable frictional heating when the probe was removed from the bottom. The reduction to equilibrium temperature for this run is given in Figure 51.

The temperatures at the seafloor for the two runs differ substantially, probably because of errors in the calibrations between the two WSTP instruments, so the differences in temperature between the seafloor and the equilibrium sediment temperature have been used at this site. The two temperatures are plotted vs. depth in Figure 52. The limited number of successful thermal conductivity measurements at this site render plots of integrated thermal resistivity meaningless. The mean thermal conductivity in the surficial sediments is close to 1.0 W/(m · K), so that value will be used to calculate the heat flow. The heat flow is a very low value of 6.9 mW/m^2, which may not be representative of the heat flow at depth. Measurements of the heat flow at Eniwetok atoll during the U.S. Atomic Energy Commission–U.S. Geological Survey drilling program in the 1950s found that the atoll was permeable to a great depth and that the surficial temperature gradient was not representative of the heat flow at depth (Swartz, 1958).

SUMMARY AND CONCLUSIONS

Site 831 is located at 16°00.56′S, 166°40.36′E in a water depth of 1066.4 mbsl. This site is located in the center of the summit platform of the Bougainville Guyot, about 42 km

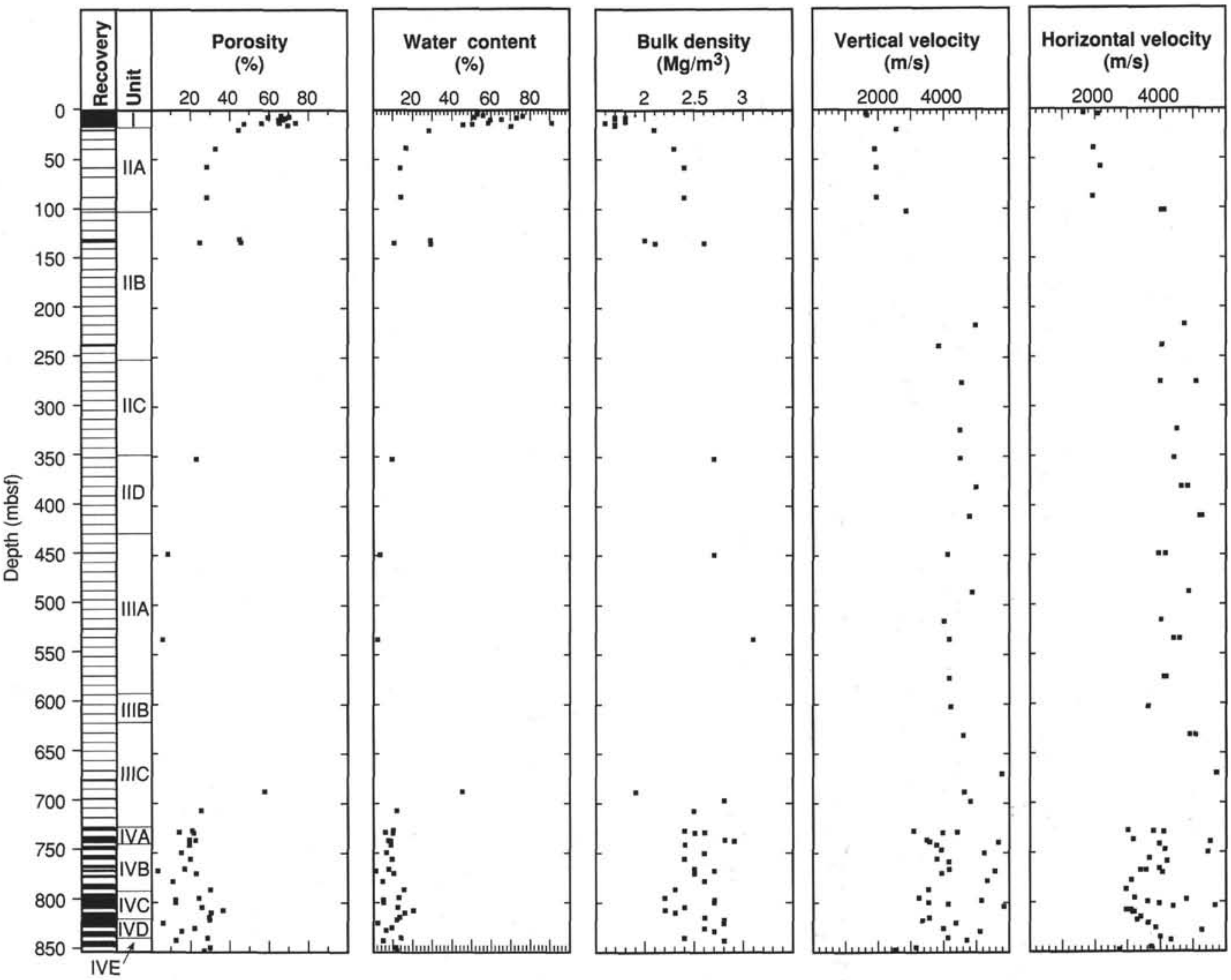

Figure 42. Porosity, water content, bulk density, and sonic velocity vs. depth, Site 831.

southwest of the southern tip of Espiritu Santo Island, about 5 km west of the collision zone between the Bougainville Guyot and the New Hebrides Island Arc, and approximately 15 km due west of Site 830 (Fig. 1). The Bougainville Guyot is a carbonate-capped, flat-topped seamount that represents the eastern end of the South d'Entrecasteaux Chain (SDC). It is being subducted beneath or accreted to the New Hebrides Island Arc where it impinges upon the forearc slope, forming a 10-km indentation. In response to the eastward-dipping subduction zone, the carbonate cap of the guyot is tilted ~5° to the east. Seismic reflection profiles indicate that about one-third of the guyot is buried beneath sediments of the forearc (Fisher et al., in press). Seismic reflection data also show that about 700 m of well-layered sediments make up the carbonate cap. These data, along with Seabeam data, dredge samples, and submersible observations and sampling, show the cap to be lagoonal deposits in an atoll setting (Daniel et al., 1986; Collot et al., 1989; Fisher et al., in press). At Site 831 this lagoon was drilled.

Two holes were drilled at Site 831. Hole 831 was drilled to a total depth (TD) of 115.5 mbsf, with only 25.85 m of core recovered for a recovery rate of 22.4%. Hole 831B was drilled to a TD of 852 mbsf, washed down to 102.4 mbsf, and cored for 749.6 m, recovering only 87.25 m of core for a 11.6% recovery rate.

Four major lithostratigraphic units were defined and described from the two holes of Site 831 (Fig. 53). Lithostratigraphic Unit I (0–16.9 mbsf) is a 16.9-m-thick Pleistocene, pelagic, brown foraminiferal ooze with partially lithified grainstone clasts. This unit has an upper (0.4–3.0 mbsf) bioclastic sed-lithic conglomerate layer and grades downhole into a light yellowish brown bioclastic foraminiferal ooze. Pteropods are especially abundant in the upper part of Hole 831A and are found to comprise an ooze that contains thin laminae of volcanic ash. A prominent black ash layer is present at 14.4 mbsf and is composed of pale brown glass (53%) and opaque grains (25%) that may have resulted from reworking or fractionation during subaerial or submarine settling. The contact between lithostratigraphic Units I and II is marked by an abrupt faunal transition from pelagic microfossils of Unit I to neritic microfossils of Unit II.

Lithostratigraphic Unit II (16.9–429.6 mbsf; 412.7 m thick) is identified and described from both holes at Site 831 (16.9–100 mbsf, Hole 831A; 102.4–429.6 mbsf, Hole 831B) and is a neritic carbonate deposit with a wide diversity of shallow-water organisms. The unit has also been divided into four

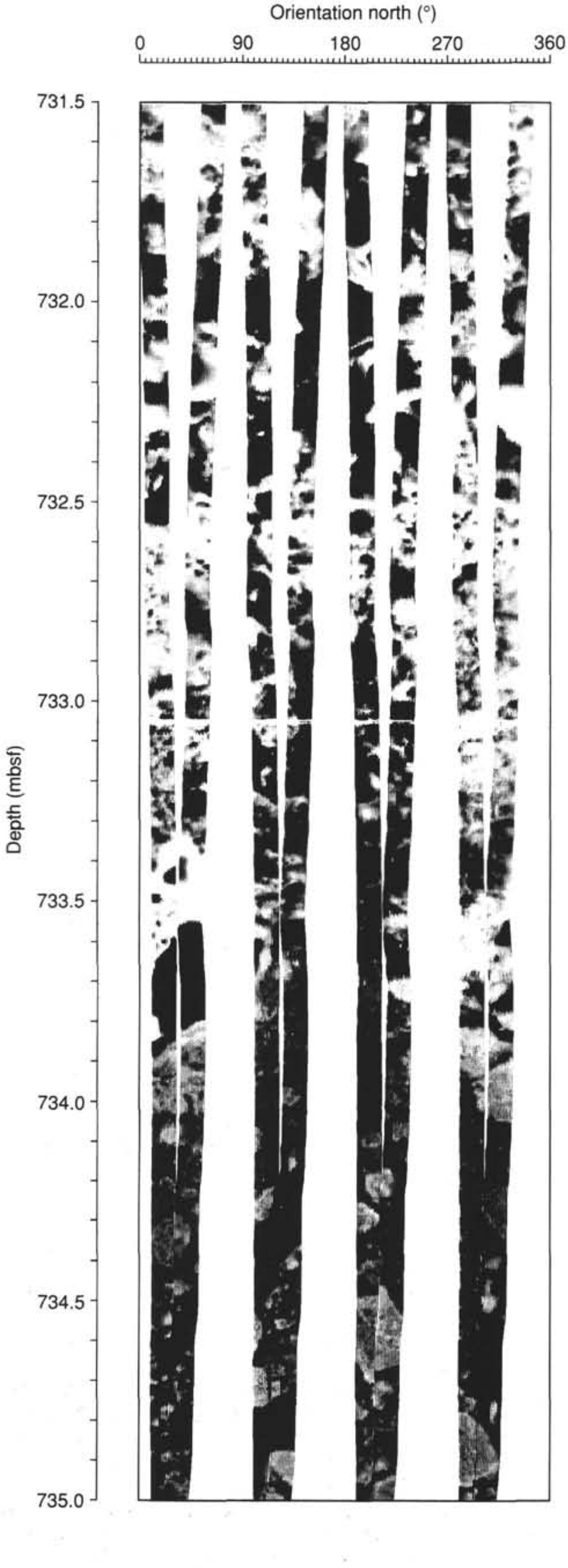

Figure 43. FMS image showing the contact between carbonates and the andesite breccia in Hole 831B. Two passes are merged which produces almost 80% coverage of the borehole (dark is conductive, white is resistive).

subdivisions. Subunit IIA (16.9–100 mbsf) is an 83.1-m-thick, Pleistocene, white coral and bioclastic grainstone and foraminiferal wackestone, which contains specimens of *Acropora* and *Porites* corals. Subunit IIB (102.4–256.0 mbsf) is a 153.6-m-thick, Pliocene(?) to Pleistocene, coral rudstone and mollusc floatstone with fragments of white *Acropora* and *Porites* coral and a large fragment of tridacnid shell; the mollusc floatstone is partially lithified by marine cementation and has abundant primary porosity. Subunit IIC (256.0–352.3 mbsf) is a 96.3-m-thick, coral rudstone and mollusc floatstone of indeterminate age with extensive carbonate dissolution (moldic and vuggy porosity forms 10%–15% of rock). A well-preserved *Porites* coral head and tridacnid shell fragment were recovered from this subunit. Subunit IID (352.3–429.6 mbsf) is a 77.3-m-thick, white, well-lithified bioclastic floatstone of indeterminate age with marine and abundant secondary carbonate cement that may have precipitated from meteoric waters.

Lithostratigraphic Unit III (429.6–727.5 mbsf) is a 297.9-m-thick, neritic carbonate deposit containing an abundance of molluscs and large benthic foraminifers. The contact between lithostratigraphic Units II and III coincides with a distinct facies change; Unit II is a coral- and mollusc-rich facies and Unit III is a mollusc- and foraminiferal-rich facies. This contact is also distinguishable by a sharp increase in carbonate dissolution and cementation. Lithostratigraphic Unit III is further subdivided into four subunits.

Subunit IIIA (429.6–592.6 mbsf) is a 163-m-thick, white, bioclastic floatstone of indeterminate age that is highly altered and extensively dissolved, with abundant secondary cement and contains coralline algae. This subunit was hard to drill.

Subunit IIIB (592.6–621.6 mbsf) is a 29-m-thick, lower Miocene, well-cemented bioclastic floatstone and foraminiferal grainstone with abundant vuggy and moldic porosity. Mottling suggests burrowing (bioturbation). This subunit was easily drilled compared to Subunits IIIA and IIIB.

Subunit IIIC (621.6–669.2 mbsf) is a 47.6-m-thick, upper Oligocene, white to very pale brown bioclastic and foraminiferal grainstone with minor amounts of moldic porosity. This subunit was hard and drilling was slow.

Subunit IIID (669.2–727.5 mbsf) is a 58.3-m-thick, upper Oligocene, well-lithified bioclastic and algal packstone and foraminiferal grainstone with distinct burrowing in the packstone. This subunit has marine cement and abundant veins of chlorite. Forty percent of the rock is composed of coralline algae (both encrusting and branching forms) and 15% of the rock shows moldic and vuggy porosity. Two soil horizons occur within Subunit IIID. The first horizon consists of a reddish brown, silty clay, sensu stricto Terra Rosa, with high water content (45%) and porosity (57.7%), and with low bulk density (1.90 Mg/m^3) at 688.1 mbsf. The second is a very pale brown foraminiferal wackestone with yellowish brown and red streaked clays at 707.6 mbsf that has lower water content (11.8%) and porosity (25.5%), and higher bulk density (2.46 Mg/m^3) than the upper soil horizon.

Lithostratigraphic Unit IV (727.5–852 mbsf) is an andesitic hyalo-breccia composed of two-pyroxene andesite clasts or blebs in a matrix of lithic fragments, crystals, and glass; in places it is a palagonite breccia. Hole 831B penetrated 124.5 m of the andesites; the TD of the hole is within this unit at 852 mbsf. Unit IV is barren of microfossils and hence its age is unknown at present. Five subunits were defined for Unit IV based on what appears to be a cyclicity of eruptive events or depositional conditions.

Subunit IVA (727–741 mbsf) is a 14-m-thick andesitic breccia with thin beds of reworked grit and sandstone,

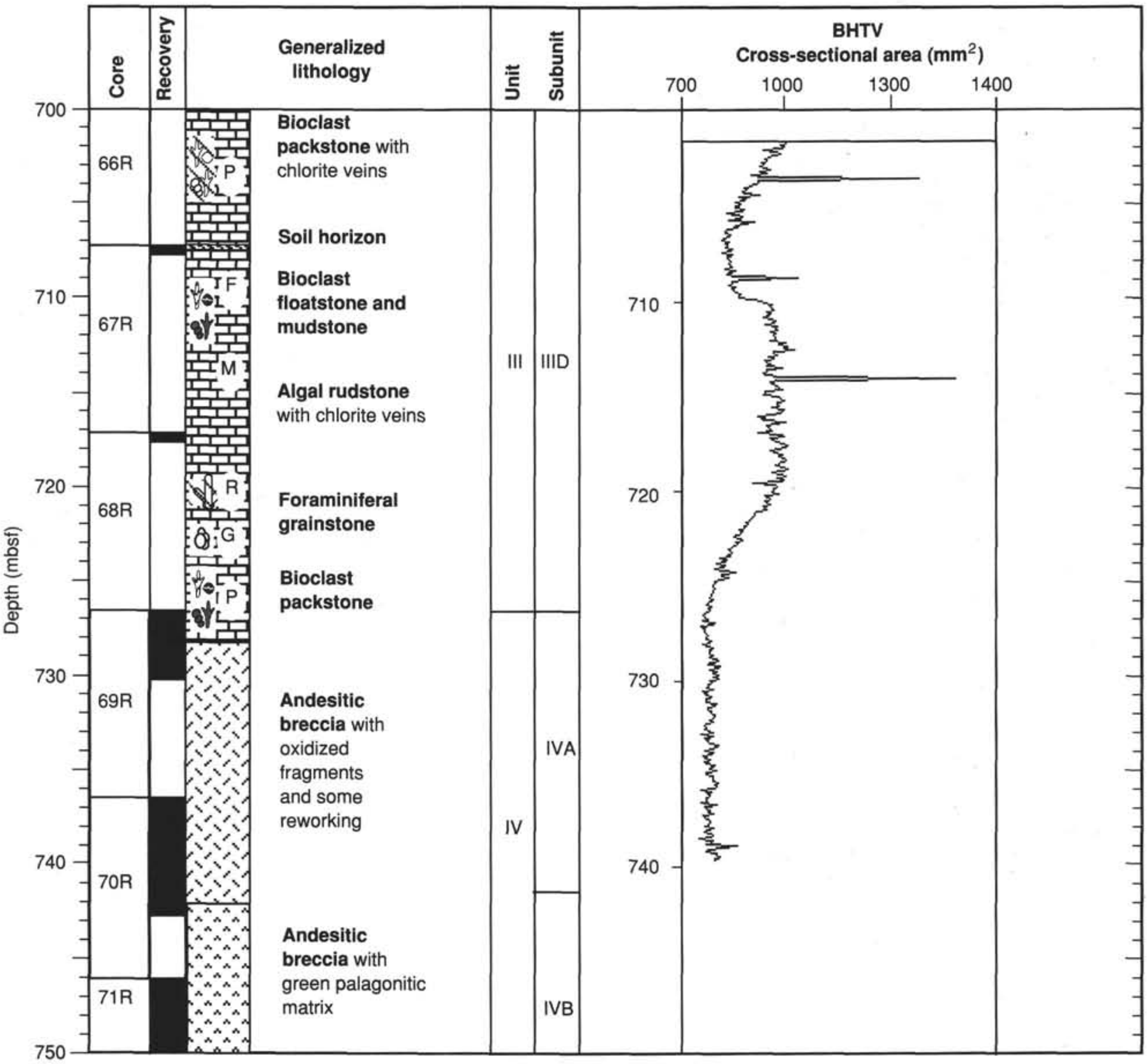

Figure 44. Change in lithology compared with cross-sectional area at the carbonate/basement contact in Hole 831B. For key to lithologic symbols, see Figure 8.

strongly oxidized at the top of the subunit (probably the result of subaerial weathering). Large clasts of volcanic fragments become progressively more abundant (20%) near the bottom of the subunit.

Subunit IVB (741–789 mbsf) is a 48-m-thick andesitic breccia composed of subrounded, wispy andesite blebs within a pale green matrix.

Subunit IVC (789–822 mbsf) is a 33-m-thick coarse-grained breccia that includes pale reddish fragments interbedded with grits and sandstone. Subunit IVD (822–838 mbsf) is a 10-m-thick breccia that consists almost exclusively of well-defined, gray, fresh andesite blebs with distinct coronas or reaction rims in a grayish matrix. Near the base (837 mbsf), blebs become more diffuse and assume irregular or wispy outlines. Subunit IVE (838–852 mbsf) is a 14-m-thick breccia with reddish lava fragments in a pale green matrix that includes abundant sand-sized fragments of lava with varying degrees of oxidation. Cross-bedded sandstone and grits mark the base of this subunit.

Nannofossils and foraminifers, including large foraminifers preserved in the neritic carbonate rocks, are the only indicators of age. However, due to the soupy nature of much of the pelagic carbonate sequence and poor core recovery of the neritic carbonate sequence, dating of cores was sketchy at best. Only the upper 20 m could be dated by both nannofossils and foraminifers. Assemblages of microfossils analyzed in cores from Site 831 revealed an age of Pleistocene for lithostratigraphic Unit I (0–16.9 mbsf) and the upper part (16.9–20 mbsf) of Unit II. The middle part of Unit II (20–246.4 mbsf) was dated as Pliocene or Pleistocene. From 246 to 563.6 mbsf (the lower part of lithostratigraphic Unit II to the upper part of Subunit IIIA) the cores were barren of microfossils and their age cannot be determined. For the interval from 563.6 to 621.6 mbsf (lithostratigraphic Unit III, from the lower part of Subunit IIIA through Subunit IIIB), an early Miocene (~21.8–23.6 Ma) age was determined based on large foraminifers. Finally, for the interval from 621.6 to 735.7 mbsf (lithostratigraphic Units III and IV and Subunits IIIC, IIID, and the

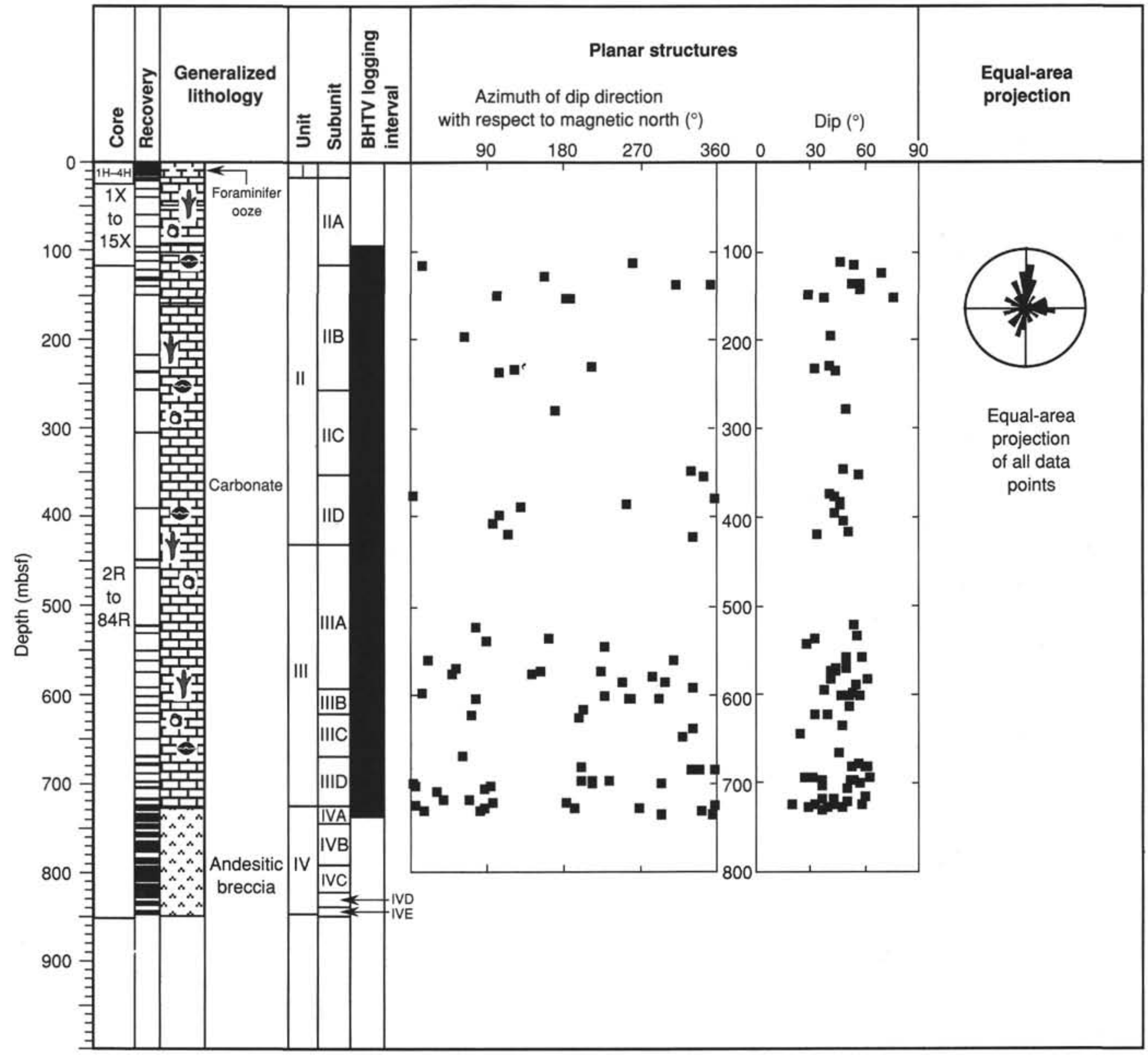

Figure 45. Variation of dip and azimuth of dip direction of planar structures detected with the BHTV at Site 831. Azimuth of dip direction is shown with respect to magnetic north. For key to lithologic symbols, see Figure 8.

upper part of IVA), a late Oligocene (~23.6–28.2 Ma) age was assigned based on large foraminifers. This interval includes the base of the carbonate sequence and the upper surface of the andesite basement rocks.

Depositional environments for the 727.5 m of epiclastic, hemipelagic, and carbonate sediments overlying the andesitic basement rocks of the Bougainville Guyot were determined using benthic foraminifers in epiclastic and hemipelagic sequence and corals and larger foraminifers, as well as the type of carbonate cementation (marine or meteoric) within the carbonate sequence. The Pleistocene pelagic deposits in the upper part (0–6.4 mbsf) of lithostratigraphic Unit I were deposited in the middle bathyal zone (500–2000 mbsl), and from 6.4 to 16.9 mbsf sediments were deposited in an outer sublittoral zone. At 16.9 mbsf, foraminifers indicate that a shallow lagoon environment existed before the drowning of the guyot. From 16.9 to 246.4 mbsf, Subunits IIA and IIB are deposited in an inner sublittoral environment. Below 246.4 mbsf, an inner or outer sublittoral zone appears to be the depositional environment based on both smaller and larger foraminifers. Lithostratigraphic Subunits IIC and IID (256–429.6 mbsf) appear to have been deposited in a shallow-water environment based on the presence of shallow-water fauna. At 612 mbsf, a foraminiferal assemblage indicates an inner shallow platform condition. Pervasive alteration and abundant secondary cement within lithostratigraphic Unit III (429.6–727.5 mbsf) suggest subaerial or near-surface conditions with alteration from meteoric processes.

Only two pore-fluid samples were collected from cores obtained at Site 831. Both samples exhibited solutes that approximate seawater concentrations, with the exception of magnesium, calcium, and sulfate. Calcium is slightly enriched at 135 mbsf and magnesium is depleted, suggesting carbonate

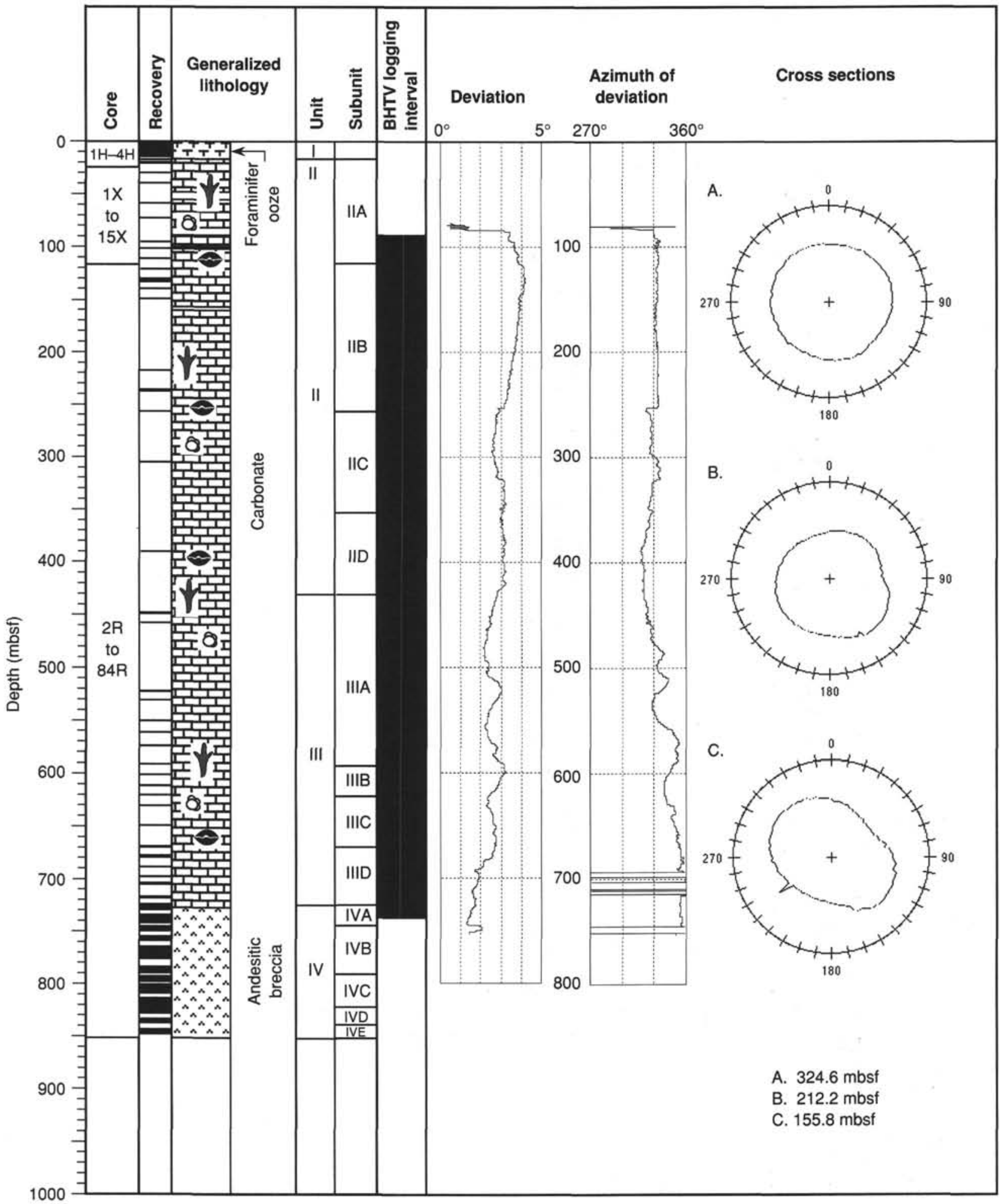

Figure 46. Change in shape of borehole cross-section from BHTV data at three depths. For key to lithologic symbols, see Figure 8.

diagenesis. Organic carbon contents are low, which may account for the minor sulfate reduction.

Based on the preliminary interpretation of the drilling results from Site 831 a general geologic history of the Bougainville Guyot can be inferred. During the late Oligocene or sometime before, late-stage volcanic eruptions completed the building of the submarine edifice or island that has become the Bougainville Guyot. Andesitic hyalo-breccias were emplaced in a manner similar to the formation of pillow lavas and the associated hyaloclastic deposition. Chilled margins or coronas around the clasts of the breccia suggest that miniature pillows developed, and the quenching in seawater caused chilled rinds to spall and be incorporated into a glassy matrix. Oxidized clasts and more vesicular fragments suggest a shallow-water

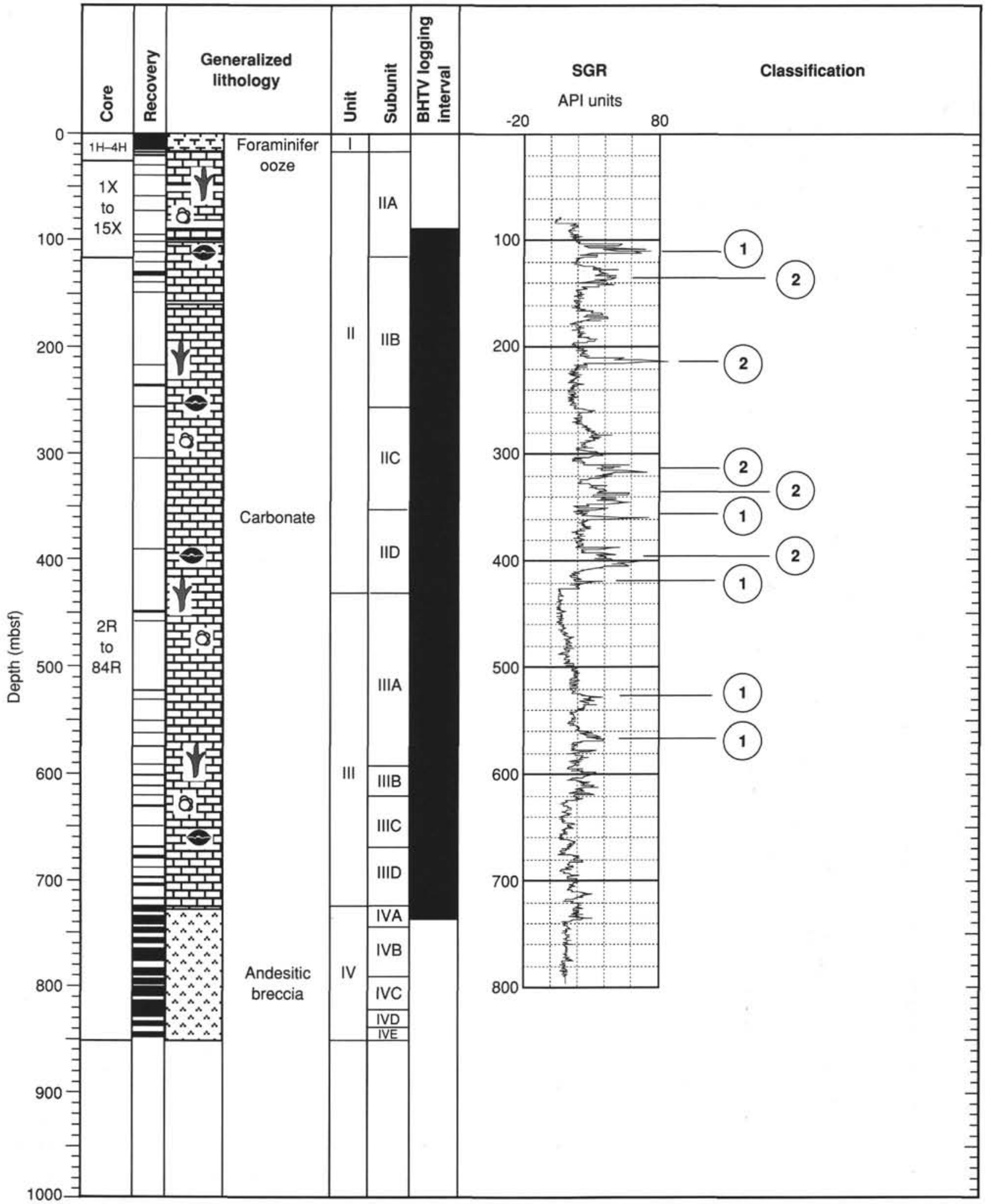

Figure 47. Comparison of change in spectral gamma-ray (SGR) measurements with changes observed in the BHTV at Site 831. Numbers identify the different characters observed in BHTV data (see also text). For key to lithologic symbols, see Figure 8.

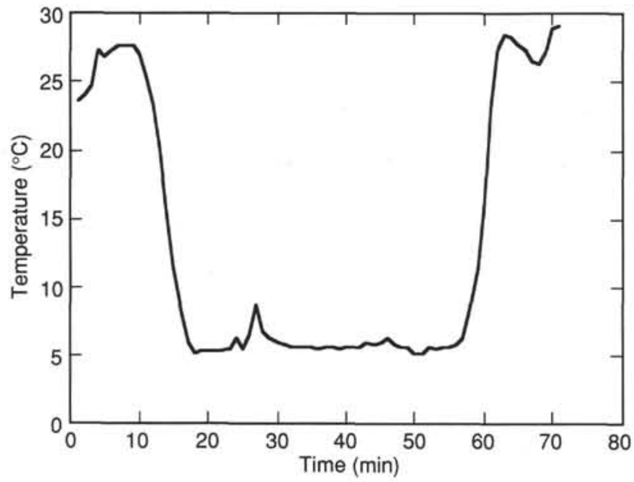

Figure 48. Temperature vs. time for WSTP run 9X in Hole 831A at a depth of 48.6 mbsf.

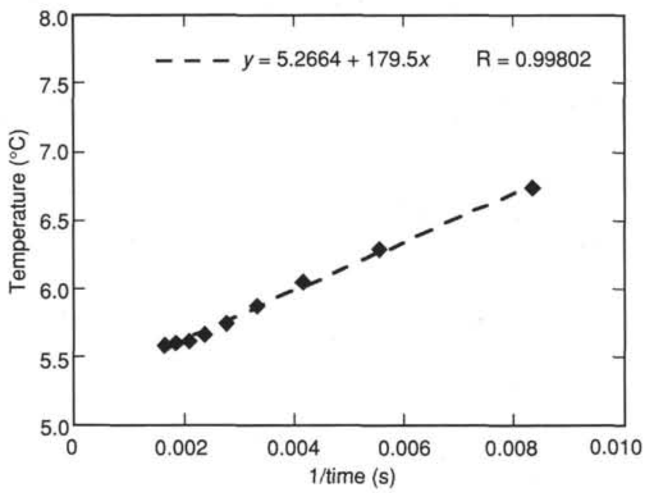

Figure 49. Reduction to equilibrium temperature for WSTP run 9X in Hole 831A. The temperature value at 1/time = 0 is the equilibrium value.

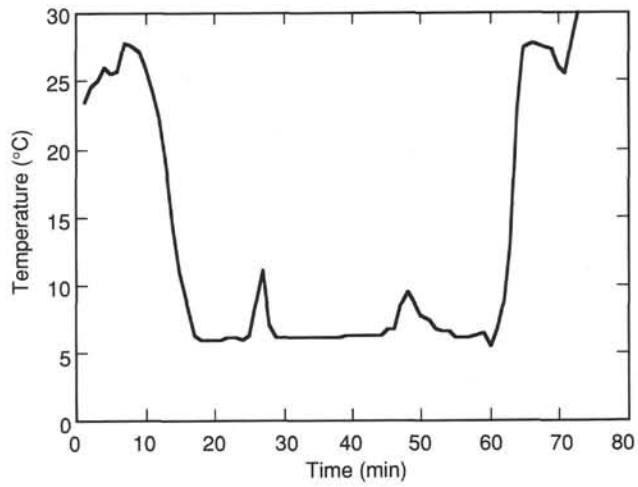

Figure 50. Temperature vs. time for WSTP run 13X in Hole 831A at a depth of 87.0 mbsf.

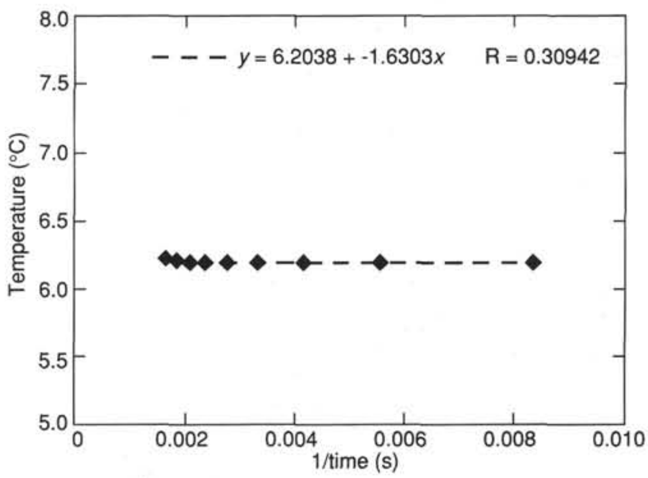

Figure 51. Reduction to equilibrium temperature for WSTP run 13X in Hole 831A. The temperature value at 1/time = 0 is the equilibrium value.

origin, and perhaps the input of subaerial material from an island source. Maximum depth of deposition is, therefore, estimated to be around a few hundred meters. The wispy shapes of the blebs suggest that the magma was still reasonably fluid or plastic at the time of deposition. Deposition of this volcanic rock probably formed an apron around the submarine volcano with some of the more chaotic breccias being deposited by avalanches or debris flows. Petrographic characteristics of the two-pyroxene andesites show calc-alkaline or island-arc tholeiite affinity, indicating that the guyot is unequivocally of island-arc origin.

The Bougainville Guyot appears to have formed along a volcanic island arc that is represented by the SDC. As proposed by Daniel et al. (1977) and Maillet et al. (1983), the DEZ may be an Eocene subduction/obduction zone. The oxidized andesitic rocks of the guyot indicate that the guyot was probably an island before subsidence during the late Oligocene, when it started accumulating the 727.5 m of carbonate rocks. Neritic carbonate sediments were deposited from the Oligocene to early Miocene and at least two episodes of emergence, as indicated by the soil horizons at 688.1 and 707.6 mbsf, occurred during this time. No middle to upper Miocene sediments were identified; the possible absence of these sediments at this site is consistent with a major Miocene hiatus similar to that observed at Site 828 and at Deep Sea Drilling Project (DSDP) Site 286 (Andrews, Packham, et al., 1975). This hiatus may coincide with a facies change in the neritic carbonate sequence at 429.6 mbsf; a coral- and mollusc-rich facies (16.9–429.6 mbsf) overlying a mollusc- and foraminiferal-rich facies (429.6–727.5 mbsf). The Pliocene to Pleistocene neritic carbonates represent lagoonal sediments associated with an atoll. Eastward transport of the guyot upon the Australia-India plate is documented by its submergence/emergence history. As the guyot approached the outer rise of the New Hebrides Island Arc it became quite shallow, similar to the condition that Sabine Bank is experiencing today (Dubois et al., 1988). Then, during the late Pliocene (~2 Ma) or early Pleistocene, the shallow-water carbonate platform drowned, as indicated by the foraminiferal assemblage recovered from 30 mbsf. Foraminiferal assemblages examined from cores at about 20 mbsf indicate that paleodepths were no greater than about 100 mbsl. Major subsidence or sea-level rise and pelagic sedimentation occurred throughout the Pleistocene, as indicated by the foraminiferal assemblages exam-

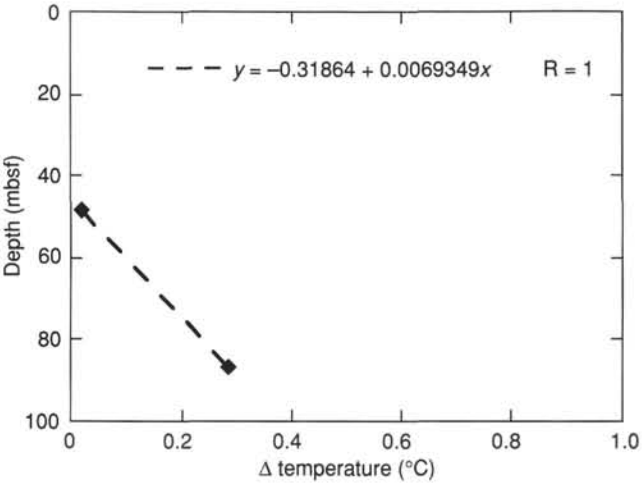

Figure 52. Delta temperature (equilibrium minus mudline temperature) vs. depth below seafloor.

ined from about 20 to 4.5 mbsf. Ash layers found within the pelagic sediments between 0 and 15 mbsf illustrate the influence of volcanic events along the Central Chain of the New Hebrides Island Arc on the guyot. Pelagic deposition and continued subsidence represent the transport of the guyot away from the outer rise and down the subduction zone to its present position on the forearc slope.

REFERENCES

Adams, C. G., 1984. Neogene larger foraminifera, evolutionary and geological events in the context of datum planes. *In* Ikebe, N., and Tsuchi, R. (Eds.), *Pacific Neogene Datum Planes: Contribution to Biostratigraphy and Chronology:* Tokyo (Univ. of Tokyo Press), 47–67.

Andrews, J. E., Packham, G., et al., 1975. *Init. Repts. DSDP,* 30: Washington (U.S. Govt. Printing Office).

Bé, A.W.H., 1977. An ecological, zoogeographic and taxonomic review of Recent planktonic foraminifera. *In* Ramsay, A. (Ed.), *Oceanic Micropaleontology* (Vol. 1): London (Academic Press), 1–100.

Boersma, A., 1978. Foraminifera. *In* Haq, B. U., and Boersma, A. (Eds.), *Introduction to Marine Micropaleontology:* New York (Elsevier), 19–77.

Collot, J.-Y., and Fisher, M. A., 1989. Formation of forearc basins by collision between seamounts and accretionary wedges: an example from the New Hebrides subduction zone. *Geology,* 17:930–933.

Collot, J.-Y., Pelletier, B., Boulin, J., Daniel, J., Eissen, J.-P., Fisher, M. A., Greene, H. G., Lallemand, S., and Monzier, M., 1989. Premiers résultats des plongées de la campagne SUBPSO1 dans la zone de collision des rides d'Entrecasteaux et de l'arc des Nouvelles Hébrides. *C. R. Acad. Sci. Ser. 2,* 309:1947–1954.

Daniel, J., Collot, J. Y., Monzier, M., Pelletier, B., Butscher, J., Deplus, C., Dubois, J., Gérard, M., Maillet, P., Monjaret, M. C., Récy, J., Renard, V., Rigolot, P., and Temakon, S. J., 1986. Subduction et collision le long de l'arc des Nouvelles-Hébrides (Vanuatu): résultats préliminaires de la campagne SEAPSO (Leg 1). *C. R. Acad. Sci. Ser. 2,* 303:805–810.

Daniel, J., Jouannic, C., Larue, B., and Récy, J., 1977. Interpretation of d'Entrecasteaux zone (north of New Caledonia). *Int. Symp. on Geodynamics in South-west Pacific, Noumea, New Caledonia, 1976.* Paris (Editions Technip), 117–124.

Dubois, J., Deplus, C., Diament, M., Daniel, J., and Collot, J.-Y., 1988. Subduction of the Bougainville seamount (Vanuatu): mechanical and geodynamic implications. *Tectonophysics,* 149:111–119.

Dupuy, C., Dostal, J., Marcellot, G., Bougault, H., Joron, J. L., and Treuil, M., 1982. Geochemistry of basalts from central and southern New Hebrides arc: implication for their source rock composition. *Earth Planet. Sci. Lett.,* 60:207–225.

Fisher, M. A., Collot, J.-Y., and Geist, E. L., in press. Structure of the collision zone between Bougainville Guyot and the accretionary wedge of the New Hebrides Island Arc, Southwest Pacific. *Tectonics.*

Fisher, M. A., Collot, J.-Y., and Smith, G. L., 1986. Possible causes for structural variation where the New Hebrides island arc and the d'Entrecasteaux zone collide. *Geology,* 14:951–954.

Fisher, R. V., and Schmincke, H.-U., 1984. *Pyroclastic Rocks:* Berlin (Springer-Verlag), 272–274.

Fryer, P., Pearce, J. A., Stokking, L. B., et al., 1990. *Proc. ODP, Init. Repts,* 125: College Station, TX (Ocean Drilling Program).

Hills, S. J., Thierstein, H. R. 1989. Plio-Pleistocene calcareous plankton biochronology. *Marine Micropaleontology,* 14:67–96.

Jakes, P., and White, A.J.R., 1972. Major and trace element abundances in volcanic rocks of orogenic areas. *Geol. Soc. Am. Bull.,* 83:29–39.

Kennett, J. P., and Srinivasan, M. S., 1983. *Neogene Planktonic Foraminifera: A Phylogenetic Atlas:* Stroudsburg, PA (Hutchinson Ross).

Maillet, P. M., Monzier, M., Selo, M., and Storzer, D., 1983. The d'Entrecasteaux zone (southwest Pacific): a petrological and geochronological reappraisal. *Mar. Geol.,* 53:179–197.

Minster, J. B., and Jordan, T. H., 1978. Present-day plate motions. *J. Geophys. Res.,* 83:5331–5354.

Okada, H., and Bukry, D., 1980. Supplementary modification and introduction of code numbers to the low-latitude coccolith biostratigraphic zonation (Bukry, 1973; 1975). *Mar. Micropaleontol.,* 5:321–325.

Pearce, J. A., 1983. The role of sub-continental lithosphere in magma genesis at destructive plate margins. *In* Hawkesworth, C. J., and Norry, M. J. (Eds.), *Continental Basalts and Mantle Xenoliths:* Nantwich (Shiva), 230–250.

Sartorio, D., and Venturini, S., 1988. *Southern Tethys Biofacies:* Agip S.p.A., S. Donato Milanese.

Saunders, A. D., Tarney, J., and Weaver, S. D., 1980. Transverse chemical variations across the Antarctic Peninsula: implications for the genesis of calc-alkaline magmas. *Earth Planet. Sci. Lett.,* 46:344–360.

Swartz, J. H., 1958. Geothermal Measurements on Eniwetok and Bikini Atolls. *Geol. Surv. Prof. Pap. U.S.,* 711–741.

Taylor, S. R., Arculus, R. J., Perfit, M. R., and Johnson, R. W., 1981. Island arc basalts. *In Basaltic Volcanism on the Terrestrial Planets* (Basaltic Volcanism Study Project): New York (Pergamon Press), 193–213.

van Morkhoven, F.P.C.M., Berggren, W. A., Edwards, A. S., et al., 1986. Cenozoic cosmopolitan deep-water benthic foraminifera. *Bull. Cent. Rech. Explor.-Prod. Elf-Aquitaine,* Mem. 11.

Wilson, M., 1989. *Igneous Petrogenesis: A Global Tectonic Approach:* London (Unwin Hyman).

Ms 134A-111

NOTE: All core description forms ("barrel sheets") and core photographs have been printed on coated paper and bound as Section 4, near the back of this volume, beginning on page 581.

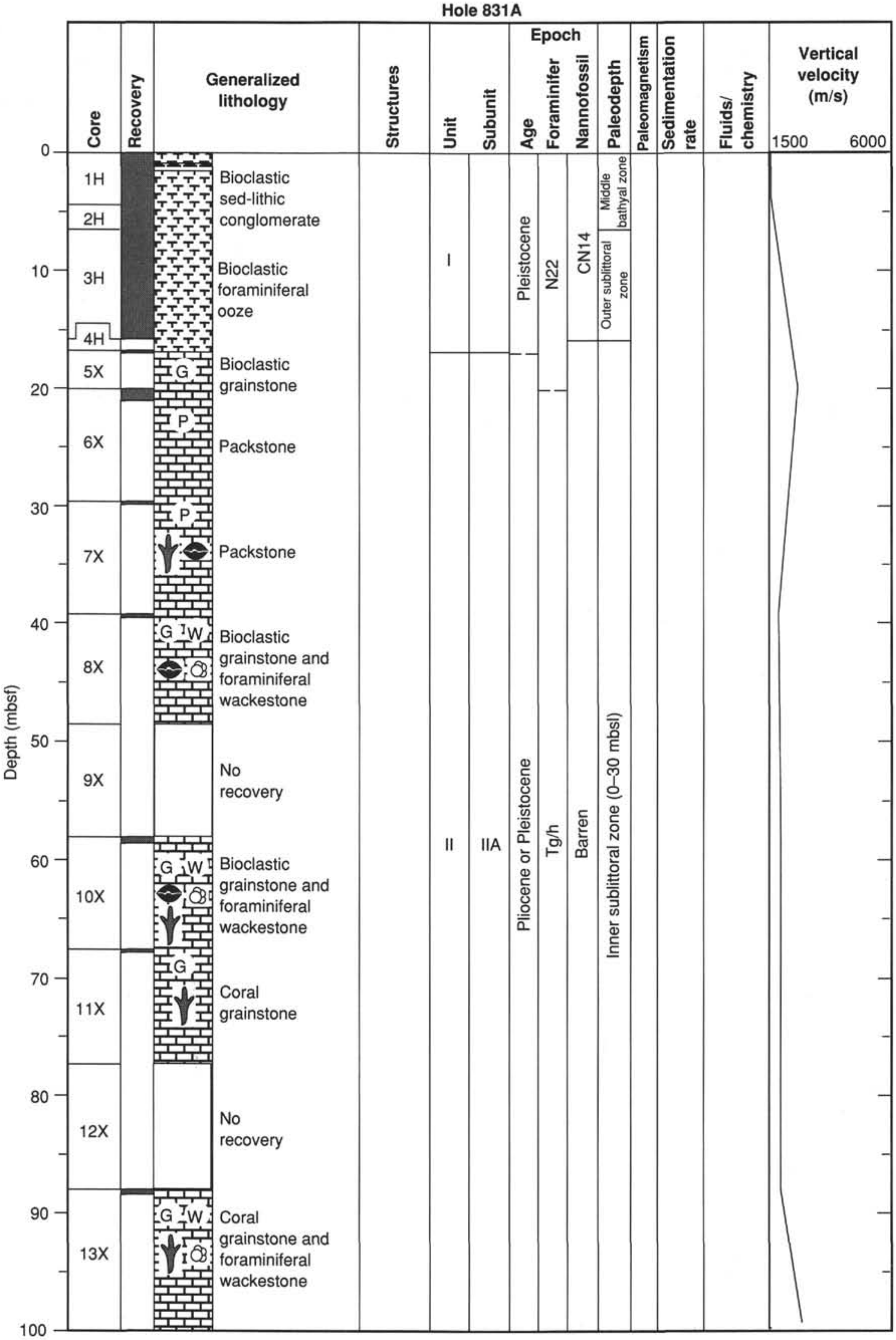

Figure 53. Generalized summary of Holes 831A and 831B (note that Core 134-831B-1W was washed down to 102.4 mbsf). If no data or annotations appear in a particular column, please refer to the appropriate section of this chapter for details.

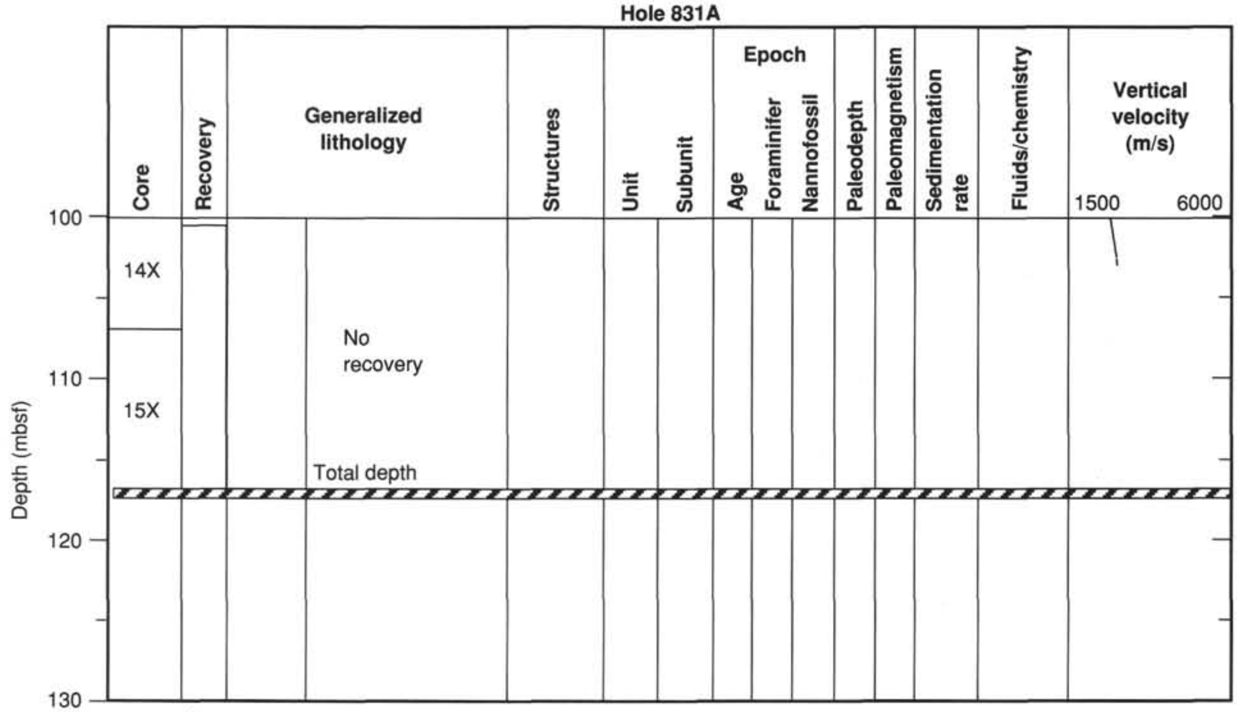

Figure 53 (continued).

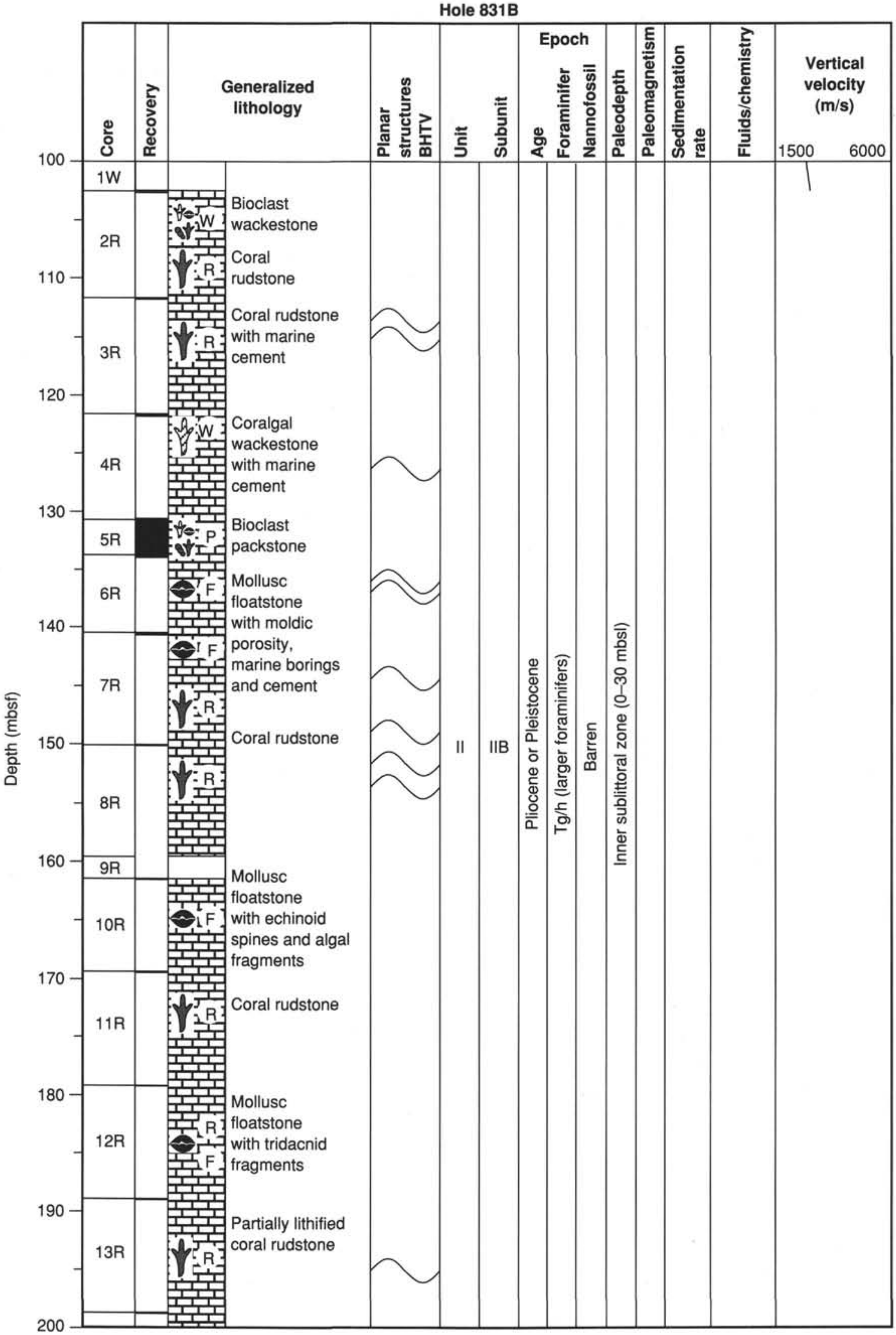

Figure 53 (continued).

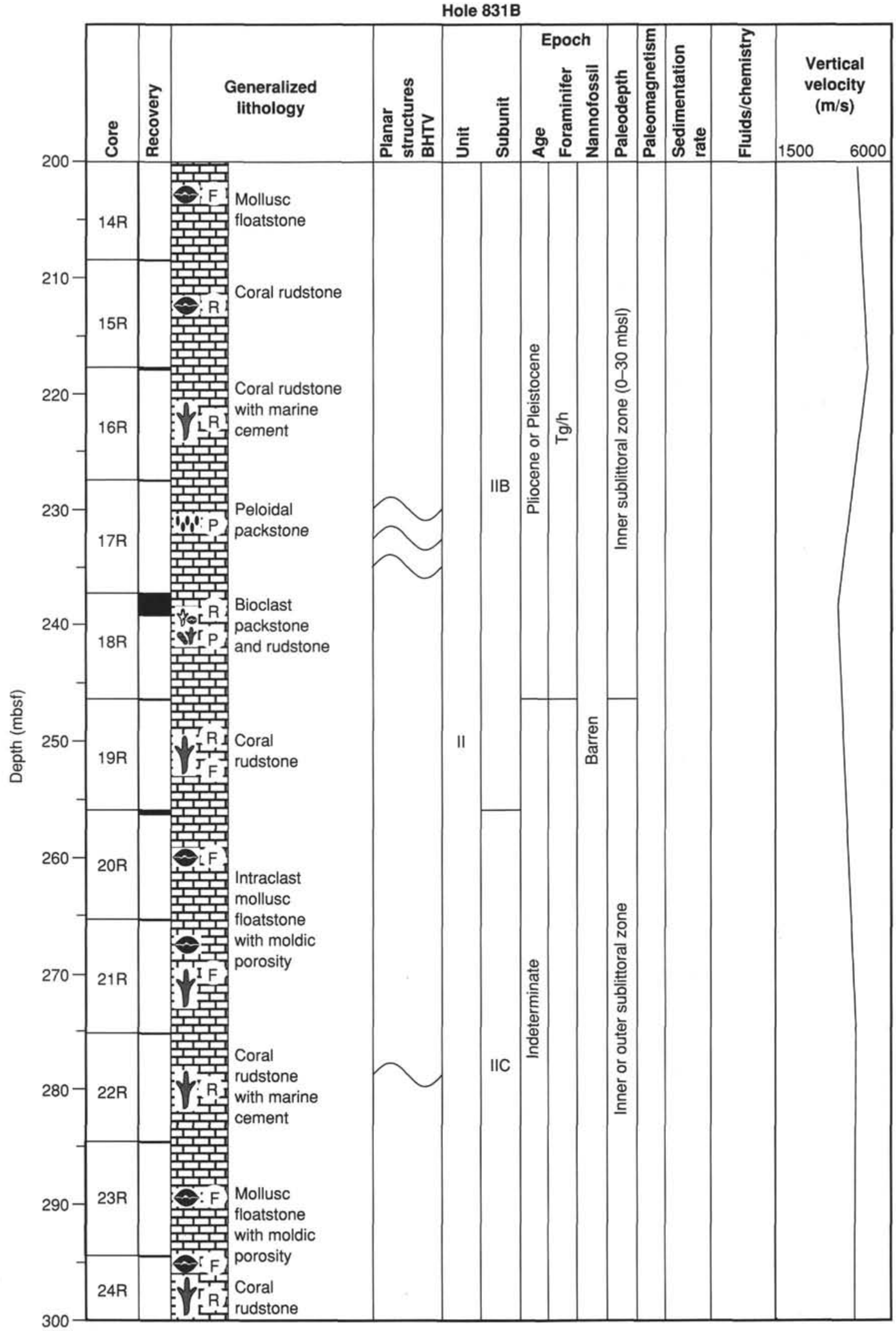

Figure 53 (continued).

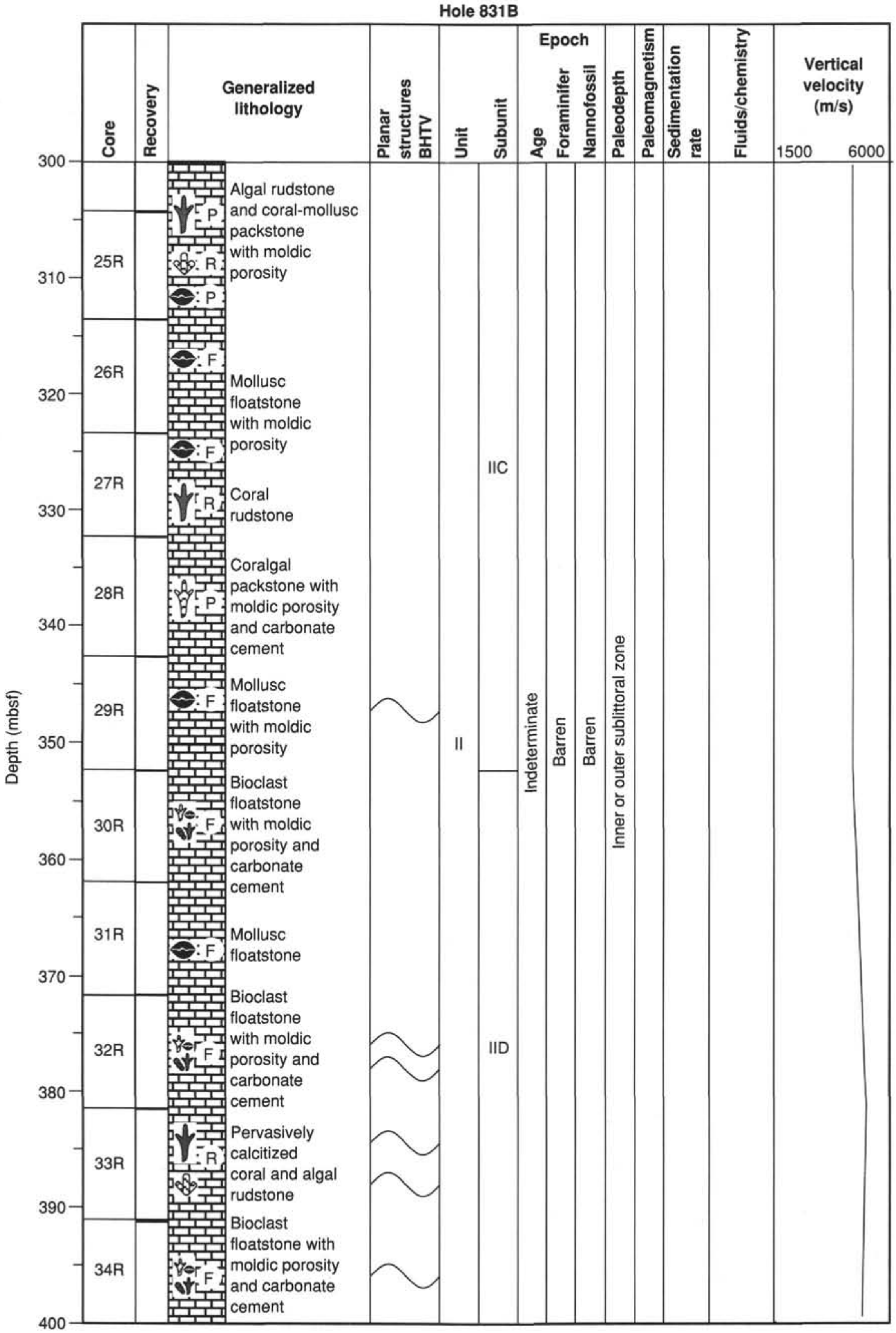

Figure 53 (continued).

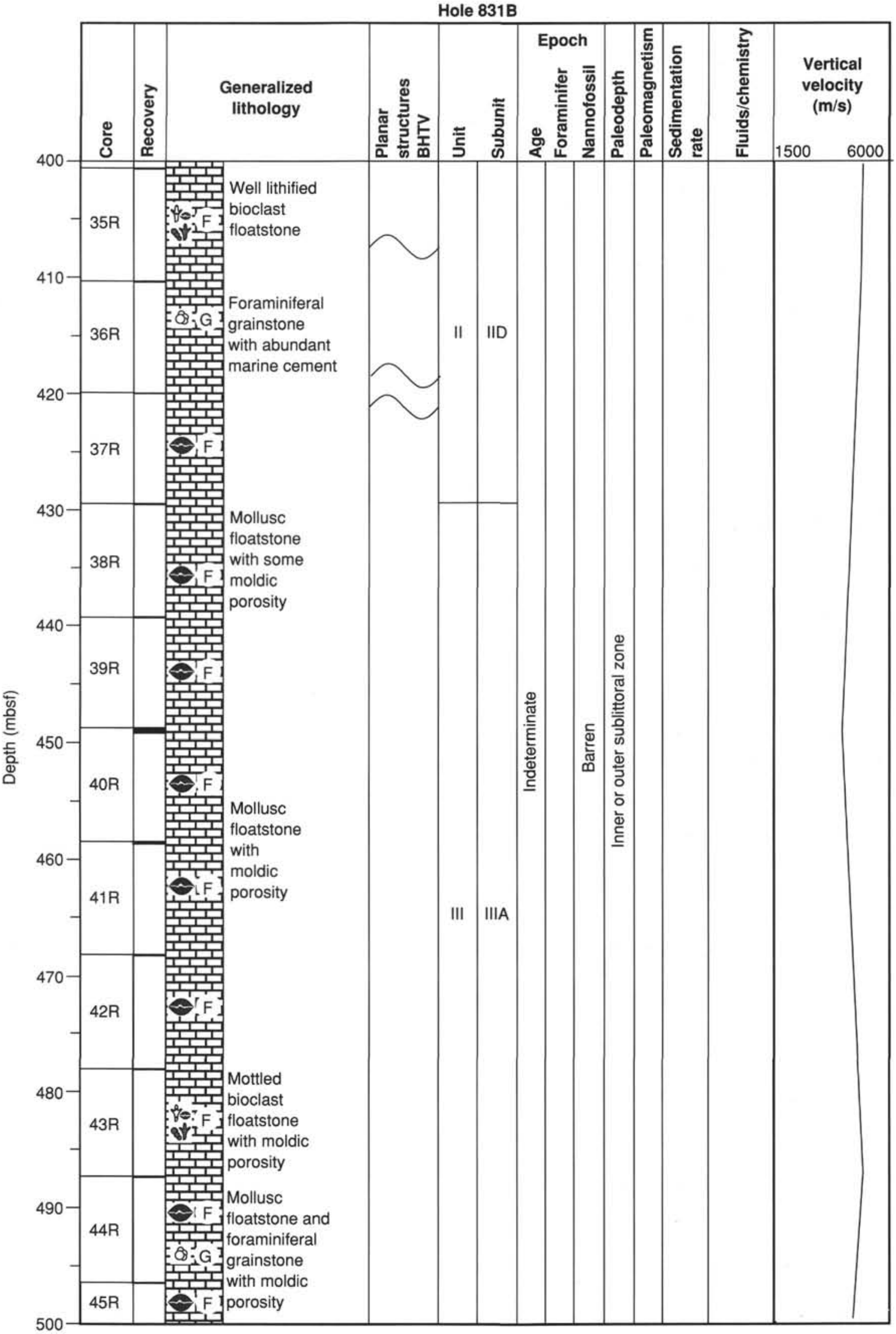

Figure 53 (continued).

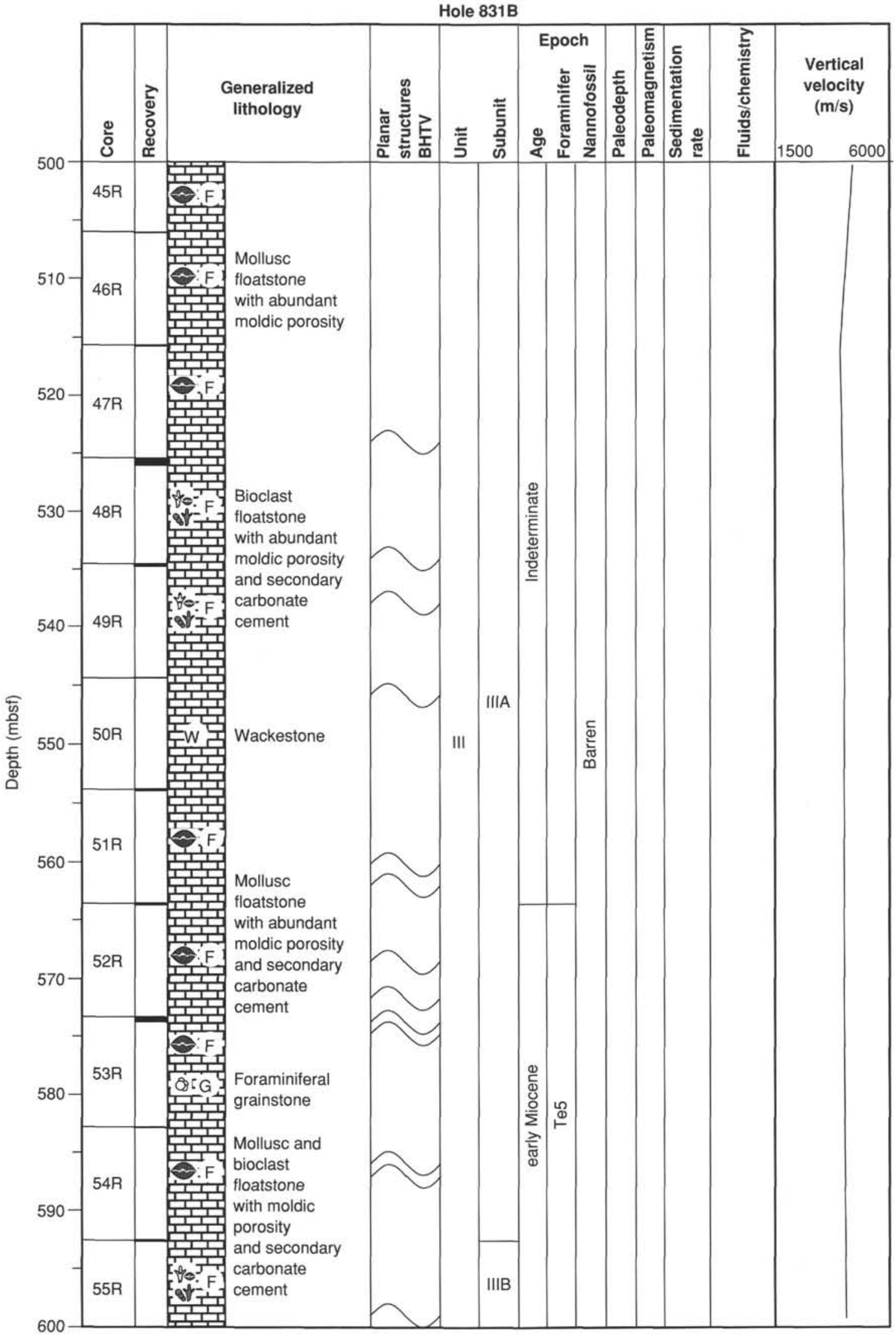

Figure 53 (continued).

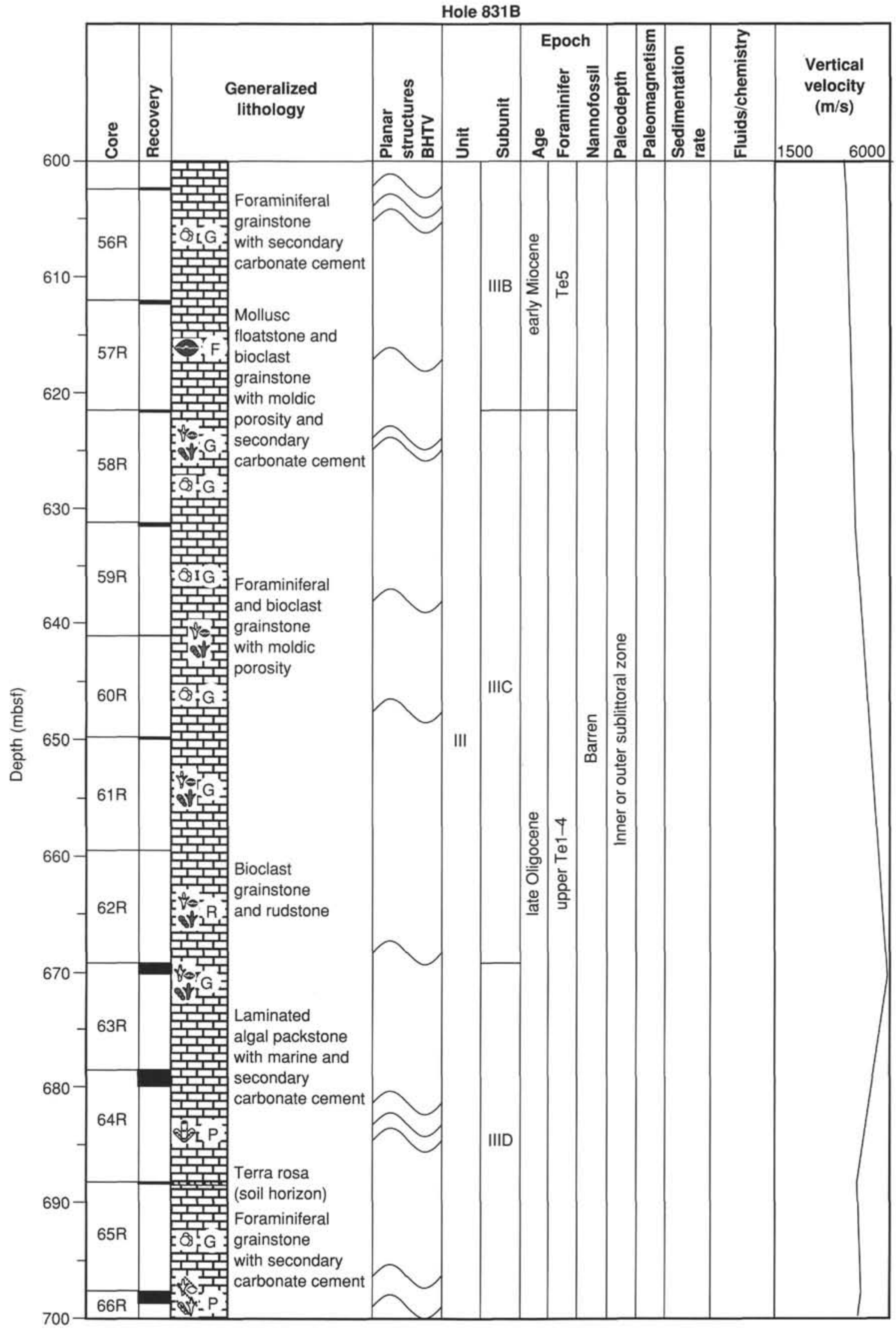

Figure 53 (continued).

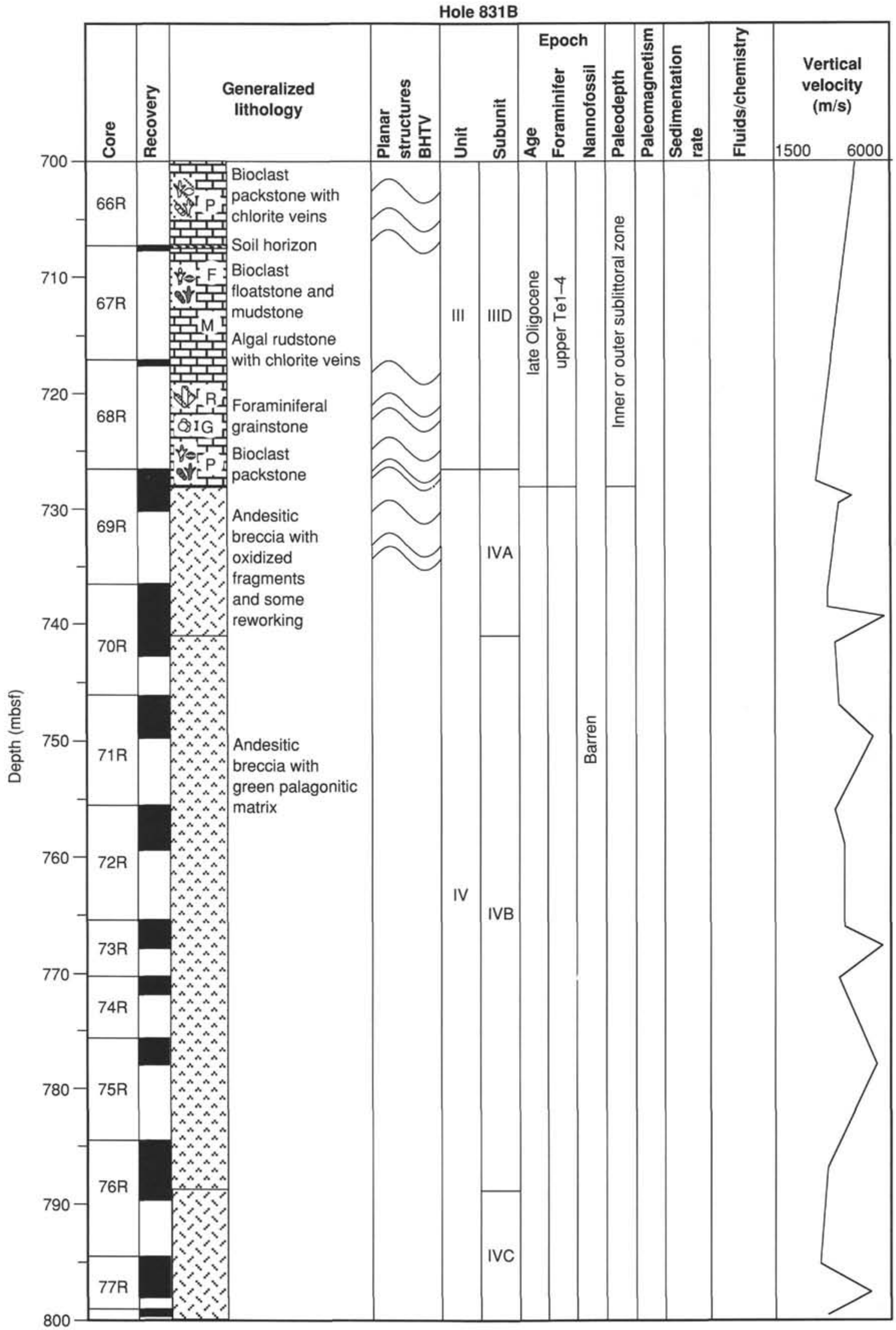

Figure 53 (continued).

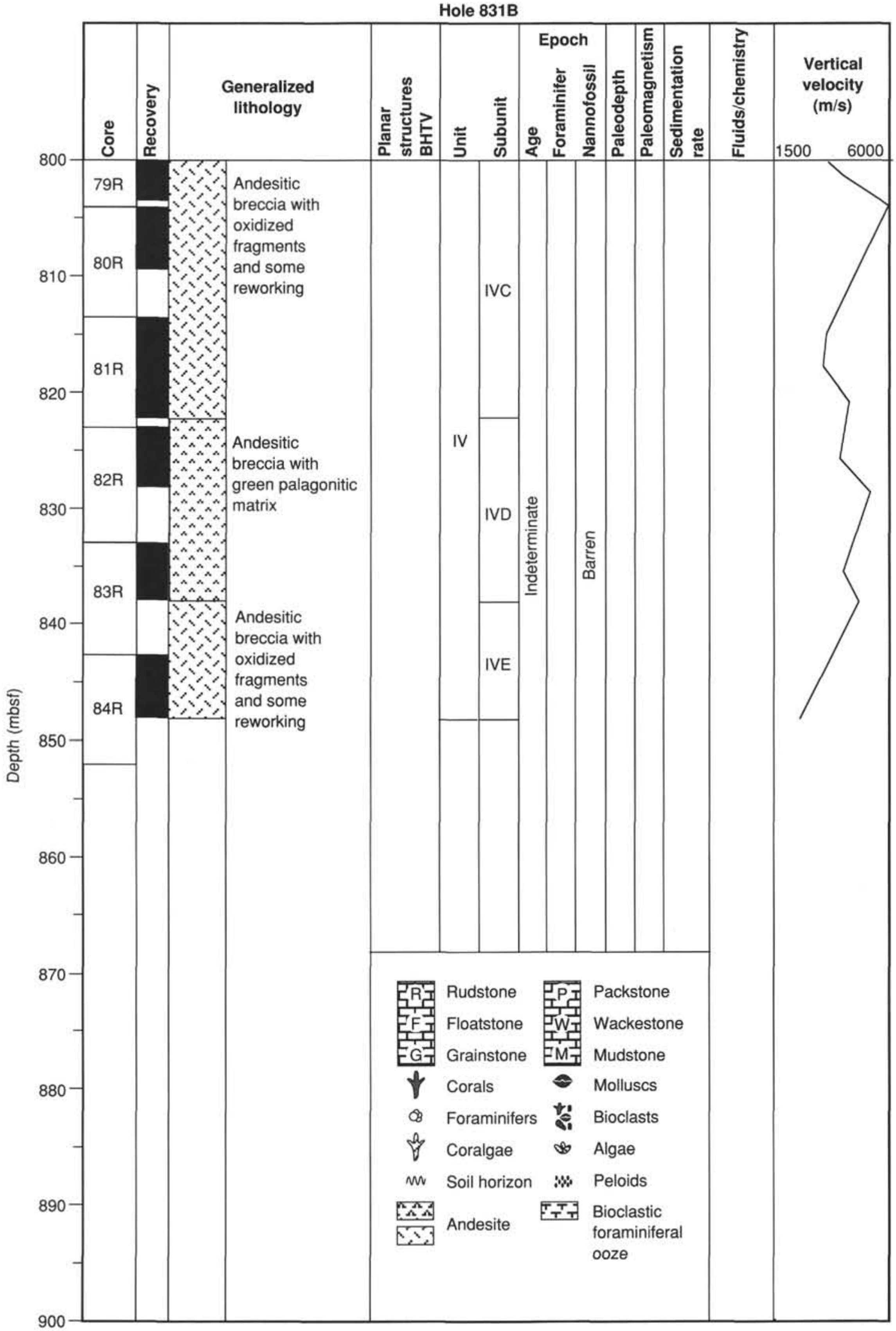

Figure 53 (continued).

Hole 831B: Resistivity-Sonic-Natural Gamma Ray Log Summary

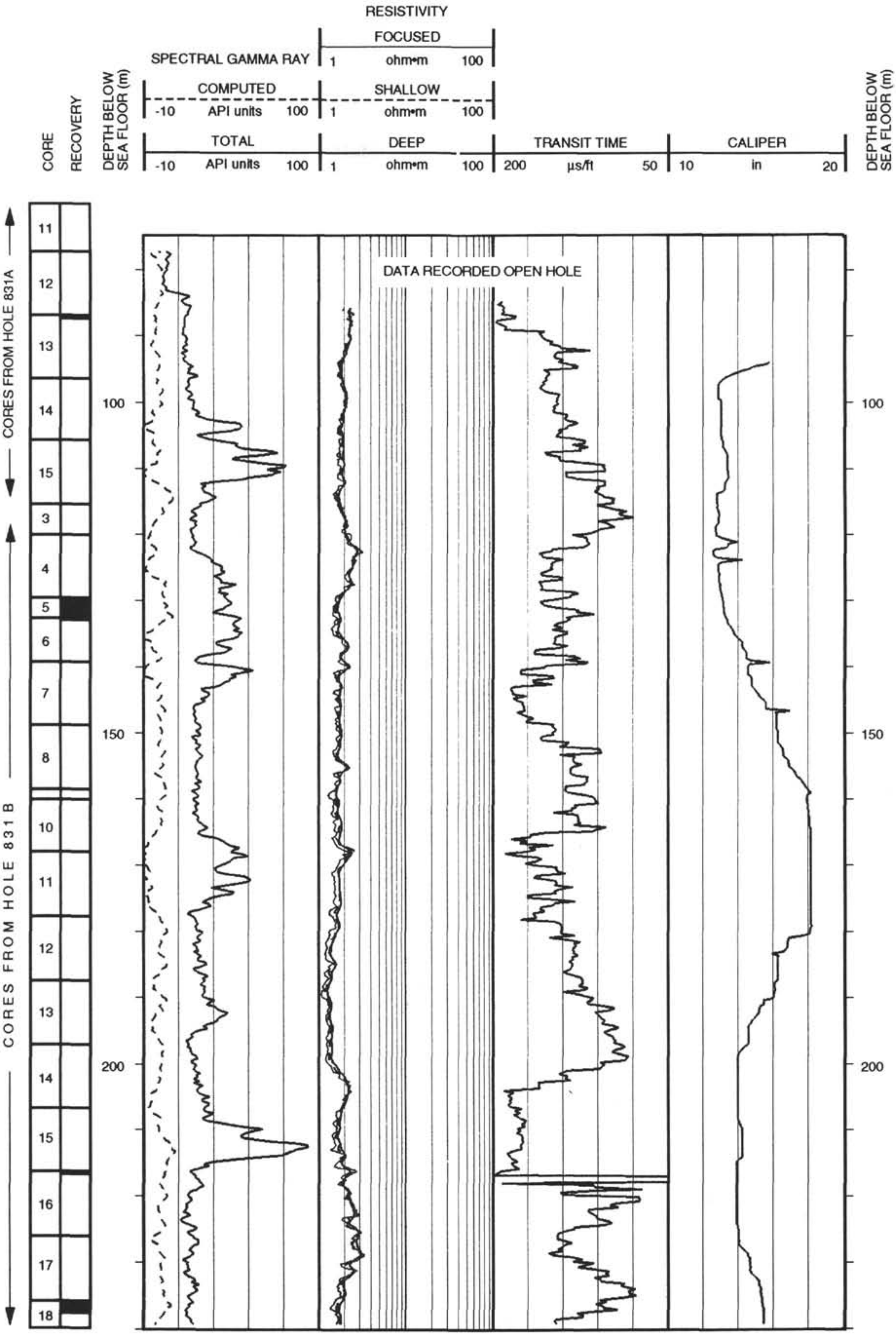

Hole 831B: Resistivity-Sonic-Natural Gamma Ray Log Summary (continued)

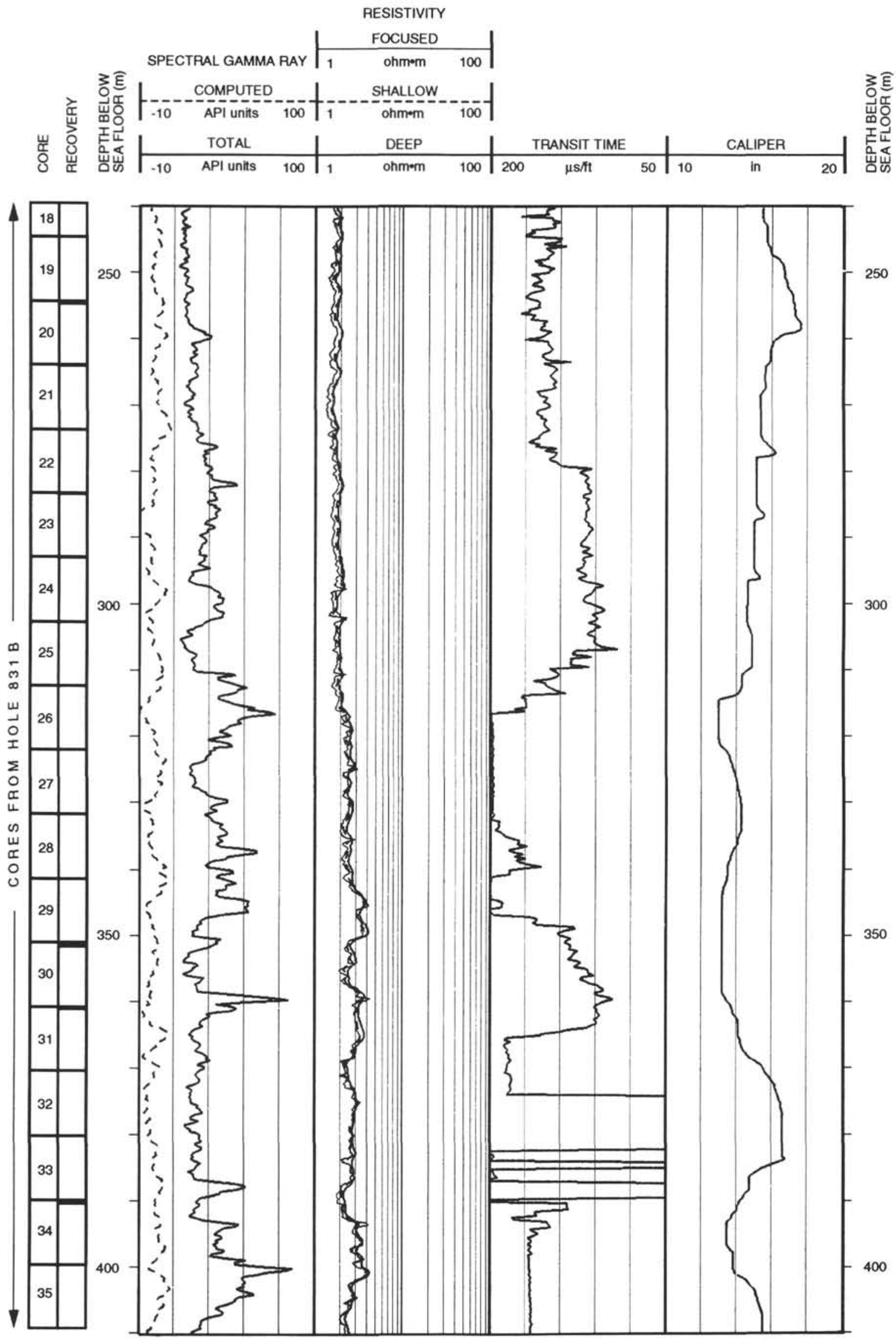

Hole 831B: Resistivity-Sonic-Natural Gamma Ray Log Summary (continued)

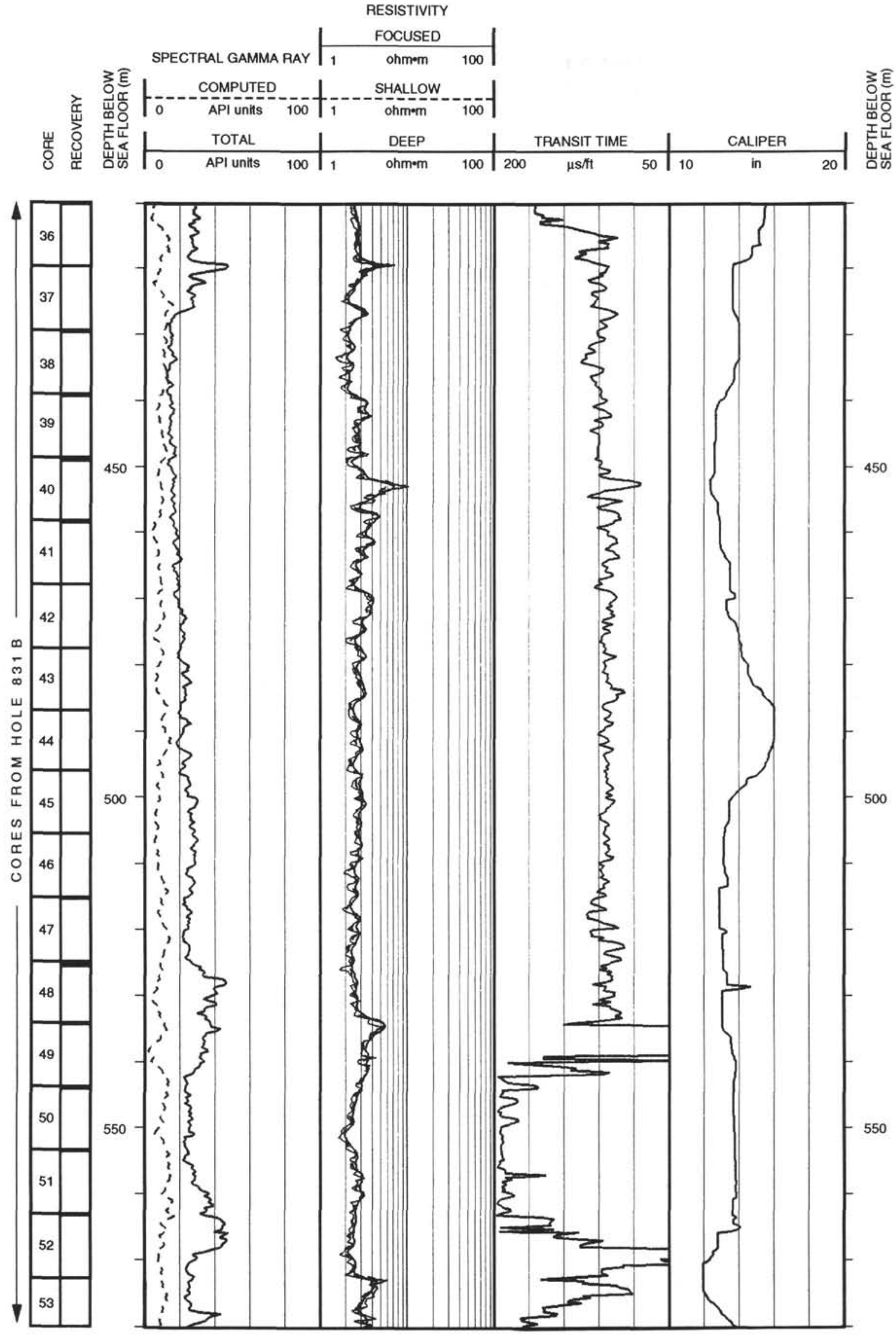

Hole 831B: Resistivity-Sonic-Natural Gamma Ray Log Summary (continued)

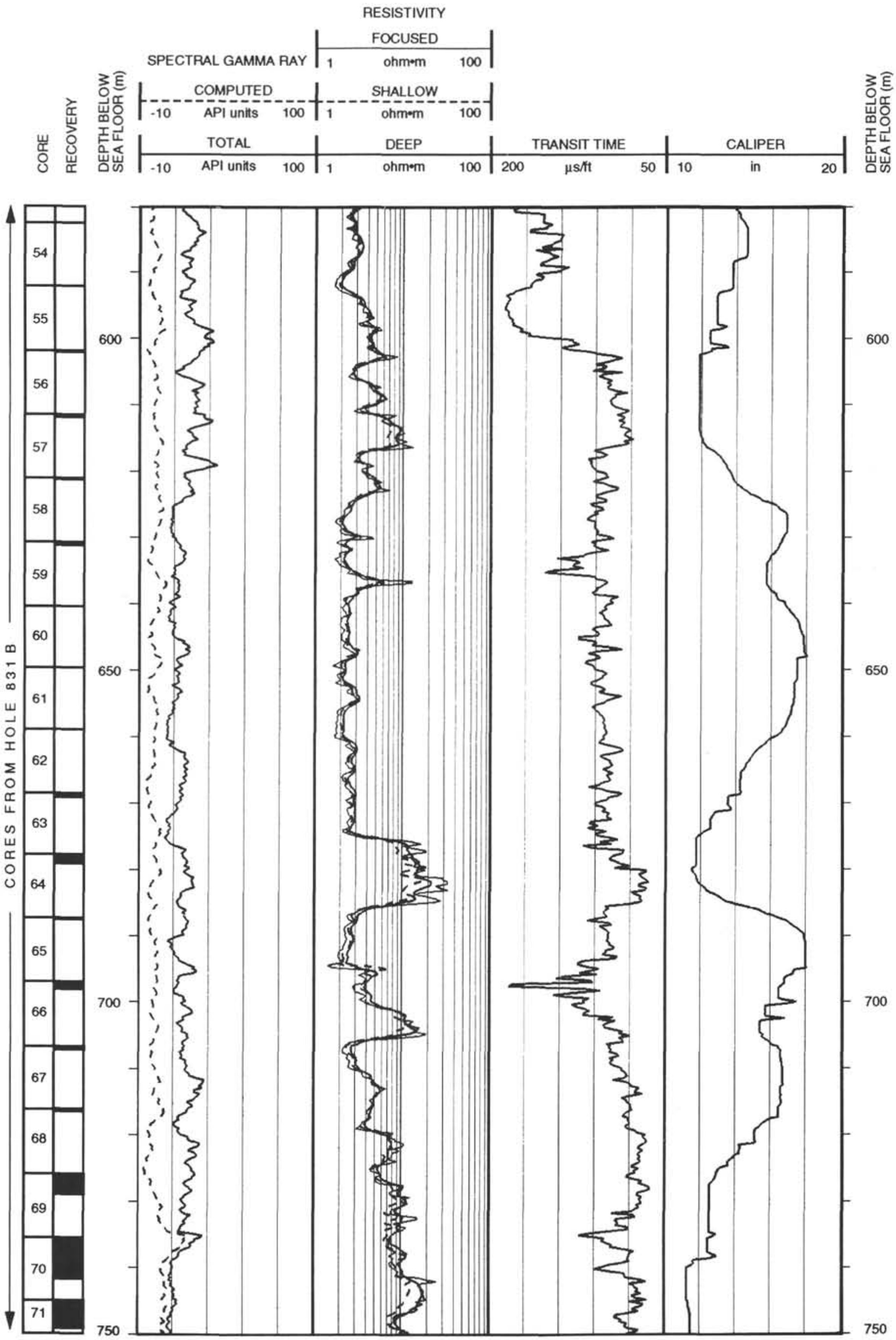

Hole 831B: Resistivity-Sonic-Natural Gamma Ray Log Summary (continued)

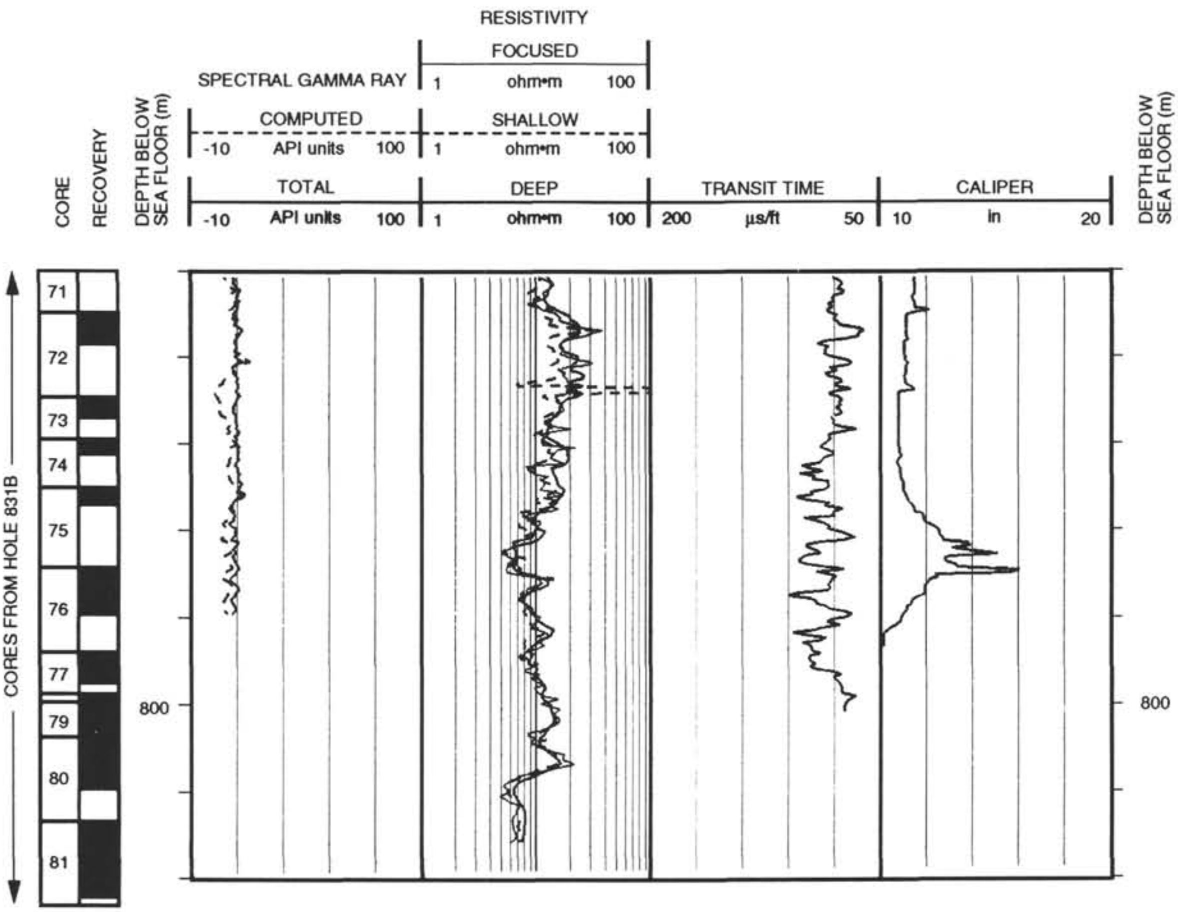

Hole 831B: Density-Natural Gamma Ray Log Summary

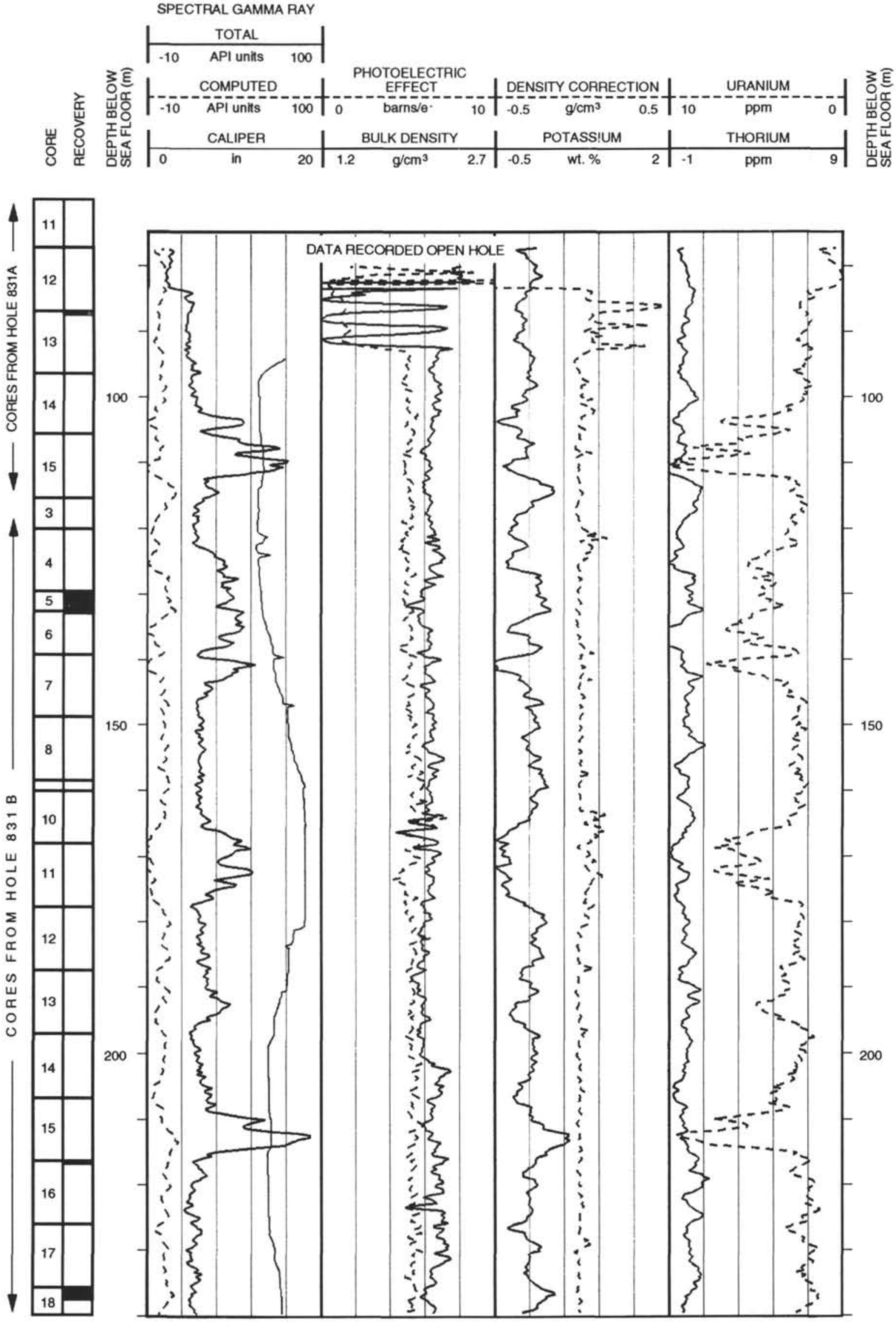

Hole 831B: Density-Natural Gamma Ray Log Summary (continued)

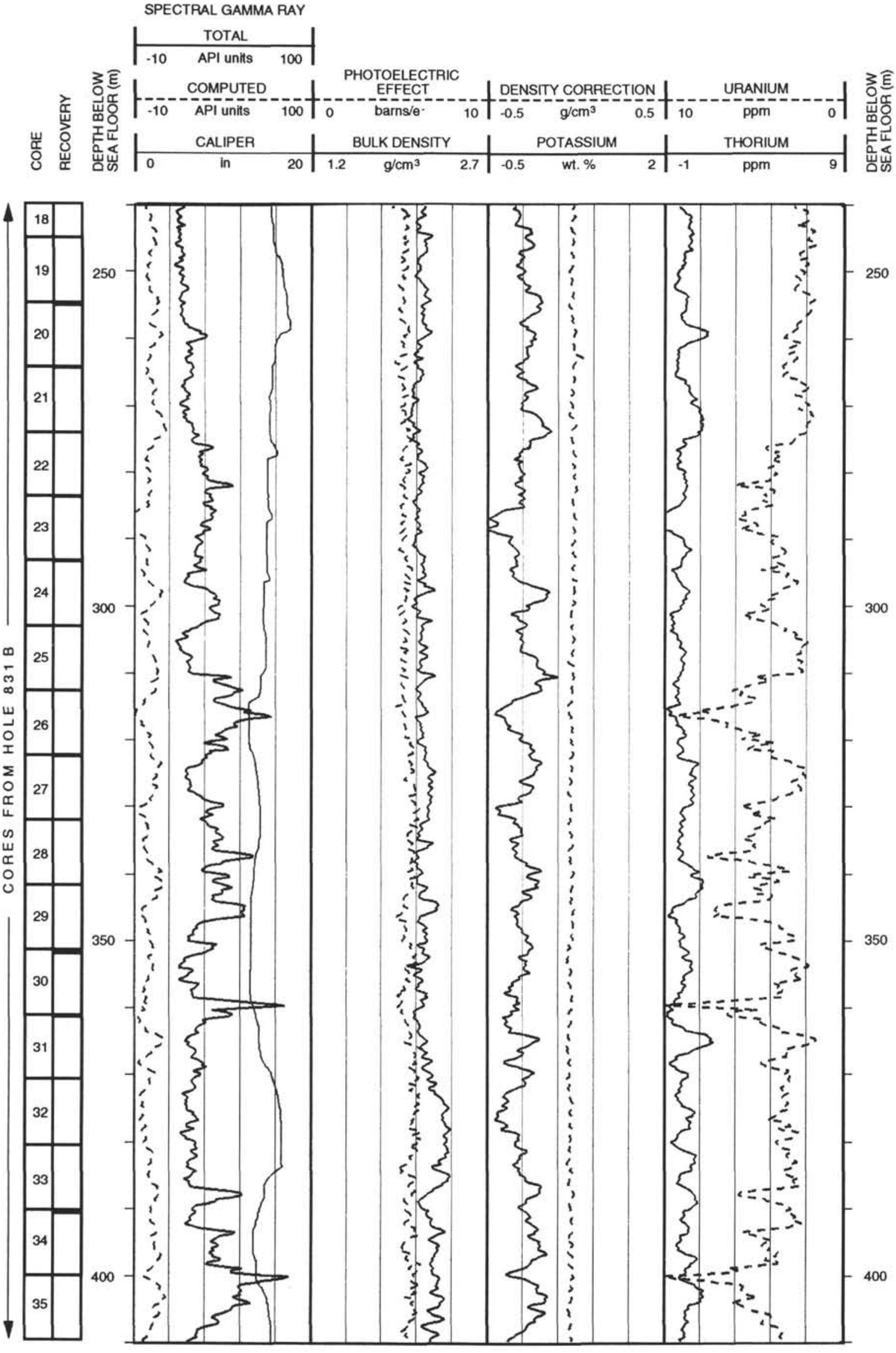

Hole 831B: Density-Natural Gamma Ray Log Summary (continued)

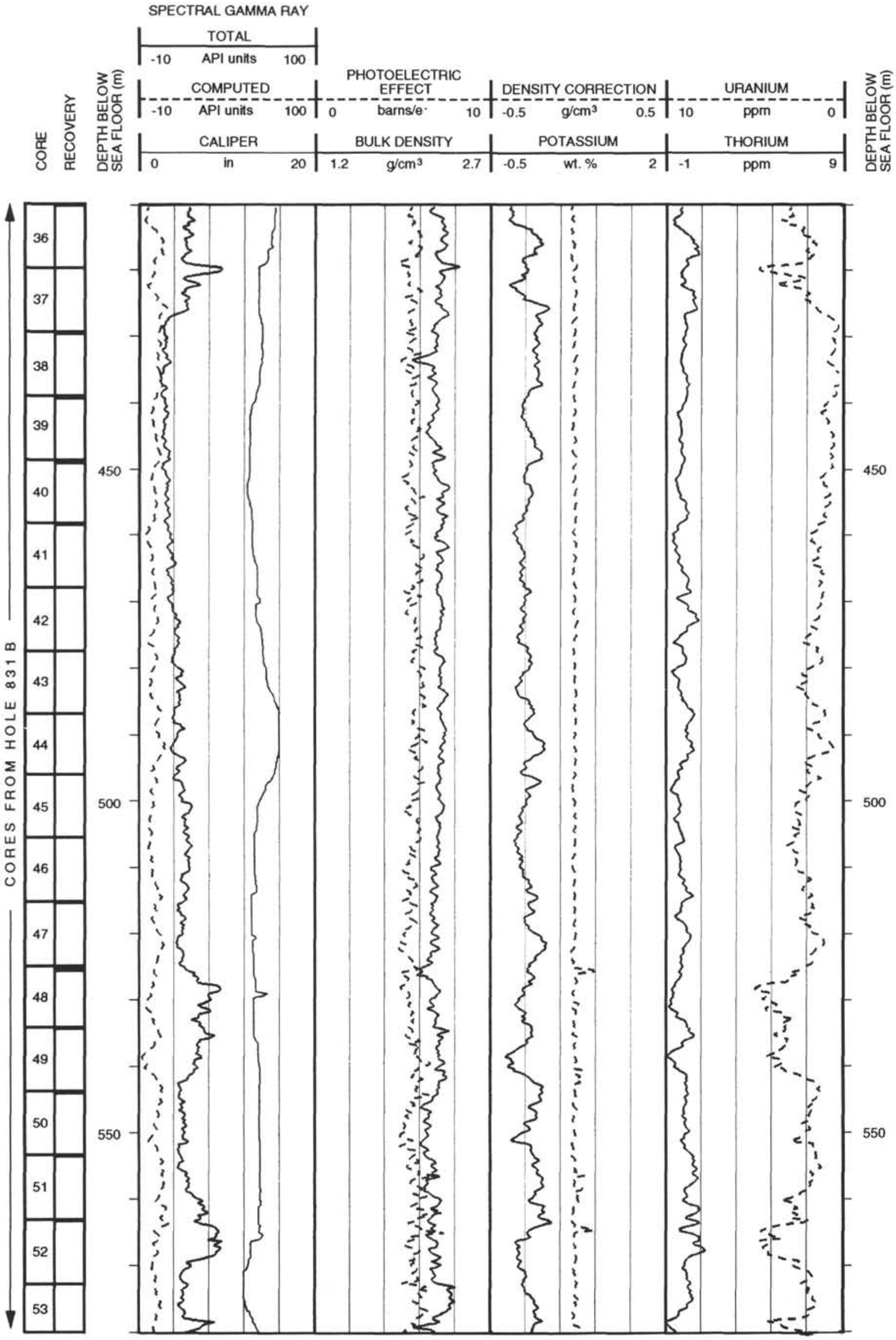

Hole 831B: Density-Natural Gamma Ray Log Summary (continued)

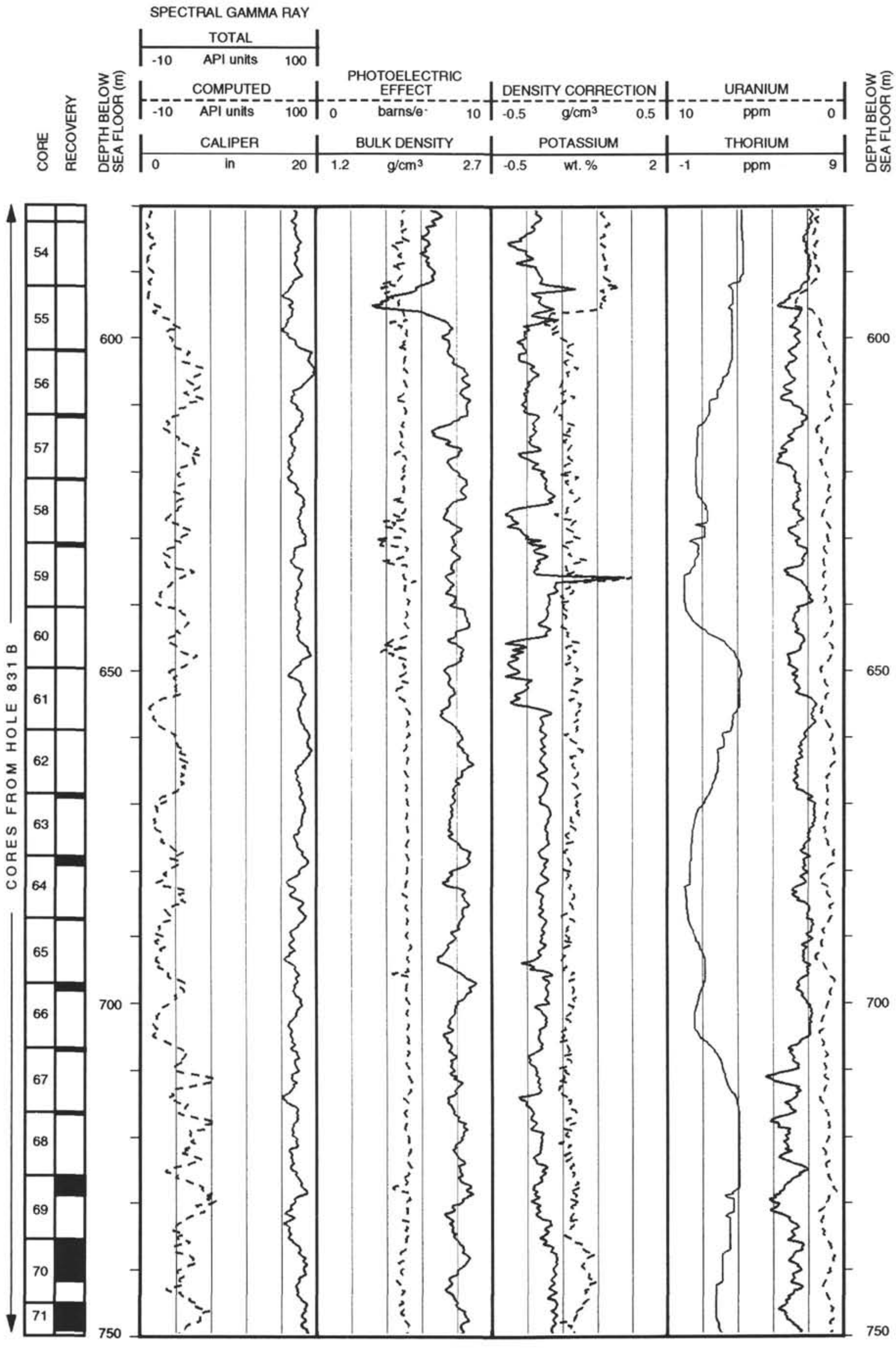

Hole 831B: Density-Natural Gamma Ray Log Summary (continued)

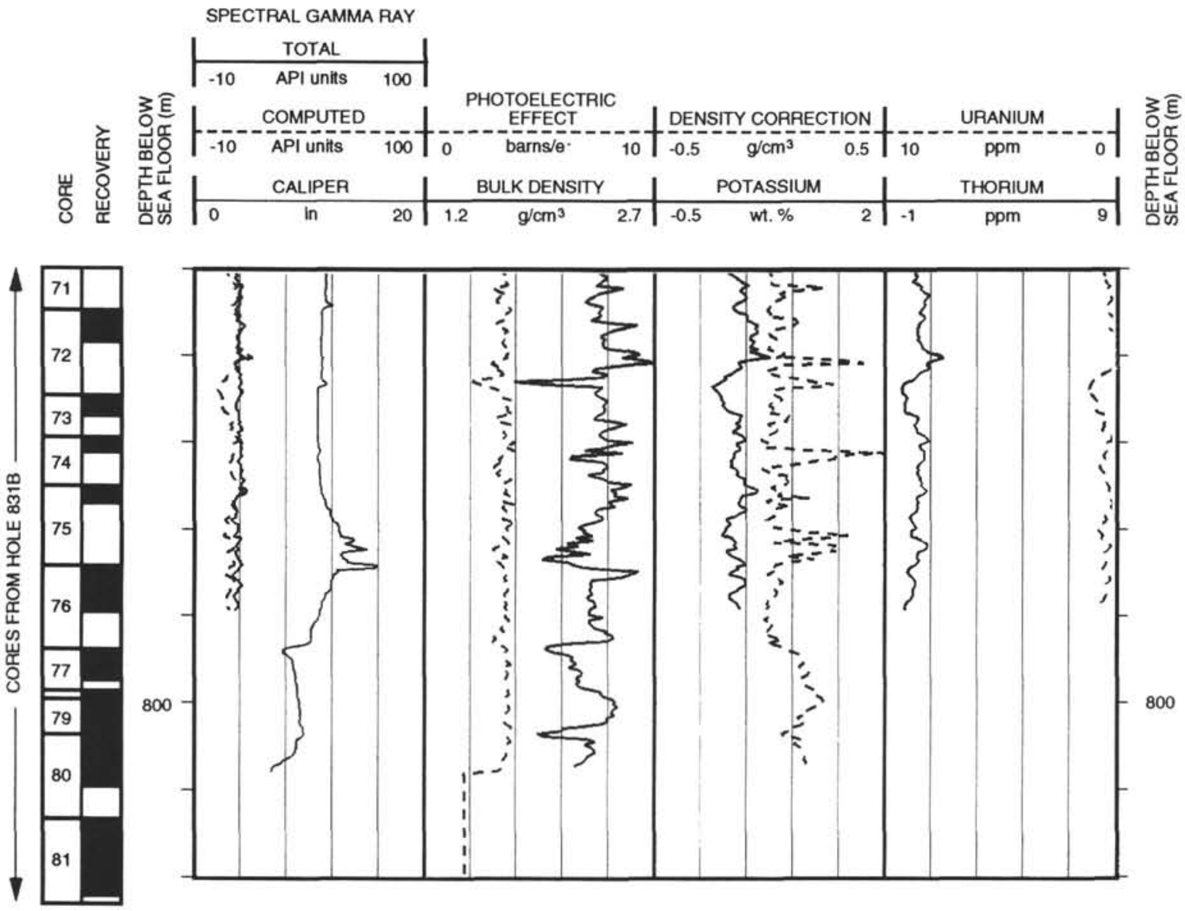

Hole 831B: Geochemical Log Summary

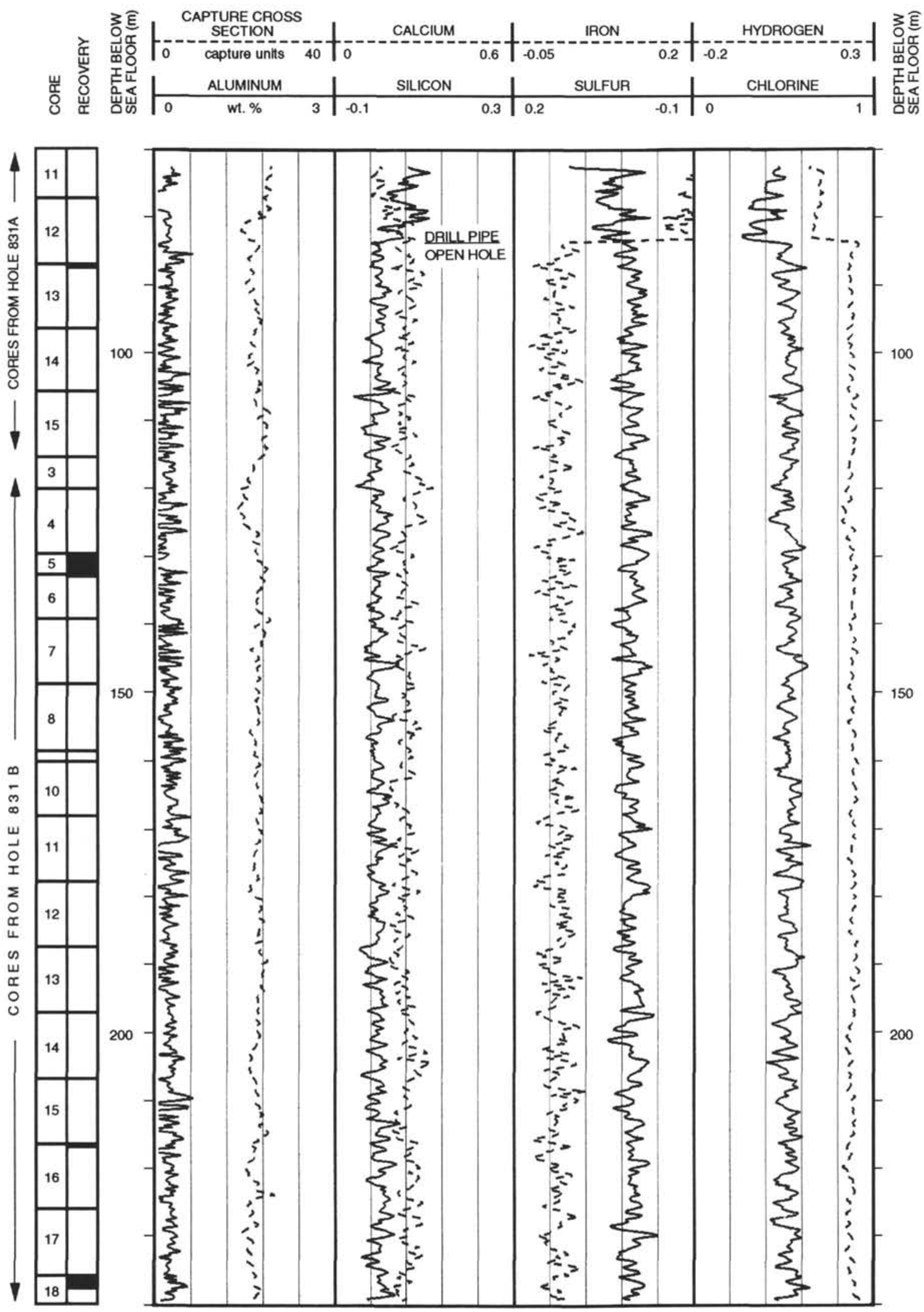

Hole 831B: Geochemical Log Summary (continued)

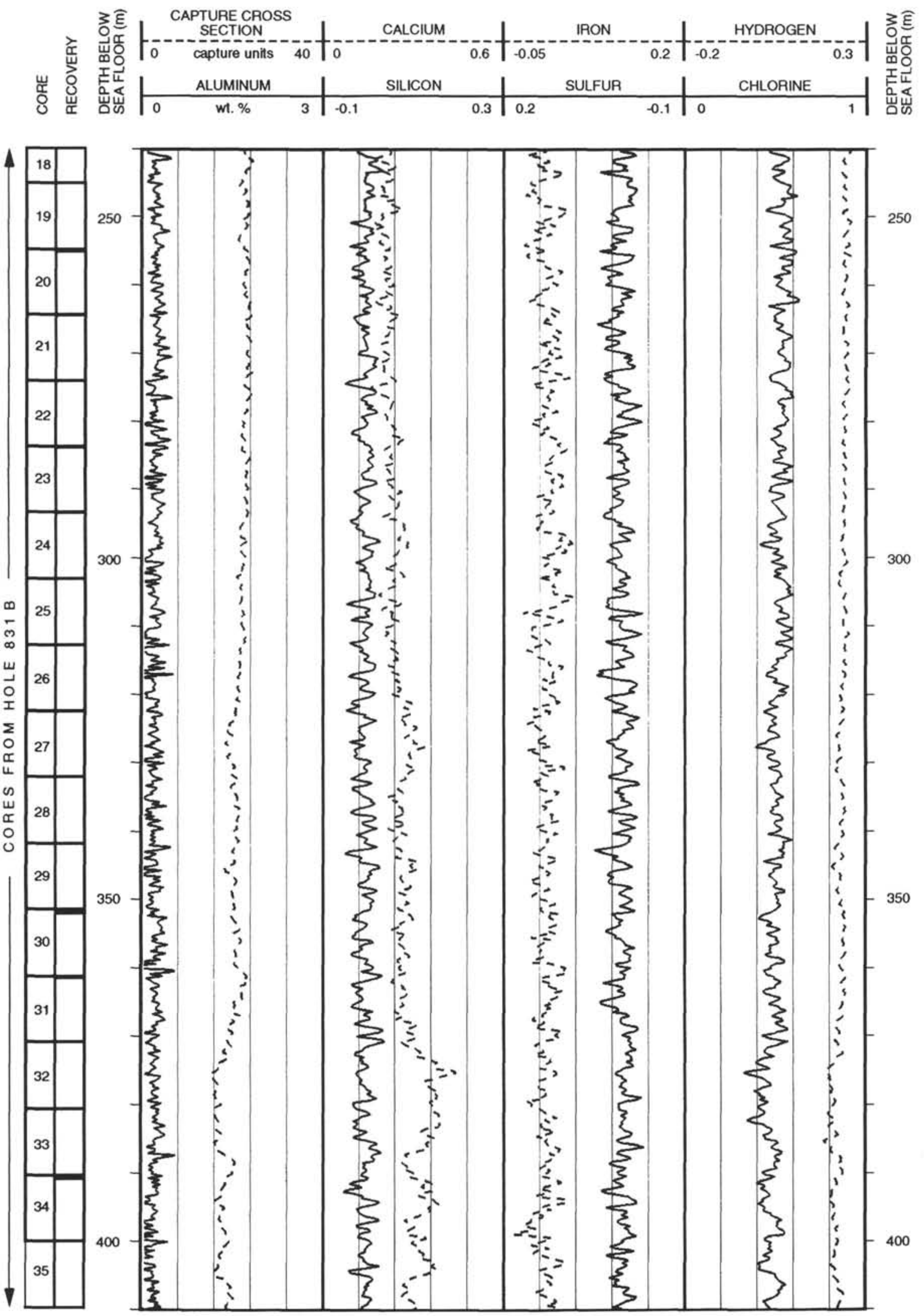

Hole 831B: Geochemical Log Summary (continued)

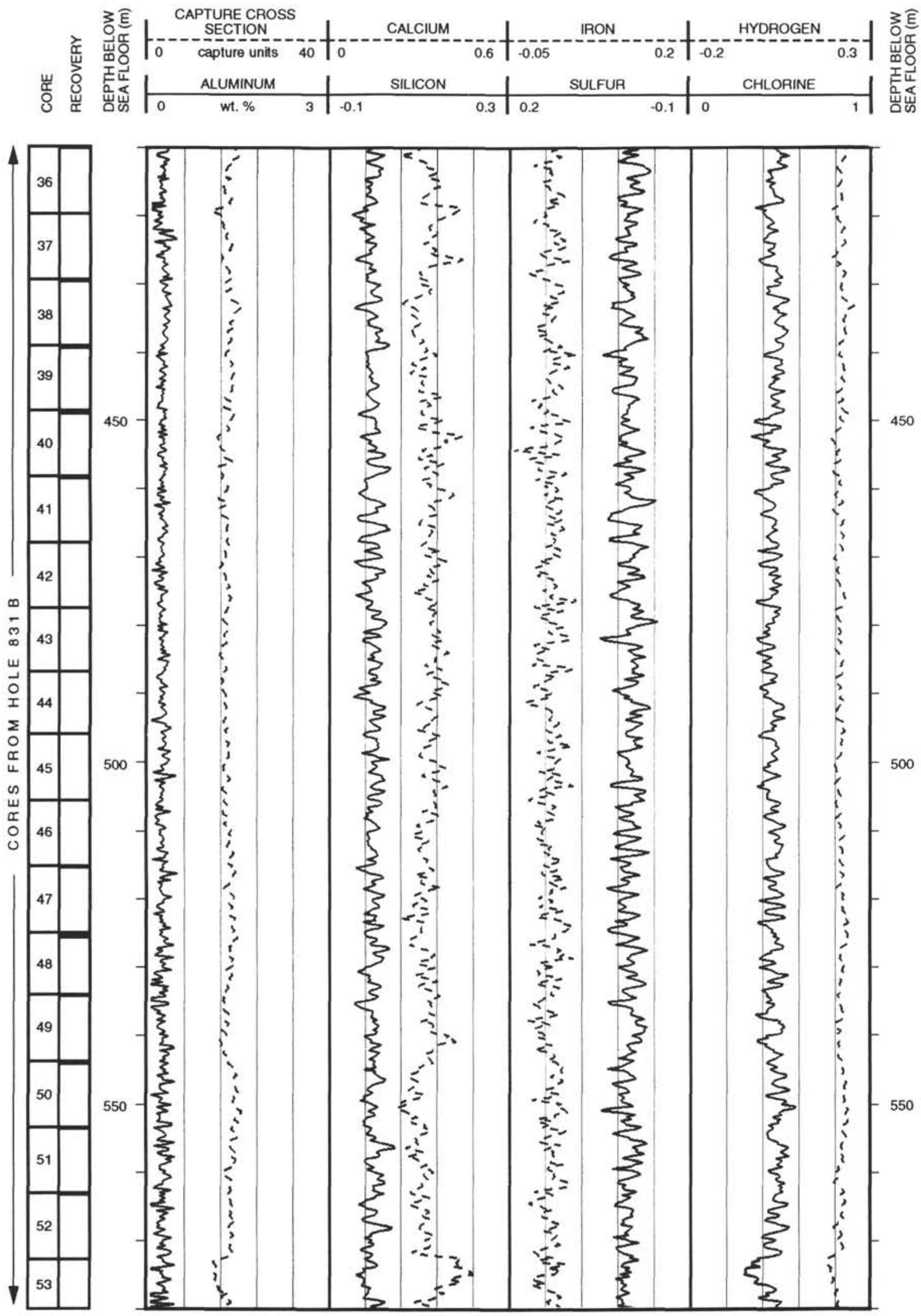

Hole 831B: Geochemical Log Summary (continued)